The Southern Ocean

A survey of oceanographic and marine meteorological research work

by Hartmut H. Hellmer and Manfred Bersch
with contributions of
Ernst Augstein and Iris Grabemann

Berichte zur Polarforschung Nr. 26 / Dezember 1985
Reports on Polar Research no. 26 / December 1985

		page
1.	Introduction	3
2.	The Southern Ocean	4
2.1	Spatial subdivision and bottom topography	4
2.2	Marine atmosphere	5
2.2.1	Sea surface heat exchange	5
2.2.2	Air temperature near the sea surface	7
2.2.3	Antarctic pressure trough	10
2.2.4	West and east wind zones	11
2.2.5	Precipitation	14
2.3	Ice distribution	15
2.3.1	Sea ice	15
2.3.2	Ice shelves	21
2.4	Hydrography	21
2.4.1	Water masses	21
2.4.1.1	Antarctic Surface Water	22
2.4.1.2	Circumpolar Deep Water	23
2.4.1.3	Antarctic Bottom Water	24
2.4.1.4	Modified Circumpolar Deep Water	24
2.4.1.5	Antarctic Intermediate Water	25
2.4.1.6	Shelf Water	25
2.4.1.7	Polar Frontal Zone	26
2.4.1.7.1	General Features	26
2.4.1.7.2	Thermohaline characteristics	30
2.4.1.8.	Weddell-Scotia Confluence	34
2.4.2	Oceanic circulation	36
2.4.2.1	Antarctic Circumpolar Current (ACC)	36
2.4.2.1.1	General features of the ACC	37
2.4.2.1.2	Atlantic sector	38
2.4.2.1.3	Indian sector	39
2.4.2.1.4	Pacific sector	42
2.4.2.1.5	Drake Passage	42
2.4.2.2	East Wind Drift	44
2.4.2.3	Antarctic Divergence	44
3.	The Weddell Sea	46
3.1	Bottom topography	46
3.2	Marine atmosphere	46
3.2.1	Surface heat budget in the pack ice zone	46
3.2.2	Air temperature at the lower boundary of the atmosphere	49
3.2.3	Antarctic pressure trough	50
3.2.4	West and east wind zones	50
3.2.5	Precipitation	52
3.3	Glaciological aspects	52
3.3.1	Sea ice	52
3.3.2	Weddell Polynya	56
3.3.3	Ice shelves	57

		page
3.4	Hydrography	58
3.4.1	Water masses	59
3.4.1.1	Winter Water	61
3.4.1.2	Warm Deep Water	61
3.4.1.3	Antarctic Bottom Water	62
3.4.1.4	Weddell Sea Bottom Water	63
3.4.1.5	Weddell Sea Deep Water	65
3.4.1.6	Shelf Water	66
3.4.1.7	Ice Shelf Water	67
3.4.2	Circulation	68
3.4.2.1	Weddell Gyre	68
3.4.2.2	Circulation on the shelf	73
4.	The Bottom Water formation	74
4.1	Influence of the wind	74
4.2	Surface cooling and salt rejection during freezing periods	75
4.2.1	Sea ice growth and haline convection	75
4.2.2	Large-scale salt and heat fluxes	77
4.2.3	Convection on the shelf	78
4.2.4	Convection in the open ocean	80
4.3	Mixing processes	86
4.3.1	Mixing on the continental slope	86
4.3.2	Mixing in the open ocean	90
4.3.3	Double diffusive convection	90
4.3.4	Cabbeling-instability	92
4.6	Spreading of Antarctic Bottom Water from the Weddell Sea	93
Subject Index		99
References		102

1. INTRODUCTION

An increasing amount of attention has been paid to the polar regions over the last three decades in the course of climate-, general circulation-, geological-, geophysical- and biological investigations. These studies document the important role of the polar oceans in the framework of the global marine ecosystem, the general oceanic and atmospheric circulation and the state of the Earth's climate. Previous work also indicates that in spite of growing understanding of the impact of the polar regions on the global bio-, hydro-, cryo- and atmospheres, considerable gaps in our knowledge have still to be filled.

This challenge has attracted numerous scientists, who have previously worked in other areas, to the field of polar research. They may benefit in particular from this literature survey, which concentrates on studies of oceanic and atmospheric physics of the Southern Ocean with special emphasis on the Weddell Sea. The latter region has been chosen as the main working area for the present and forthcoming German marine research in Antarctica.

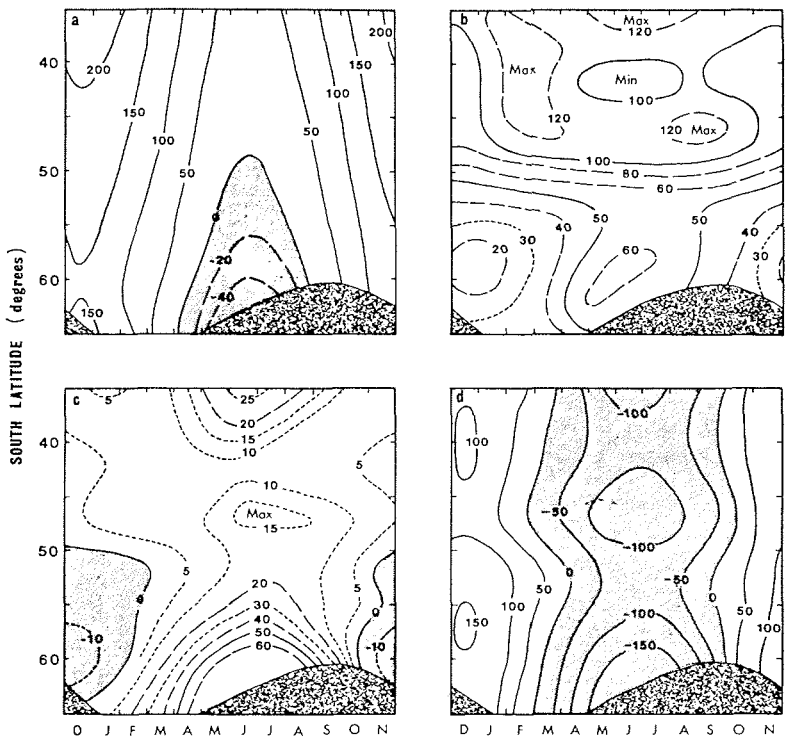

Figure 2: Sea surface components of the ocean heat budget south of Australia (115-160°E). The strongly shaded area represents the pack ice extent.

a) Radiation balance (positive for an oceanic gain)
b) Latent heat flux
c) Sensible heat flux (positive for fluxes from the ocean to the atmosphere)
d) Net heat gain (positive) of the ocean (Zillmann, 1972).

On an annual average the ocean looses heat at the sea surface. This loss increases with latitude from 3 Wm^{-2} at 50°S to 18 Wm^{-2} at 60°S (Zillman, 1972).

The following conclusions based on measurements may have a rather general validity for the ice free water belt:

- The ocean is generally warmed up by a net downward radiation flux north of the ice edge, with the exception of the area south of 50°S from April to August (Fig. 2 a)

- The sea continuously looses heat through evaporation in the entire open water area (Fig. 2 b)

- Similar effects result from the transfer of sensible heat from the water to the air. Only during the summer months and for latitudes higher than 50°S is this flux directed oceanwards (Fig.2c)

- The combination of the radiative and turbulent heat and water vapour fluxes at the sea surface (Fig.2d) result in a net heat gain of the ocean from October to February and a loss during the rest of the year.

Slightly different results are obtained by Taylor et al. (1978) who, for the longitudes from 115°E to 140°E south of the Antarctic Convergence (AAC) (55°-60°S), derive an ocean heat gain of 10 Wm^{-2}, whilst their calculations show a heat loss of 15 Wm^{-2} north of the AAC up to 45°S. Similar results were obtained for 0° - 10°E.

The inclusion of pack ice to the calculations lead Gordon and Goldberg (1970) to estimate an annual heat loss for the entire ocean south of the AAC (incl. pack ice zone) of 19 - 25 Wm^{-2}. This value has more or less been confirmed by Gordon and Taylor (1975 a), who arrived at 20 Wm^{-2}.

2.2.2 Air temperature near the sea surface

The annual oscillation of the air temperature at the lower boundary of the atmosphere follows the annual cycle of the solar radiation with a time-lag of 0.5 to 1 month. The temperature maximum occurs in December/January and the minimum in July.

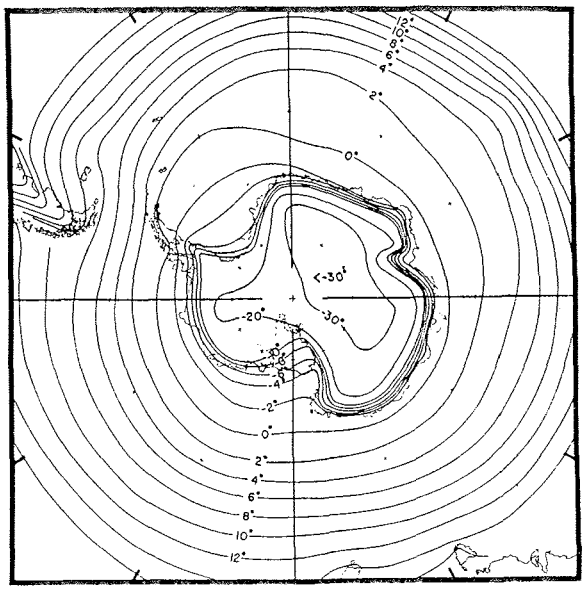

Figure 3: Monthly averaged air temperature (°C) at the earth surface for January (Schwerdtfeger, 1970).

Figures 3 and 4 show the monthly averaged air temperature at the earth surface south of about 45°S for January and July. Over the

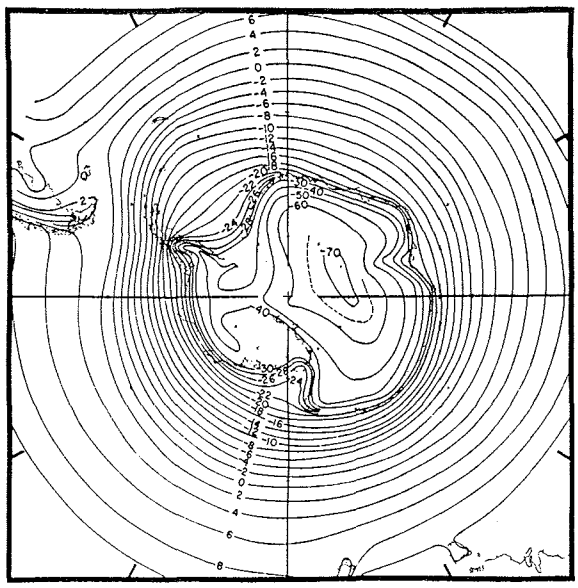

Figure 4: Monthly averaged air temperature (°C) at the earth surface for July (Schwerdtfeger, 1970).

ocean, the lowest temperatures occur in the southern Weddell Sea and the southern Ross Sea. Due to the asymmetry of Antarctica and the northward deflection of cold water and air masses by the Antarctic Peninsula, positive temperature deviations from the zonal mean appear in the Pacific sector and negative temperature deviations in the Atlantic and Indian sectors. The largest meridional temperature gradients are situated in summer to the north, and in winter to the south, of the AAC. Streten (1977) compares the seasonal temperature fluctuations of distinct oceanic regions. He divides the meteorological stations of the Southern Ocean (Table 2) into 3 categories:

Station	Position		Abbr.	Region
Campbell Island	52.5°S	169.1°E	CA	2
Chatham Island	46.0°S	176.5°E	CH	1
Deception Island	63.0°S	60.6°W	D	3
Gough Island	40.3°S	9.9°W	GO	1
Grytviken (South Georgia)	54.2°S	36.6°W	GR	3
Heard Island	53.1°S	72.5°E	H	3
Ile Nouvelle, Amsterdam	37.8°S	77.6°E	NA	1
Macquarie Island	54.5°S	159.0°E	MC	2
Marion Island	46.9°S	37.8°E	M	2
Orcadas (Laurie Island)	60.7°S	44.7°W	O	3
Port aux Francais (Kerguelen)	49.3°S	70.2°E	K	2

Station	Position		Abbr.	Region
Signy Islands	60.7°S	45.6°W	SG	3
Stanley (Falkland Islands)	51.7°S	57.9°W	ST	2
Tristan Da Cunha	31.1°S	12.3°W	T	1

Table 2: Meteorological stations of the Southern Ocean (Streten, 1977).

1. Stations near the Subtropical Convergence
   (T 10°C in summer, T 5°C in winter)

2. Stations between the Subtropical Convergence and the Antarctic Convergence
   (10°C T 5°C in summer, 5°C T 0°C in winter)

3. Stations south of the Antarctic Convergence
   (T 5°C in summer, T 0°C in winter)

Except for stations in the Scotia Sea (D, SG, O, GR, ST) perennially averaged temperatures are higher in autumn than in spring (Fig. 5). The anomaly in the Scotia Sea region is produced

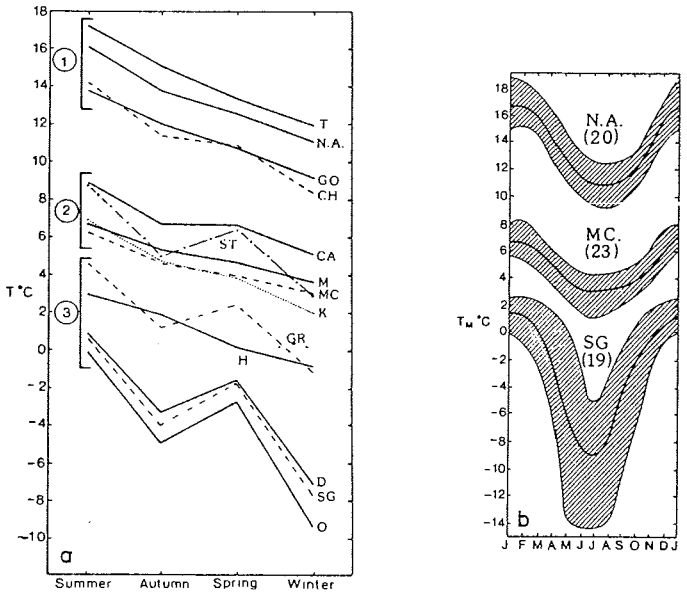

Figure 5: a) Seasonally averaged surface temperatures at meteorological stations of 3 different regions in the Southern ocean.
b) Monthly averaged temperatures of New Amsterdam (NA), Macquarie (MC) and Signy (SG). The heavy lines indicate the record averages (the numbers in brackets denote the record lengths in years). The hatched area comprises the range of the monthly averaged temperatures (Streten, 1977).

by the northward transport of cold water masses and newly formed sea ice in the Weddell Gyre. Temperatures at stations of the third group exhibit the largest annual oscillations and the largest interannual fluctuations due to the annual and interannual variations of the pack ice extent. Due to regular ice growth, temperatures at stations in the eastern hemisphere show less variability (Streten, 1977).

2.2.3 Antarctic pressure trough

The stationary high pressure area over the Antarctic Plateau with its centre at about 83°S 90°E is surrounded by a circumpolar low pressure belt between 60°S and 73°S (Antarctic trough) with local pressure minima at 20°-30°E, 90°-110°E, 130°-150°W,

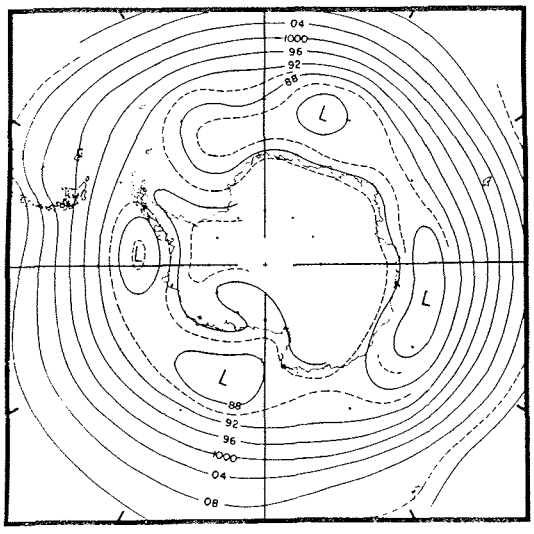

Figure 6: Monthly averaged pressure (hPa) at the sea surface for January (Schwerdtfeger, 1970).

80°-90°W and 30° - 50°W (Fig. 6; Streten, 1980). Using 3 day averaged pressure values, the circumpolar pressure field reveals a strong temporal variability with 2 - 4 low pressure centres (Cavalieri and Parkinson, 1981). An investigation by Streten (1980) shows a more frequent occurrence of cyclones for the Weddell Sea than for the Bellingshausen Sea. The Antarctic trough is formed by cyclones, which are generated predominantly at the atmospheric polar front and travel southeastwards to the Antarctic coast. However, less than 10 % of these cyclones cross the coastline of Antarctica (Taljaard, 1972).

The minimum pressure axis of the Antarctic trough oscillates meridionally with a half year period around an annually and zonally averaged position of 65.9°S. The amplitude of this variation amounts to 2.5 degrees of latitude. The southernmost position is reached mid-March and mid-October when the pack ice extent is respectively at a minimum and a maximum. The northernmost position appears late in June and late in December. At this time there is maximum pressure at the axis, whereas lowest pressures occur when the axis is nearest to the Antarctic coast. The perennial zonally averaged pressure amounts to 984 hPa at the sea surface (Van Loon, 1972 b).

Due to the asymmetry of the Antarctic continent with respect to the South Pole, the most northerly axis of the Antarctic trough is situated (60° -63°S) at 90°- 30°E (southwest of Australia), and the southernmost axis (70°-73°S) at 110°-160°W (central South Pacific). The seasonal meridional oscillations of the axis are largest in the eastern Weddell and Ross Seas (Streten, 1980).

2.2.4 West and east wind zones

The circumpolar west wind zone extends between the subtropical high pressure belt and the Antarctic trough (about 30°S-65°S) with a maximum annually and zonally averaged zonal geostrophic velocity at the sea surface of $10ms^{-1}$ at 51°S. The meridional distribution for January and July are presented in Fig. 7. Computations of the corresponding wind stress maximum amount to 0.145 - 0.185 Nm^{-2} (Eyre, 1972; Hellerman, 1967).

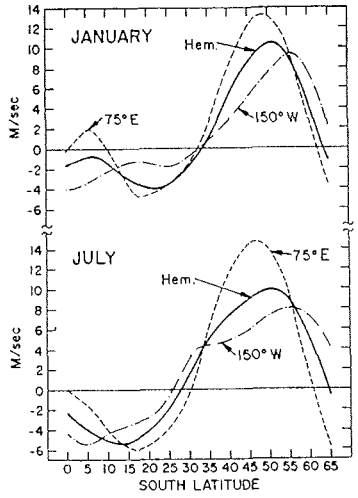

Figure 7: Meridional distributions of the zonally averaged zonal geostrophic wind velocity component at the sea surface and profiles along 75°E and 150°W (Van Loon, 1972 d).

Similar to the pressure variations of the Antarctic trough, the geostrophic west wind exhibits a half year oscillation with a maximum amplitude between 60°S and 65°S (Fig. 8). The strongest geostrophic west winds appear in February/March and September/October.

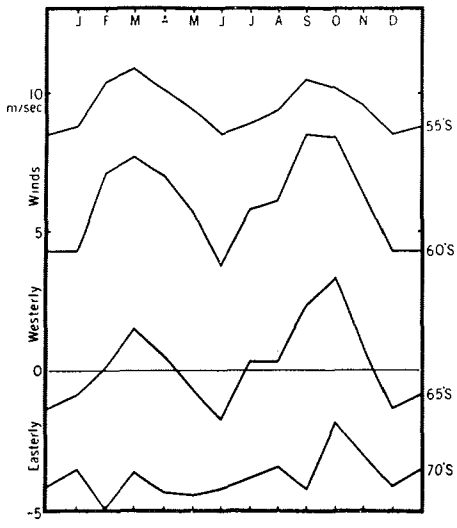

Figure 8: Annual variation of the monthly and zonally averaged zonal geostrophic wind velocity component at the sea surface (Schwerdtfeger, 1970).

On an annual average the maximum geostrophic west wind velocities occur over the South Atlantic and South Indian Ocean (55°W -115°E) between 47°S and 50°S, and over the South Pacific (160°E -90°W) between 55°S and 59°S (after Taylor et al., 1978). During the whole year the Indian sector shows the strongest geostrophic west wind and the Pacific sector the weakest one. Occasionally, besides the maximum at 76°-100°E and the minimum at 128°-175°W a secondary maximum appears at 80°-90°W and a secondary minimum at 50° - 60°W (Fig. 9). A detailed geographic distribution of the geostrophic wind field over the Southern Ocean is given in Jenne et al. (1971). Seasonal fluctuations of the maximum geostrophic west wind over the South Indian Ocean are only small. The largest seasonal fluctuations occur south of Australia and New Zealand (Streten, 1980).

A comparison of the circumpolar pressure field and the zonal average position of the pack ice edge by Streten and Pike (1980) reveals the following correlations of the atmospheric circulation and the pack ice extent: a) the weakest west wind appears when the ice edge is situated between 62°S and 65°S; b) there is a

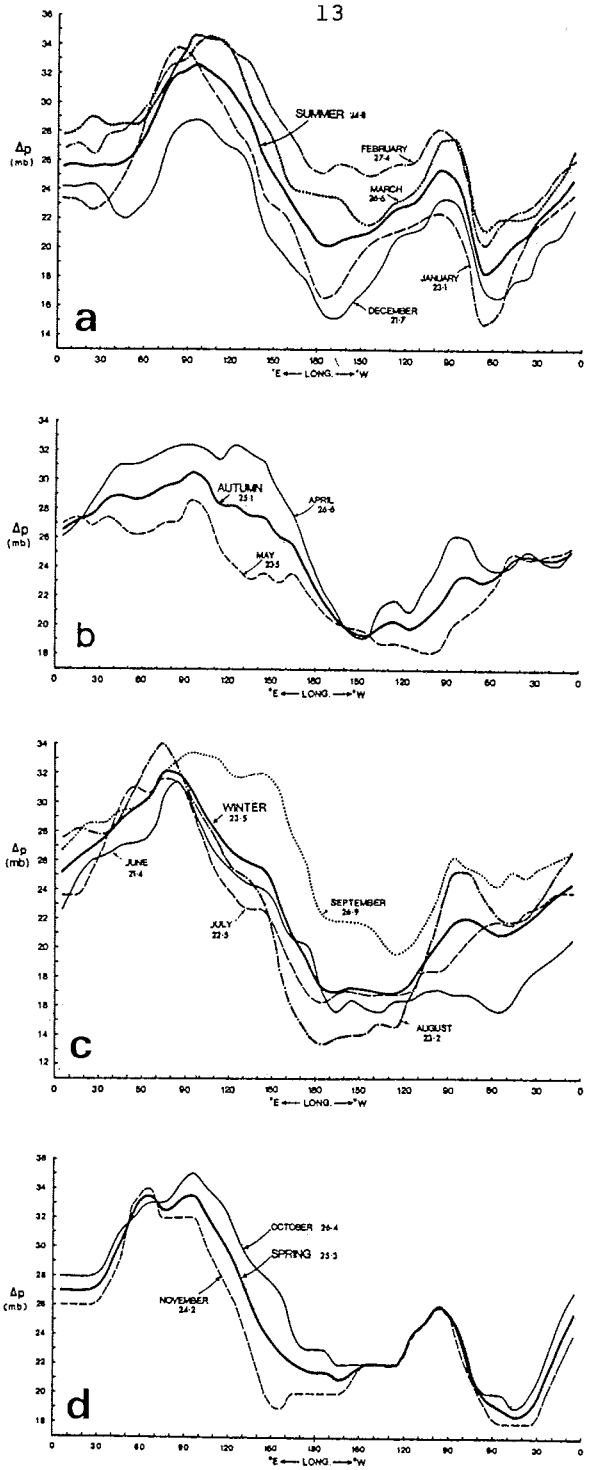

Figure 9: Zonal distribution of the meridional pressure difference at the sea surface $\Delta p = p(40°S) - p(60°S)$ for summer a), autumn b), winter c) and spring d). The numbers at the curves denote the zonal averages (Streten, 1980).

linear dependence and positive correlation between west wind strength and ice extent, when the ice edge is situated between 61°S and 62°S (northernmost range of the ice extent); c) south of 65°S the retreat of the pack ice cover is accompanied by increasing west wind; d) the variability of the west wind grows with increasing ice extent, as well as with the variability of the ice extent.

The meridional component of the geostrophic wind is weak in the west wind zone. Along 50°S it is directed southwards south of Africa, Australia, west of South America and northwards over the central oceans. Generally, the monthly averaged speed is less than 2ms^{-1} south of Australia only whilst at the west coast of South America it exceeds 3 ms^{-1} (Van Loon, 1972 d). At the Drake Passage the meridional component is directed southwards and amounts to about one fourth of the zonal component (Fig. 10).

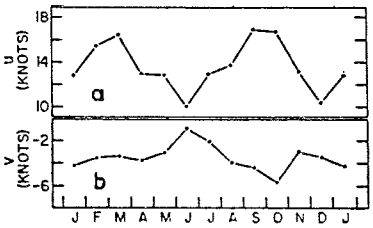

Figure 10: Annual variation of the geostrophic wind at the sea surface in the area 56°-60°S 66°-80°W:
a) west-east component
b) south-north component (Baker, 1979).

The transition between the west and east wind zones occurs in summer and winter at 60°-65°S, and in spring and autumn at 65°-70°S (Schwerdtfeger, 1970). South of it the maximum zonally averaged zonal geostrohpic component of the east wind amounts to about half of that of the west wind (Fig. 8). The corresponding wind stress is given by - 0.10 Nm^{-2} (Eyre, 1972). The east wind zone is influenced by katabatic winds which descend from the Antarctic Plateau to the coast and are deflected to the west by the Coriolis force.

2.2.5 Precipitation

A large amount of precipitation falls as snow on an ice covered ocean so that fresh water input does not take place before the sea ice melts. Additionally, there is an indefinite quantity of snow, transported by southern winds from the Antarctic continent into the sea. The annual averaged precipitation decreases from the Subtropical Convergence southwards: 1500 - 2000 mma^{-1} at 40°S, 500 - 1000 mma^{-1} at 55°-65°S, 200 - 500 mma^{-1} at 65°-70°S, < 200 mma^{-1} at 70°-90°S (Tchernia, 1980).

At the Subtropical Convergence and south of the Antarctic Convergence the largest amount of precipitation falls in autumn and winter, whilst between both convergences it is during spring and summer. In the latter region the seasonal variations are smaller (Streten, 1977).

2.3 Ice distribution

2.3.1 Sea ice

Since the routine use of satellites, the temporal and spatial variations of the Antarctic pack ice have been investigated more systematically. In contrast to the Arctic, the Antarctic pack ice extends equatorwards without being limitated by continents. Seasonal variations are therefore large for the latter. The Antarctic sea ice reaches its maximum extent of 16.9-20.5 million km^2 (range of the maximum extent from 1973 to 1982; Ropelewski, 1983) in August/September and its minimum extent of 2.7 to 5.6 million km^2 in January/February. For comparison, the ice of the Antarctic continent covers an area of 14.1 million km^2. The ratio of maximum to minimum total sea ice extent is largest in the sector between 10°W and 70°E (Southeast Atlantic and Southwest Indian Ocean), where the ice edge retreats to the Antarctic coast in summer (Ropelewski, 1983). Only a small part of the sea ice is perennial ice. This is predominantly found in the western Weddell Sea, the eastern Ross Sea, the central Amundsen Sea, and at the coast of Oates Land (Fig. 11).

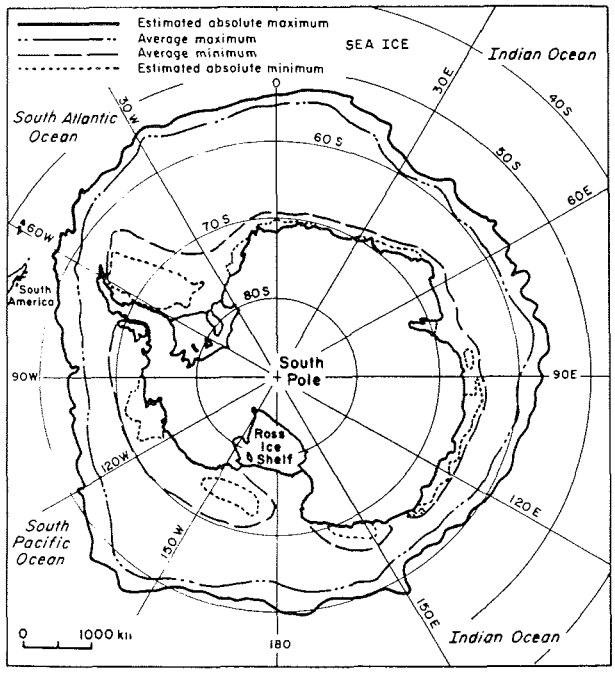

Figure 11: Sea ice extent 1971-1976 (Ackley, 1981 a).

The growth of sea ice takes about 7 months, somewhat more than its retreat (Fig. 12). The mean growth rate between March and

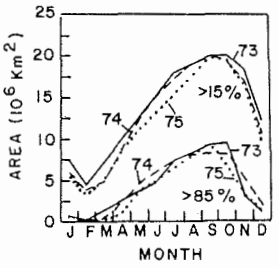

Figure 12: Annual variation of the Antarctic sea ice cover for the area with an ice concentration > 15%, resp. > 85% (Zwally et al., 1979).

August amounts to about $3 \cdot 10^6$ km^2 per month (after Ackley, 1981a) with a maximum of $3.4 \cdot 10^6$ km^2 per month in May and June (Ropelewski, 1983). From August to the end of October there are only small changes in the sea ice extent. The main retreat of the sea ice cover lasts from November through January with a maximum rate of $6.4 \cdot 10^6$ km^2 in December (Ropelewski, 1983). The annual cycle of the sea ice extent follows the cycle of the air temperature at the sea surface with a time lag of 1.5 - 3 months.

On a perennial and zonal average the pack ice edge is situated at 64°S. It reaches the monthly averaged northernmost position of 60.9°S in September/October, the corresponding southernmost position of 68.3°S in March (Streten and Pike, 1980).

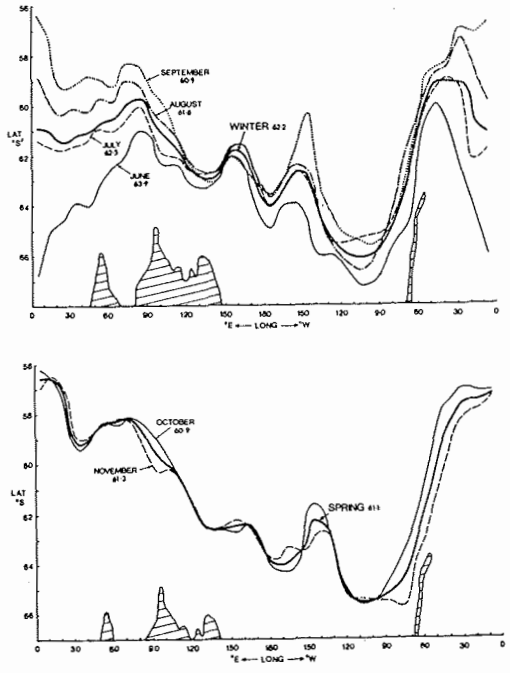

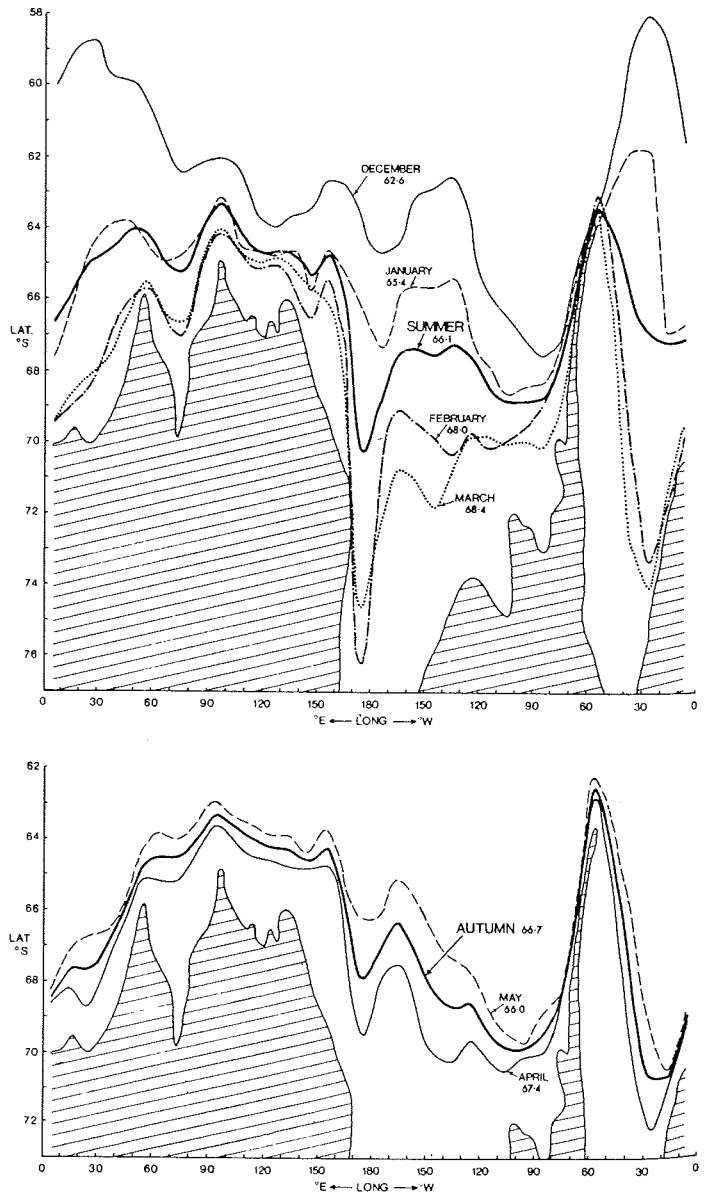

Figure 13: Monthly averaged position of the pack ice edge around Antarctica (hatched area) from observations between Dec. 1972 to Nov. 1977. Numbers at the curves denote the zonal averages (Streten and Pike, 1980).

The zonal variation of the pack ice edge reflects the coastal configuration of the Antarctic continent and is closely associated with local atmospheric and oceanic circulations (Fig. 13). Due to the polar wind system, which produces the Antarctic Divergence, ice also forms in the interior of the pack ice zone and is advected northwards into warmer waters where it melts (Gordon and Taylor, 1975 b). In summer the extent of the pack ice zone partially compensates for the asymmetry of the Antarctic continent with respect to the South Pole (Rayner and Howarth, 1979). The Weddell and Ross Seas exhibit the largest seasonal variations. Generally, the annual variation is larger in regions where the pack ice transport is intense.

The northernmost extent of pack ice (56°-57°S) occurs northeast of the Weddell Sea at 30°W - 20°E in September/October. The rather high latitude ice edge at the same time in the Bellingshausen Sea documents the strong influence of the Antarctic Peninsula on the oceanic and atmospheric circulations of the Weddell Sea region.

The southernmost pack ice edge position of 76°S appears in the western Ross Sea in February. In the same way as in the western Weddell Sea, southern winds cause an intense northward sea ice transport in the western Ross Sea. In contrast to the Weddell Sea, the western continental boundary of the Ross Sea does not extend into the west wind zone, so the northward transported pack ice accumulates north of Oates Land. The heat transport of the Antarctic Circumpolar Current,which is deflected southwards by the Macquarie Ridge, hampers the northward advection of the pack ice (Ackley, 1981 a). For several years the annual variation of the pack ice extent in the Ross Sea shows a primary maximum in July and a secondary maximum in October. This is also true for some other regions of the pack ice belt. Possibly the secondary maximum is due to a break-up of the ice cover and a subsequent northward transport of pack ice in late winter (Ropelewski, 1983).

The smallest seasonal variations of the Antarctic pack ice extent take place at 80°-150°E and in the Bellingshausen und Amundsen Seas, where the pack ice advection is weak.

From 1973 to 1983 variations from year to year of the maximum and minimum Antarctic sea ice cover range between 0.3 and 1.9 million km^2 (Ropelewski, 1983). On a monthly and zonal average the largest interannual variation appears in January, the smallest in April. Maximum interannual variations are found in the Weddell and Ross Seas (Streten and Pike, 1980). The zonal distribution of the range of the pack ice edge position between December 1973 and November 1977 is presented in Fig. 14. Primary maxima occur in the region of the central Weddell Sea and the western and eastern Ross Sea; secondary maxima occur in the region of Prydz Bay and the western Bellingshausen Sea. The east Antarctic sea ice at 90°-150°E shows the smallest fluctuations.

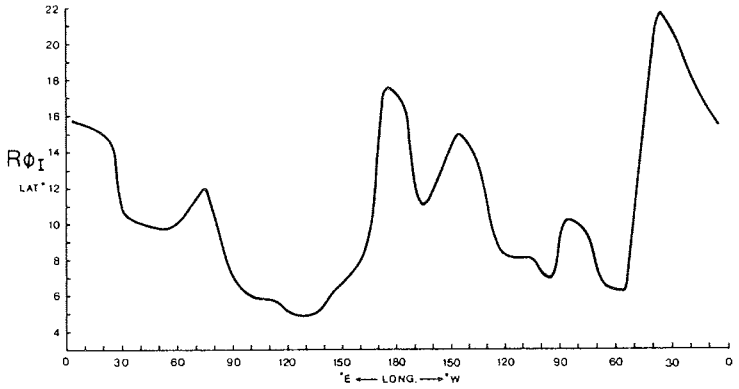

Figure 14: Zonal distribution of the range of the pack ice edge position ($R\Phi_I$) between Dec. 1973 and Nov. 1977 (Streten and Pike, 1980).

On the average Antarctic sea ice is more saline than its Arctic counter part. This may be due to faster growth rates and the generation mechanism leading to large amounts of frazil ice in the south (Gow et al., 1982).

Ice concentration in the Southern Ocean is on the average lower than in the Arctic since no compression takes place due to continental boundaries. A rapid decay of Antarctic sea ice starts in regions with high ice concentrations ($>$ 85%) in mid-October and in regions with low ice concentrations ($>$ 15%) at the end of November (Fig. 12). This phase shift of 1 to 1.5 months is caused by the formation and the existence of polynyas and leads due to the divergent wind field in areas with an ice concentration $>$ 85% (Gordon, 1981). Deep ocean convection, which transports deep water heat to the surface water and high absorption of solar radiation by the ocean in the ice-free areas lead to melting of the surrounding pack ice. Whereas in areas with an ice concentration $>$ 15% at mid-October the atmosphere-to-ocean heat flux serves mainly to increase the ice temperature.

Near the Antarctic coast there are several semi-permanent polynyas which are caused by katabatic winds which push the newly formed sea ice off the coast. Consequently a large sea ice production takes place within these regions caused through cooling of the surface water by cold continental air (Ledenev, 1964). Other coastal oceanic and/or atmospheric processes also occasionally generate polynyas in areas with low ice concentration (Fig. 15).

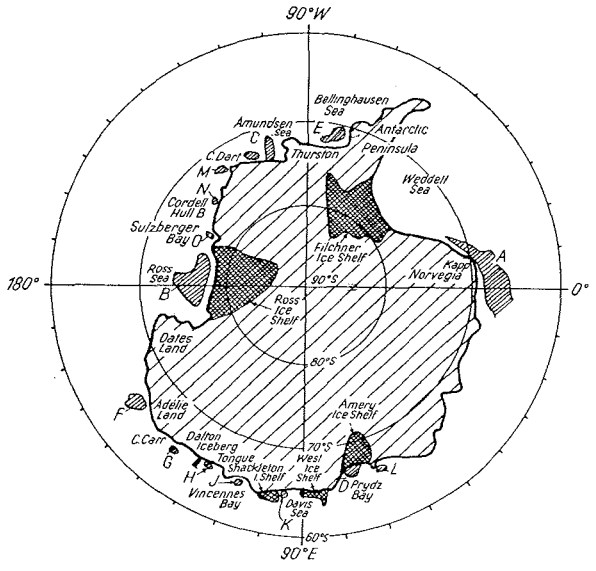

Figure 15: Locations of frequently appearing polynyas (slanting hatched) and ice shelves (cross hatched). The observations refer to satellite images, received in the summer months (October to March) between Dec. 1968 and Dec. 1970 (Streten, 1973).

The meridional extent and the concentration of the Antarctic sea ice result from the dynamic and thermodynamic balances of the ocean-atmosphere system. For September 1974 Parkinson and Cavalieri (1982) detect a lower ice concentration around Antarctica in comparison with September 1973 and 1975. This is correlated with an intensified variability of the circumpolar pressure field at the sea surface. In spring 1973, a premature retreat of the pack ice edge in the Bellingshausen Sea lead to enhanced cyclonic activities which contribute to the maintainance of diminished ice cover (Ackley and Keliher, 1976). Generally, intense cyclones force the sea ice to the north at their western flanks and to the south at their eastern flanks. Therefore, the sea ice area appears to be large at the west coast of the Ross Sea in winter 1977 (Streten and Pike, 1980). Equivalent relations exist for anticyclones, which occasionally connect the subtropical with the Antarctic Plateau high pressure regions (Cavalieri and Parkinson, 1981). Regions with frequent southerly winds show a larger variability of the sea ice cover (Streten and Pike, 1980).

Untersteiner (1966) estimates the mean thickness of the annual Antarctic sea ice at 1 to 1.5 m. Convergences of the ice velocity field can cause pressure ridges of more than 10 m thickness. In contrast divergences stretch the pack ice field so that thin ice sheets can form. On the average, thickness increases with ice concentration. Weller (1981) supposes that about 10% of the pack ice area with a concentration > 85% has a thickness of less than 40 cm. In areas with a concentration between 15% and 85% this portion amounts to 35%.

2.3.2 Ice shelves

About 45% of the Antarctic coastline is occupied by floating ice shelves. The ice shelf area amounts to about 1.54 million km^2 (11% of the Antarctic continental area; Jacobs et al., 1979 b). The largest ice shelves are the Ross Ice Shelf (0.53 million km^2) and the Filchner-Ronne Ice Shelf (0.47 million km^2). At the ice front the thickness ranges from 200 to 300 m with one quarter above sea level. This grows gradually to about 1000 m at the grounding line.

The ice shelves melt at the bottom at a mean rate of 0.3 ma^{-1} (Jacobs et al., 1979 b). The melting rate depends locally on the circulation of the shelf water under the ice shelves. Generally, melting occurs when shelf water is forced downwards and is freezing when water ascends along the rising ice shelf bottom. The freezing rate is restricted by the poor heat conduction across the ice shelves so that ice growth is limited to a few centimeters per year (Jacobs et al., 1979a).

The Ross and the Filchner-Ronne Ice Shelves migrate with up to 1100 ma^{-1} and up to 1500 ma^{-1}, respectively (MacAyeal, 1984; Robin et al., 1983), into the ocean. The continuous supply of glacial ice from the interior of Antarctica is balanced by iceberg calving of about 1600 km^3a^{-1} at the ice front (Jacobs et al., 1979 b). The predominant tabular icebergs have draughts of up to 350 m. On the average their life-span amounts to 4 years (Radok et al., 1975).

2.4 Hydrography

2.4.1 Water masses

The water mass of the Southern Ocean with a total volume of $137.6 \times 10^6 km^3$ can be subdivided into the following basic components:

- the Antarctic Surface Water (AASW)
- the Circumpolar Deep Water (CDW)
- the Antarctic Bottom Water (AABW).

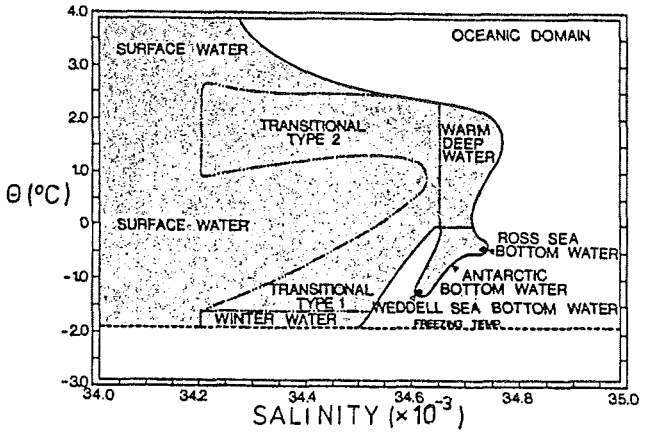

Figure 16: Θ/S-diagram of water masses of the Southern Ocean deep sea area (Carmack, 1977).

The different water masses are characterized by the potential temperature/salinity diagram of Figure 16 and the values of Tables 3 and 4. Apart from these main water masses, various secondary categories will be discussed later.

2.4.1.1 Antarctic Surface Water (AASW)

In winter, the AASW is a nearly homogeneous water mass which extends down to about 250 meters depth. Its salinity varies from 34.0 x 10^{-3} to 34.5 x 10^{-3}. The temperature increases from a value near freezing at the Antarctic Divergence (AAD) to 2°C at the Polar Front (PF) (Tchernia, 1980).

In summer, the mixed layer of the AASW has a 30 to 80 m thickness which warms up to -1.8°C at the ice edge and to 6°C at the PF while the salinity drops to 33.6 x 10^{-3} and 34.2 x 10^{-3}, respectively (Gordon and Molinelli, 1982). Winter Water (WW) occupies the levels below the mixed layer.

The low temperature WW is a remnant of wintertime convection with temperatures near freezing and salinities approaching the critical value of cabbeling instability (Foster, 1972 a). It is believed that WW takes part in the formation of Antarctic Intermediate Water at the Polar Front.

Water mass	potential temperature interval θ (°C)	salinity interval S ($x10^{-3}$)	oxygen interval O_2 ($x10^{-3}$)
Winter Water (WW)	$-2 \leqslant \theta \leqslant -1.5$ (I)	$34.2 \leqslant S \leqslant 34.5$ (I)	
Circumpolar Deep Water (CDW)	$0 < \theta \leqslant 2.5$ (I)	$34.65 \leqslant S \leqslant 34.8$ (I)	
Antarctic Bottom Water (AABW)	$-1.5 < \theta \leqslant 0$ (I)	$34.6 \leqslant S \leqslant 34.75$ (I)	$5.0 \leqslant O_2 \leqslant 6.2$ (IV)
Ross Sea Bottom Water (RSBW)	$-0.5 \leqslant \theta \leqslant -0.2$ (II)	$34.72 \leqslant S \leqslant 34.75$ (II)	$5.3 \leqslant O_2 \leqslant 5.6$ (II)
Adélie Coast Bottom Water (ACBW)	$-0.7 \leqslant \theta \leqslant -0.6$ (II)	$34.65 \leqslant S \leqslant 34.66$ (II)	$O_2 = 5.9$ (II)
Low Salinity Shelf Water (LSSW)	$-2 \leqslant \theta \leqslant -1.6$ (I)	$34.0 \leqslant S \leqslant 34.6$ (I)	
High Salinity Shelf Water (HSSW)	$-2 \leqslant \theta \leqslant -1.8$ (I)	$34.6 \leqslant S \leqslant 35.0$ (I)	
Ice Shelf Water (ISW)	$-2.4 \leqslant \theta < -2$ (I)	$34.4 \leqslant S \leqslant 34.9$ (I)	
Antarctic Intermediate Water (AAIW)	$3.3 \leqslant \theta \leqslant 6.2$ (II)	$34.15 \leqslant S \leqslant 35.56$ (III)	$4.0 \leqslant O_2 \leqslant 6.0$ (III)

Table 3: Potential temperature θ (°C), salinity S ($x10^{-3}$) and oxygen O_2($x10^{-3}$) intervals for the water masses of the Southern Ocean given by:

I: Carmack (1977); II: Gordon (1974); III: Jacobs and Georgi (1977); IV: Gordon and Molinelli (1982).

Oceanic domain

water mass	volume (km^3)	percent of TV0
AASW	7.4×10^6	5.4
WW	0.607×10^6	0.4
CDW	81×10^6	58.8
AABW	38×10^6	27.5
Atlantic	18.8×10^6	13.5
Indic	15.8×10^6	11.5
Pacific	3.4×10^6	2.5
RSBW	2.5×10^6	1.7
ACBW	0.015×10^6	0.01
MCDW	2.6×10^6	1.9
Transition zone 2	8.6×10^6	6.4
total volume (TV0)	137.6×10^6	100

Shelf domain

		TVS
AASW	0.49×10^6	37.9
LSSW	0.48×10^6	37.1
HSSW	0.29×10^6	22.6
ISW	0.03×10^6	2.4
total volume (TVS)	1.29×10^6	100

Table 4: Volume and percent of the total volume for the water masses listed in table 3.
TVO: total volume of the oceanic domain
TVS: total volume of the shelf domain

2.4.1.2 Circumpolar Deep Water (CDW)

The CDW is generally characterized by a temperature maximum and an oxygen minimum beween 500 to 1200 m depth and a salinity maximum between 750 to 1500 m depth (Gordon and Molinelli, 1982; Table 210); no O_2-minimum exists however in the Indian Ocean sector (Callahan, 1972). According to the extreme values of state, CDW can be subdivided into an upper and a lower regime (Gordon, 1971 b). Figure 17 shows that a further subdivision is possible into Warm Deep Water (WDW), which is restricted to the Weddell Sea, and warmer Southeast Pacific Deep Water (SPDW) with a slightly higher salinity.

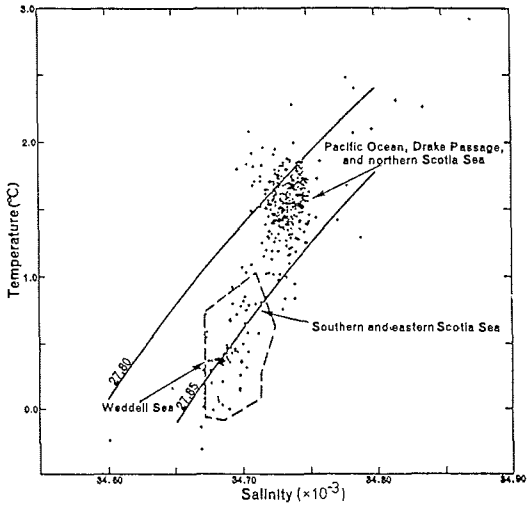

Figure 17: Potential temperature/salinity correlation curve of the S_{max}-layer between 20° to 170°W (Gordon, 1967).

CDW, with a mean thickness of about 2000 meters, occupies about 58% of the total volume of the Southern Ocean. It encompasses the density range of the North Atlantic Deep Water (NADW) (Reid et al., 1977) due to an influx of the latter at 1000 m depth at about 45°S in the western South Atlantic (Georgi, 1981; Gordon and Goldberg, 1970). Consequently, two oxygen minima exist one above and the other below the NADW.

At the Antarctic Divergence, the CDW ascends to a level of 150 to 100 meters where it causes a relatively shallow temperature and salinity maximum (Tchernia, 1980).

2.4.1.3 Antarctic Bottom Water (AABW)

AABW is characterized by a temperature minimum and an oxygen maximum near the bottom. This water mass occupies a layer with a mean thickness of 1100 meters.

It is assumed that the Weddell Sea is the main source of the low-salinity and the Ross Sea of the high-salinity AABW (Gordon, 1974). About 71.6% of the total AABW is produced in the Weddell Sea, while only 6.6% has its origin in the Ross Sea (Carmack, 1977). The rest is formed at various locations off the Adélie Coast (Gordon and Tchernia, 1972), off the Enderby Land-/Prydz Bay Coast (Jacobs and Georgi, 1977), in the Davis Sea (Carmack, 1977) and off the Amery Ice Shelf (Gordon, 1974).

Ross Sea Bottom Water (RSBW)

RSBW has the highest temperature and highest salinity of the Antarctic Bottom Water (see Fig. 16). It is characterized by a second salinity maximum below the main one.

At the shelf break, a mixing of Modified Circumpolar Deep Water with High Salinity Shelf Water and Ice Shelf Water takes place. This mixture, which has a higher density than CDW descends along the continental slope and mixes once more with CDW. This new water body is called Ross Sea Bottom Water (Jacobs et al., 1970). It spreads in a layer of about 600 m thickness along the continental rise to the west. Near Balleny Island the bottom current splits into two branches. The first one advances to the north through the Balleny Fracture Zone (ca. 160°W), the other one continues in a westerly direction into the South Indian Basin and finally mixes with the Adélie Coast Bottom Water (Rodman and Gordon, 1982). The latter is rather similar to the bottom water of the Weddell Sea with respect to its Θ/S values. It occupies a thin layer over the continental slope off the Adélie Coast.

Bottom water with a potential temperature of -0.75°C and a relatively high O_2-value of 6.1×10^{-3} was found over the continental rise at 60°E. Its characteristics differ from those of the bottom waters of the eastern Weddell Sea and of the South Indian Basin. Jacobs and Georgi (1977) conclude that this water mass is formed along the Enderby Land-/Prydz Bay Coast.

2.4.1.4 Modified Circumpolar Deep Water (MCDW)

MCDW represents the water mass of the transition zone between Winter Water and Circumpolar Deep Water (see Fig. 16). It has a rather weak static stability. In meridional sections across the shelfbreak MCDW appears as a warm tongue between the surface water and the shelf water and compensates for the discharge of shelf water masses.Through mixing with High Salinity Shelf Water,

it contributes to the bottom water formation. In the Weddell Sea MCDW is called Modified Warm Deep Water (MWDW) for historical reasons. West of 40°W MWDW exists only at the shelf break (Foster and Carmack, 1976 a), but in the Ross Sea the influence of MCDW could still be proved at the shelf ice edge at 100 meters depth (Jacobs et al., 1970).

2.4.1.5 Antarctic Intermediate Water (AAIW)

AAIW is characterized by a salinity minimum and an oxygen maximum near the sea surface north of the Polar Front. These features are apparent at depths of more than 1000 meters at mid-latitudes (Piola and Georgi, 1982).

In the Atlantic the AAIW flows northwards with the Falkland Current predominantly along isopycnal surfaces (Kuksa and Poyarkow, 1977) to about 40°S. Further downstream it turns eastwards into the anticyclonic subtropical gyre and reaches finally the coast of South America north of 30°S. The salinity minimum can still be detected as far as 25°N - 20°N (Reid et al., 1977 and Wüst, 1935).

In the Indian Ocean the AAIW terminates at about 5°S and in the Pacific Ocean at 10°S (Wyrtki, 1971). The reason for the differences of the meridional distribution lies presumably in the special bottom topography of the three oceans. The regional production rate may also contribute to this distribution (Jacobs and Georgi, 1977).

The water mass of the transition zone 2 (see Fig. 16), with a maximum potential temperature of $\Theta = 2.5°C$ and a minimum salinity of $S = 34.2 \times 10^{-3}$, is restricted to the Indian ($3.6 \times 10^6 km^3$) and Pacific ($3.3 \times 10^6 km^3$) sectors (Carmack, 1977). Such characteristics could result from a mixture of CDW and AAIW.

2.4.1.6 Shelf Water

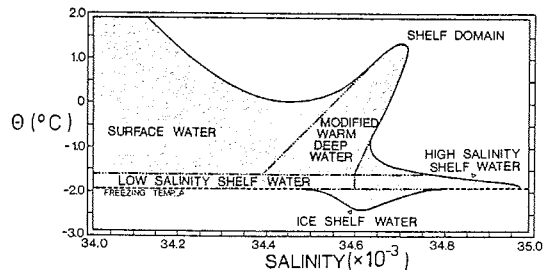

Figure 18: Θ/S diagram of water masses of the Southern Ocean shelf domain (Carmack, 1977).

The shelf water masses originate from winter time convection. They can thus be compared with the WW of the deep ocean. In respect to bottom water production, a distinction must be made between Low Salinity Shelf Water (LSSW) and High Salinity Shelf Water (HSSW). Only shelf water with a salinity > 34.6 x 10^{-3} contributes to bottom water production (Mosby, 1934).

Shelf water is seperated from water masses of the deep ocean by a frontal zone along the continental slope. Gordon (1974) shows that topography, especially the shelf widths and the existence of depressions, cause differences in shelf water salinities. Shelf water with salinities > 34.75 x 10^{-3} (HSSW) covers most of the shelf of the Ross Sea, which is 600 km wide and extends also below the ice shelf (MacAyeal, 1984). The salinity of the water masses of the Weddell Sea shelf, which is about 500 km wide, assumes values of up to 34.8 x 10^{-3} whilst over the shelf off Adélie Land, salinities > 34.6 x 10^{-3} are also to be found.

The interaction of HSSW with the Filchner and Ross Ice Shelves in the frame work of basal melting in about 200 meters water depth leads to the formation of Ice Shelf Water (ISW) (Jacobs et al., 1970; Carmack and Foster, 1975 a). The potential temperature here drops below the sea surface freezing temperature. In the course of local circulation, ISW can be detected off the ice front at intermediate depths (MacAyeal, 1984; Rohardt and Augstein, 1985).

2.4.1.7 The Polar Frontal Zone (PFZ)

2.4.1.7.1. General Features

At the Antarctic Convergence, cold, less saline Antarctic Surface Water (AASW) meets warmer, more saline Subantarctic Surface Water (SASW). The transition zone (Polar Frontal Zone) is bounded by two fronts: the Polar Front (PF) to the south and the Subantarctic Front (SF) to the north. Large horizontal density gradients associated with these fronts can also be detected in the deep waters. They are related to current cores of the Antarctic Circumpolar Current (Nowlin et al., 1977; Sciremammano et al., 1980). Most of the horizontal temperature and salinity changes across the fronts can be explained by a vertical offset of the isopycnals. This is particularly true for deep waters where the horizontal water mass zonation is due to isopycnal tilting (Nowlin and Clifford, 1982). Large meridional shifts of the Polar and Subantarctic Fronts cause considerable temporal and spatial variability of the PFZ width. South of Australia the width is about 500 km whilst in the Drake Passage it is reduced to 250 km (Sciremammano et al., 1980).

The Polar Front is mainly characterized by a horizontal temperature variation in the range of 1°C to 3°C across the front in the upper 500 m of the ocean. Due to heating in spring and summer,

the maximum sea surface temperature gradient decreases and shifts to the south by 1 to 2 degrees of latitude. Satellite observations at the Drake Passage between August and November reveal sea surface temperature gradients at the PF of 0.05-0.25°C km^{-1} (Legeckis, 1977). The position of the PF is defined by

- the northernmost position of the 2°C isotherm in the AASW (Botnikow, 1963),
- the salinity minimum at the 200 m depth level (see Fig.19) which is caused by increasing thickness of the AASW to the north (Ostapoff, 1962),
- the northern termination of the temperature minimum layer of the AASW (Gordon, 1967).

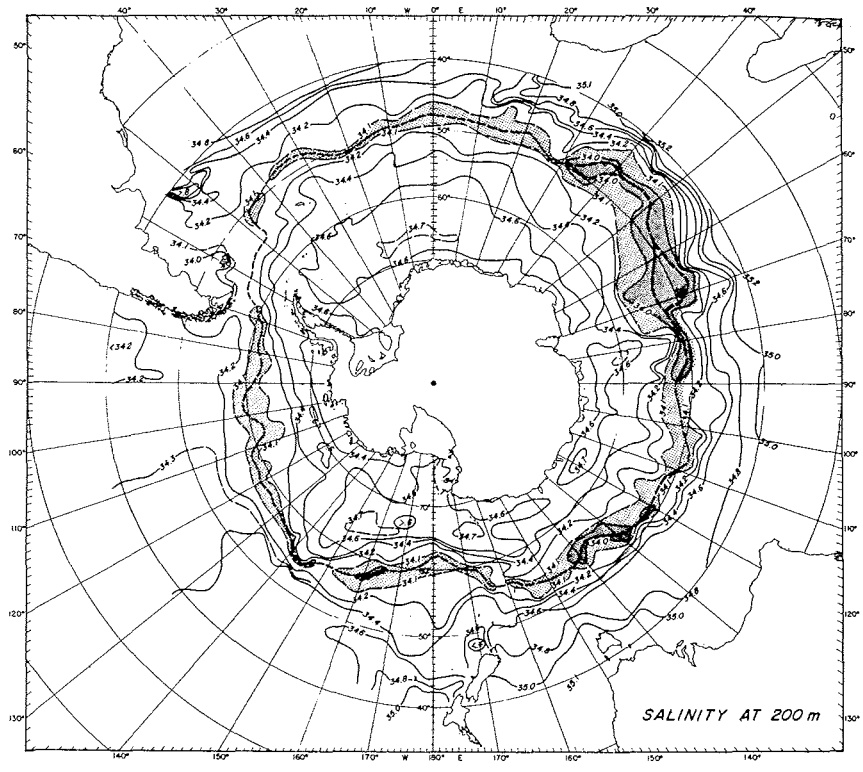

Figure 19: Salinity distribution at the 200 m depth level south of 40°S. The dotted line indicates the salinity minimum (Gordon et al., 1978).

The circumpolar average of the PF is situated at 52°-53°S (Treshnikov et al., 1980). Deviations from the mean position are due to the asymmetry of the Antarctic continent and the associated atmospheric fields. Striking meridional shifts of 5 to 10 degrees of latitude occur between 150° and 170°E due to the Macquarie Ridge, and between 45° and 70°W due to the continental boundaries of the Drake Passage and the bottom topography of the Scotia Sea. In the Drake Passage, the PF is at least 30 km wide (Nowlin and Clifford, 1982).

The position of the PF varies seasonally by 1 to 2 degrees of latitude. Meanders of the PF have characteristic wave lengths of 100 -250 km and phase velocities of 10-15 cms^{-1}. They cause meridional shifts of the PF of up to 2 degrees of latitude in the course of a few weeks (Legeckis, 1977; Sievers and Emery, 1978; Sciremammano et al., 1980). These waves can develop into deep reaching cold core rings, with diameters of 60 - 100 km, which drift in the Antarctic Circumpolar Current or migrate northwards across the PFZ (Sievers and Emery, 1978; Savchenko et al., 1978; Joyce et al., 1981; Peterson et al., 1982). Figure 20a shows a large surface temperature gradient at the PF and a weak Subantarctic Front. Ten days later there is a cold core ring of AASW in the PFZ, generated at the PF (Fig. 20b). The PFZ has widened due to the northward shift of the Subantarctic Front, which is intensified by the cyclonic circulation of the ring. After a further 14 days period, the eddy has been advected away or is dissipated and the Subantarctic Front shows a double-front structure (56.5°S and 58°S; Fig. 20c). Computations by De Szoeke and Levine (1981) suggest that ring formation seems to provide an important contribution to the total meridional heat transport. Interannual meridional variations of the PF amount to about 4 degrees of latitude (Botnikov, 1964).

Maximum temperature changes across the Subantarctic Front (SF) occur in the range of 3°C to 9°C in the upper 500 meters. The intensity of the SF varies distinctly with longitude. If neither continental boundaries nor zonal submarine ridges affect the Antarctic Circumpolar Current, the SF is weak as in the Southeast Pacific Basin (Emery, 1977). In the Indian Ocean and the Southwest Pacific, between 20°E and 160°W, the SF is strong due to the influence of the Agulhas Current and the Southeast Indian Ridge. In the Drake Passage, the meridional width of the SF amounts to at least 37 km (Nowlin and Clifford, 1982).

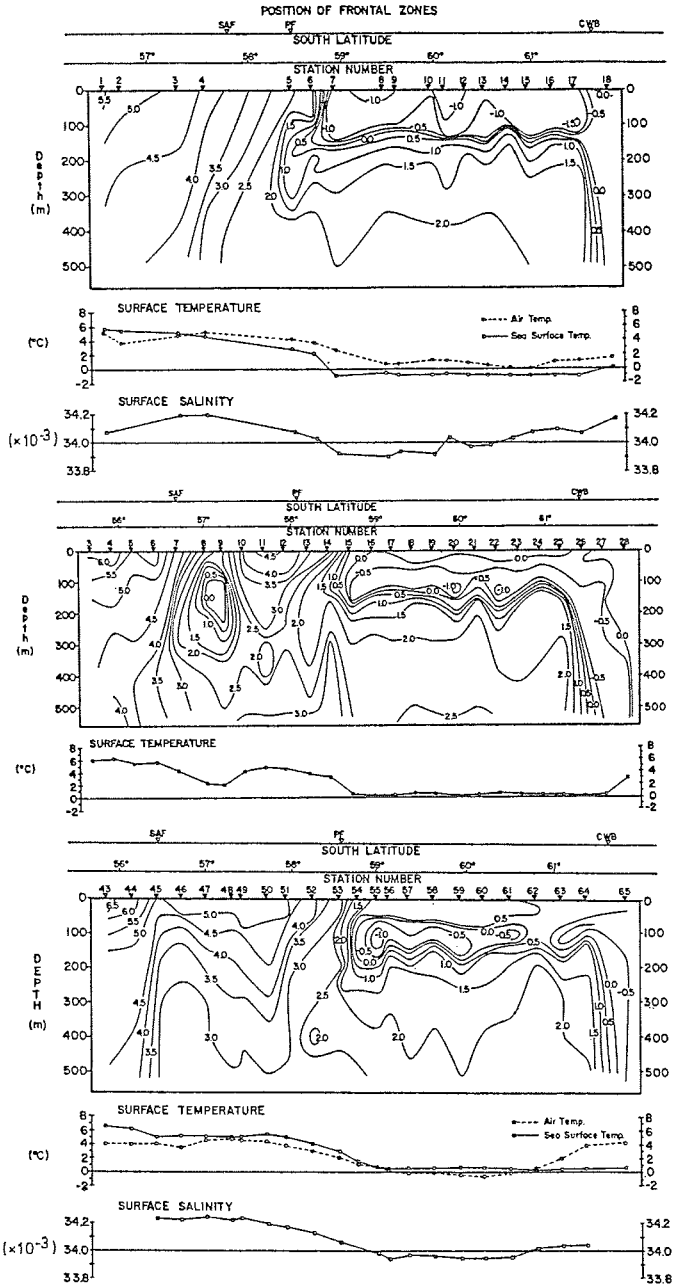

Figure 20: North-south temperature sections from XBT-observations and surface temperature and salinity distributions along these sections across the Drake Passage. PF, SAF, CWB denote the positions of the Polar Front, the Subantarctic Front and the Continental Water Boundary. a) 17 - 18 November, b) 27 - 29 November, c) 13 -14 December 1976 (Sievers and Emery, 1978).

2.4.1.7.2 Thermohaline characteristics

The Subantarctic Surface Water (SASW) is characterized by a nearly isohaline layer starting between 100 m and 400 m depth at the SF. Northwards this regime becomes thicker, warmer, and more saline.

To the south of the PF isotherms and isohalines generally have a smaller vertical slope than to the north. In the region of the PFZ, a stepwise rise of isotherms and isohalines related to the SF and PF can be observed. In the upper 500 m of the PFZ, in the Pacific sector, the temperature ranges from 2°C to 7°C and salinity from 33.85 x 10^{-3} to 34.35 x 10^{-3}. The temperature minimum layer of the WW does not always exist.

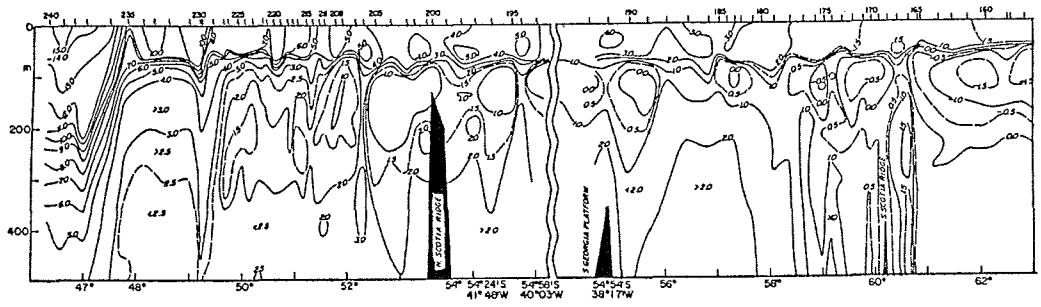

Figure 21: Thermal structure of the upper 500 m along 40°W. The section was recorded in January and February 1977 by XBT-probes (Taylor et al., 1978).

On the meridional temperature section along 40°W (Fig. 21) the PFZ lies between 47.5°S and 49.5°S. South of 48°S, a distinct thermocline has formed in about 80m depth due to solar heating. The temperature minimum layer below the thermocline is governed by a cellular structure.

Along 132°E, the PFZ is broadened from 48°S to 58°S in the summer (Fig. 22). During winter the frontal region has practically no vertical temperature gradient in the upper 500 m of the water column.

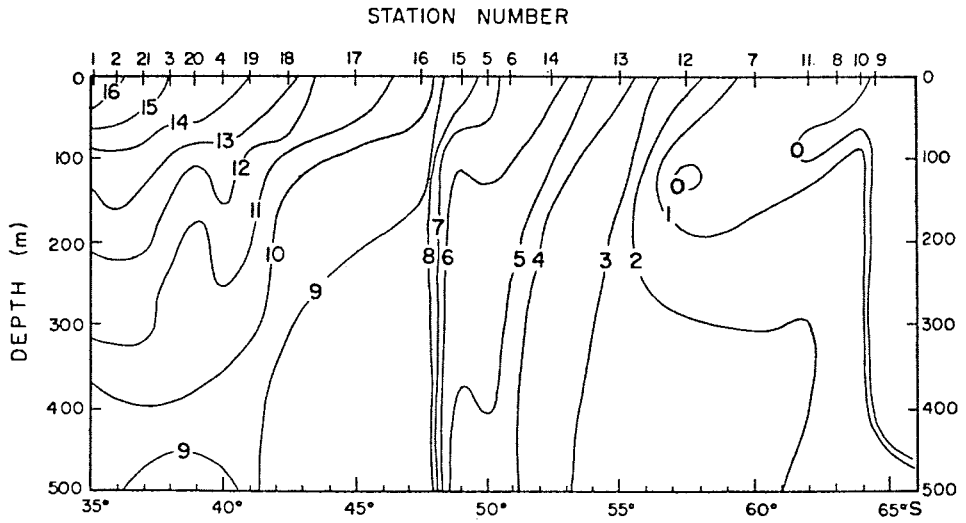

Figure 22: Thermal structure of the upper 500 m along 132°E. The section was recorded in December 1969 and January 1970 by STD-probes (Emery, 1977).

East of the USARP Fracture Zone (140°W) and east of the Macquarie Ridge (165°E), cold cells with temperatures <2°C frequently occur in the PFZ. These features may originate from rings formed at the Polar Front, local divergences generated by cyclonic activities in the atmosphere, and breaking internal waves which migrate northwards along the Antarctic pycnocline (Gordon, 1971 a). In the Pacific sector the largest horizontal temperature gradients can be observed at the southern boundary of the PFZ, whereas the largest horizontal salinity gradients occur at the northern boundary (Moroz, 1979).

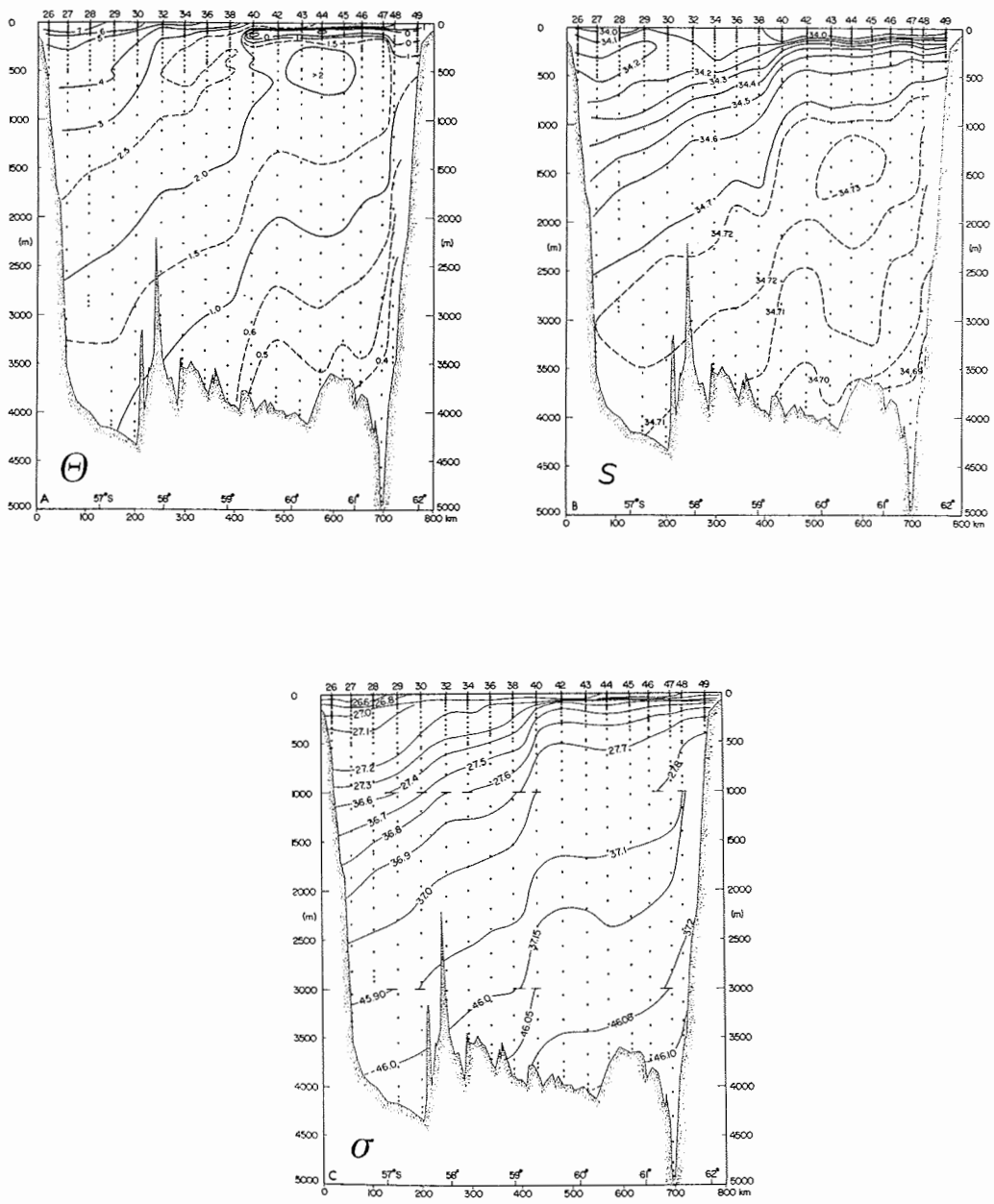

Figure 23: North-south profiles of potential temperature, salinity and potential density relative to 0, 20 and 40 MPa across the Drake Passage. The PF is situated between stations 38 and 40, the SF near station 30 (Joyce et al., 1978).

Profiles of temperature and salinity across the Drake Passage (Fig. 23) indicate a rise of the highly saline CDW from 3000 m in the north to 800 m in the south. The SF and PF extend down to the ocean floor. In the upper 500 m, large-scale respective thermal and haline gradients along density surfaces amount to about 2.5 x 10^{-2}°Cm^{-1} and 3.1 x 10^{-9} m^{-1} across the PF (Joyce et al., 1978). XBT surveys from 1975 to 1979 across the Drake Passage display variations of the PFZ width from 80 to 340 km. Lateral deviations from the mean position of PFZ range between 70 km to the north and 120 km to the south (Whitworth, 1980). A mean meridional slope and the meander structure of the PFZ in the western Scotia Sea during summer is indicated on Fig. 24.

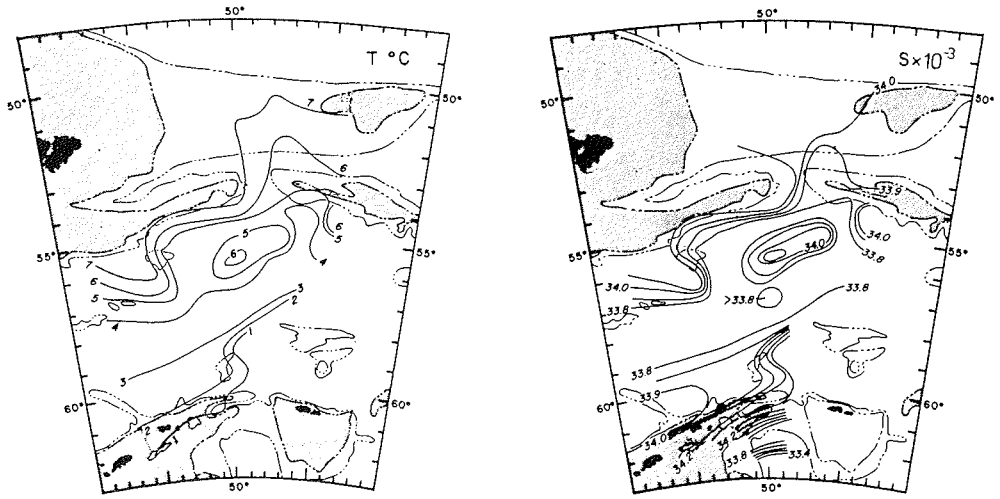

Figure 24: Surface distribution of temperature and salinity in the western Scotia Sea in summer 1975 (Gordon et al., 1977 b).

From 70°W to 45°W, the PFZ is shifted to the north by about 10 degrees of latitude.This northward migration from west to east takes place in three steps forced by lateral boundaries and bottom topography. The 4°C isotherm and the 33.8 x 10^{-3} isohaline mark the position of the PF at the sea surface whilst the 6°C isotherm and 34.0 x 10^{-3} isohaline indicate the SF. Vertical profiles of temperature and salinity (Fig. 25) in the western Scotia Sea reveal the distinct meridional differences in the vertical temperature and salinity distribution across the Polar Front. The different thermohaline states of the three areas are also shown on Fig. 25.

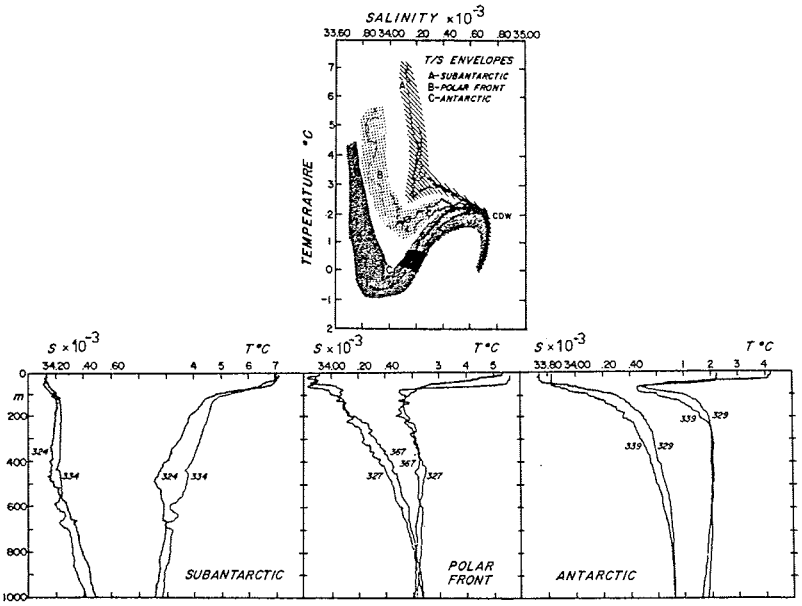

Figure 25: Characteristic T/S-curves and vertical distribution of temperature and salinity for the Subantarctic, Polar Frontal and Antarctic Zones in the western Scotia Sea (Gordon et al., 1977 b).

2.4.1.8 Weddell-Scotia Confluence (WSC)

The WSC, about 150 km in width, separates the Scotia Sea and Weddell Sea waters. It follows the South Scotia Ridge from the tip of the Antarctic Peninsula to the South Sandwich Islands.

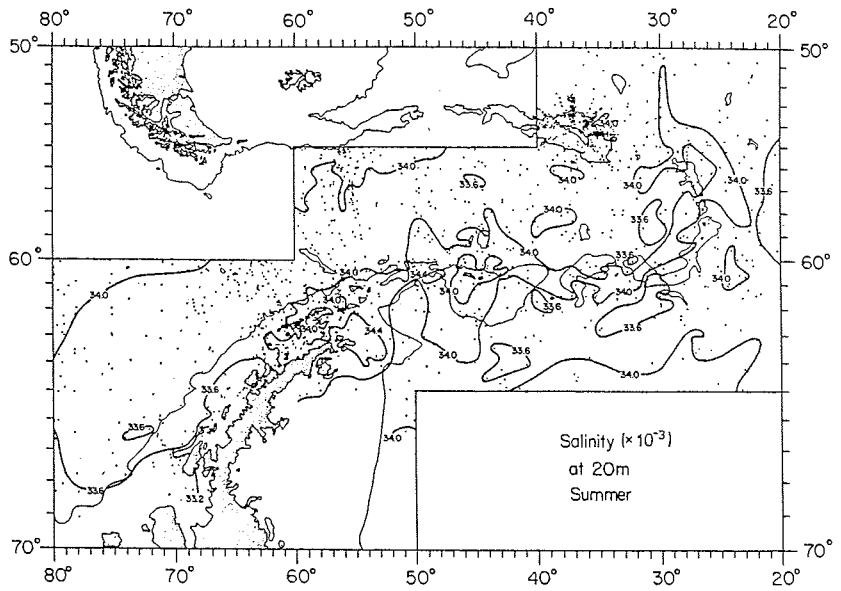

Figure 26: Horizontal distribution of salinity at 20 m depth in summer (Patterson and Sievers, 1980).

At the surface, the WSC is characterized by high salinity values ($S > 34.0 \times 10^{-3}$, Fig. 26) in summer (Gordon et al., 1977 b). East of 33°W, the surface of the WSC detaches from the deep signature in turning to the north of the South Scotia Ridge (Patterson and Sievers, 1980).

During winter, the western part of the WSC (west of the South Orkney Islands (45.5°W)) is vertically well-mixed. Its water mass is clearly separated from the waters of the Weddell and Scotia Seas as shown in Fig. 27. WSC deep waters are colder, less saline and more oxygenated than those of the Weddell and Scotia Seas. With increasing distance from the Antarctic Peninsula the influence of the Weddell and Scotia Seas on the WSC increases again.

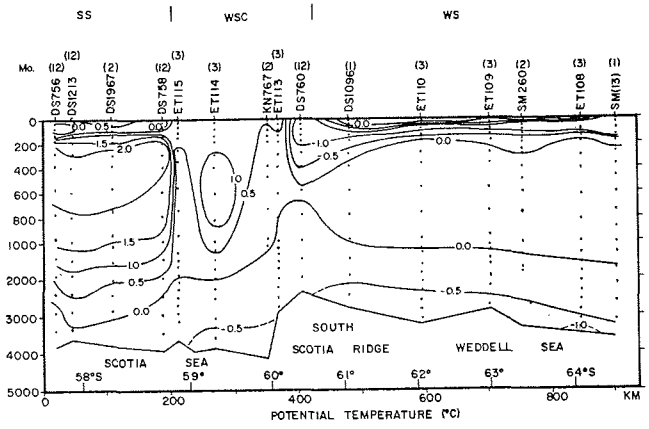

Figure 27: Vertical distribution of potential temperature along 49°W.
SS: Scotia Sea
WSC: Weddell-Scotia Confluence
WS: Weddell Sea
(Patterson and Sievers, 1980).

The origin of the western WSC seems to be due to the mixing of waters from the Bransfield Strait and waters which are transported to the north along the east and west coast of the Antarctic Peninsula (Patterson and Sievers, 1980; Gordon and Nowlin, 1978). A possible contribution to deep convection southwest of Elephant Island is the sinking of shelf water down the continental slope

from the east coast of the Antarctic Peninsula during winter (Gordon and Nowlin, 1978). Further eastwards, the WSC becomes less significant due to lateral mixing. East of Elephant Island the WSC forms a quasi-stationary meander forced by bottom topography and the northward advection of Weddell Sea waters (Stein, 1981; SCAR, 1983).

2.4.2 Oceanic circulation

2.4.2.1 Antarctic Circumpolar Current (ACC)

Meridional density distribution and westerly winds cause circumpolar eastward motions of the water north of the Antarctic Divergence. Wind stress, bottom topography and lateral friction produce deflections from a purely zonal, geostrohpically balanced current. The meridional extension of the ACC ranges from 1000 to 2000 km. The main flow axis lies between 45°S and 60°S (De Szoeke and Levine, 1981). Current measurements in the Drake Passage reveal three cores of the ACC associated with deep reaching thermohaline fronts (PF, SF, Continental Water Boundary). Their geostrophic mass transports account for about three quarters of the total baroclinic transport relative to 2500 m depth (Nowlin et al., 1977; Pillsbury et al., 1979; Nowlin and Clifford, 1982). Maximum velocities occur in the Atlantic and Pacific sectors at the PF and in the Indian sector at the SF. On the average, surface velocities of the current cores amount to 25 -30 cms^{-1}. Surface speeds are greater at the SF and PF than at the Continental Water Boundary (Gordon et al., 1978; Gordon, 1980; Nowlin and Clifford, 1982).

The transports of the ACC south of South America, Africa and Australia are, by and large, identical. They amount to about 130 x 10^6 m^3s^{-1}, with a barotropic contribution of 20 - 40 %, which increases to the south due to the growing homogeneity of the water column (Gordon, 1980; Fandry and Pillsbury, 1979). In winter, the transport is slightly higher than in summer (Neal and Nowlin, 1979). The ACC generally follows the contours of constant potential vorticity. Thus, eastward flow is deflected to the north where the ocean bottom rises and to the south where the bottom deepens. According to kinetic energy considerations the ACC is intensified along the northern flanks and weakened along the southern flanks of zonal ridges (Thompson, 1971). The baroclinicity of the ACC is closely related to bottom topography (Fig. 28). At some locations bottom topography and the northward spreading of AABW cause rather steady counter currents.

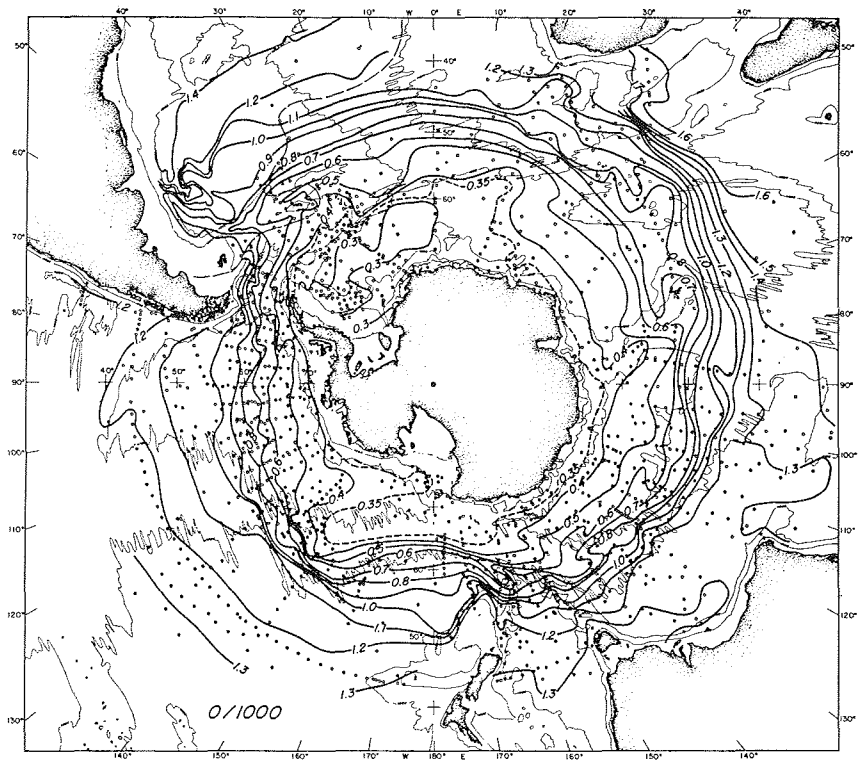

Figure 28: Geopotential anomaly of the sea surface relative to 10 MPa in dyn m. (Gordon et al., 1978).

2.4.2.1.1 General Features of the ACC

Trajectories of drifters in the ACC reveal undulatory displacements with characteristic wave lengths of 200 - 400 km and periods of 5 - 20 days (Kort, 1981). Pressure gauge measurements at 500 m depth at the Drake Passage between 1976 and 1978 display pressure fluctuations up to 2.5 x 10^3 Pa, with periods ranging from some weeks to more than one year. Pressure fluctuations of periods > 28 days are strongly correlated with the circumpolar averaged geostrophic wind field with a response time of 5.5 to 9.5 days, indicating the existence of long barotropic gravity waves with phase speeds of up to 3000 kmd^{-1}. Fluctuations with periods < 20 days are mainly caused by the local wind field with a response time of 1 - 3 days. Clarke's (1982) computations show that the response of the ACC to wind variations with periods less than a few years is predominantly barotropic. Baroclinic fluctuations are found for periods greater than 70 years caused by long period upper ocean temperature variations. Signals of the Southern Ocean with time scales from 30 to 100 years are possibly transmitted to the world ocean by the Antarctic Intermediate Water and Subantarctic Mode Water (Fletcher et al., 1982).

Numerous meso-scale eddies, presumably initiated by baroclinic instabilities (Bryden, 1979; Sciremammano et al., 1980; Wright, 1981), migrate eastward within the ACC. Most of them have radii of less than 100 km and a characteristic rotation velocity of 25 cms^{-1}. High eddy concentration, found in the Scotia Sea and northwest of the Kerguelen-Plateau, is probably generated by the bottom topography of these regions (Kort, 1981). A statistical analysis by Lutjeharms and Baker (1980) reveals a decreasing variability of the ACC with increasing distance from the PFZ. Local differences from this rule exist in the Southwest Atlantic, where the Falkland Current meets the Brazil Current, and in the Southeast Atlantic, where the ACC meets the Agulhas Current. Satellite images frequently show distinct eddy structures in these regions.

2.4.2.1.2 Atlantic sector

The continental boundaries of the Drake Passage and the ridge system of the Scotia Sea force the ACC to the north after passing the Drake Passage (Fig. 29). The northern part of the ACC turns to the north east of the Tierra del Fuego, follows the east coast of the Falkland Islands and converges further north. At 45°S the transport of the Falkland Current amounts to 30 - 40 x 10^6 m^3s^{-1} (Zyryanov and Severov, 1979). At 56°-57°S, 55°W the main flow axis of the ACC splits in two branches. The northern one follows the southern flank of the North Scotia Ridge eastwards. It crosses the ridge at 48°-49°W where bottom water from the Scotia

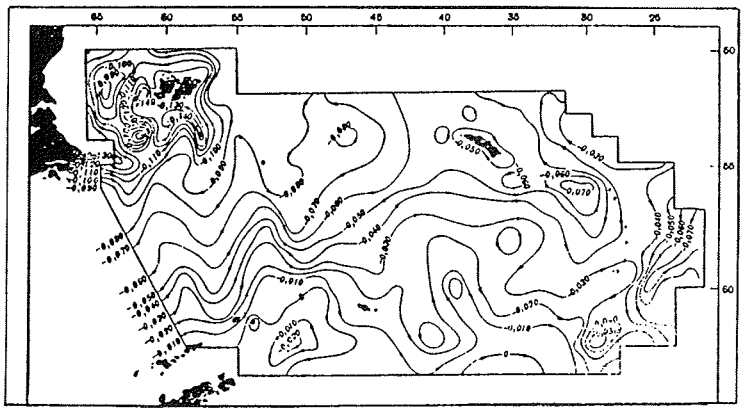

Figure 29: Isolines of the total stream function in the Scotia Sea. The scale factor for the total transport is $10^9 m^3 s^{-1}$ (Zyryanov et al., 1976).

Sea flows into the Argentine Basin (Zenk, 1981). The southern branch surmounts the North Scotia Ridge farther east at 43°-44°W, where it creates a cyclonic circulation in the area 52°-53°S/43° - 47°W (Gordon et al., 1977b). The southern ACC exhibits large meanders through interaction with the Weddell Sea circulation (Zyryanov et al., 1976). The isolines in Figure 28 indicate a nearly divergent flow of the ACC between 30°W and 0°.

2.4.2.1.3 Indian sector

South of Africa the main flow axis of the ACC crosses the Atlantic-Indian Ridge between 25°E and the Prince Edward Islands. Farther north the Agulhas Current transports relative warm water masses southwards. The southerly Agulhas Return Current creates a zone of enhanced baroclinicity which extends into the ACC up to the Macquarie Ridge (160°E). The Agulhas Return Current crosses the Atlantic-Indian Ridge north of the Crozet Plateau. Between Crozet and Kerguelen Islands several weak counter currents can be observed in the ACC, resulting in a net eastward volume transport in the upper 1000 m of up to only 6×10^6 m^3s^{-1} (Jacobs and Georgi, 1977). Anticyclonic eddies with radii of about 100 km and a propagation speed of about 6 cms^{-1} are caused by the Crozet Islands (Colton and Chase, 1983). Crossing the Crozet and Kerguelen Plateaus, the southern part of the ACC is meridionally deflected in a way that a southward heat transport is maintained (Deacon, 1983). At 110°E the northern part of the ACC feeds into the West Australian Current.

South of Australia, the ACC follows the zonal Indian-Antarctic Ridge. The northern part of this water mass recirculates anticyclonically in the Australian Basin. At about 125°E parts of the ACC move over the Indian-Antarctic Ridge southwards through the Antarctic Discordance. Current measurements and geostrophic computations indicate an intensified flow with speeds at the sea surface of 20 - 25 cms^{-1} along the northern flank of the ridge (Fig. 30). On the crest a westward barotropic current appears

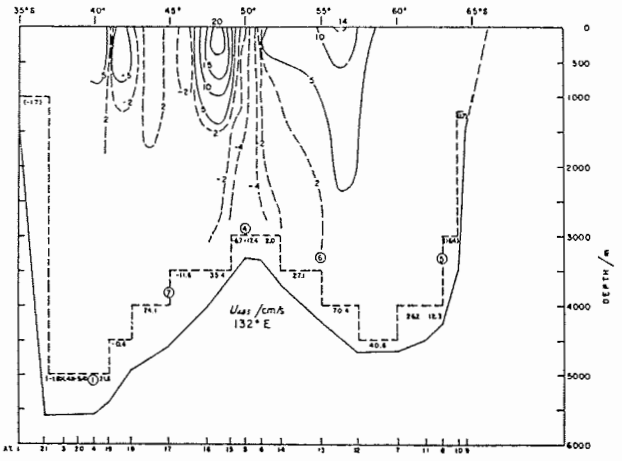

Figure 30: Absolute geostrophic velocities in cms^{-1} and absolute transports in $10^6 m^3s^{-1}$ along 132°E. The circles refer to the locations of current meters (Callahan, 1971).

with speeds of 4 - 6 cms^{-1}. South of the ridge a secondary maximum, which is related to the PF, is present in the eastward flow of the ACC. Along 140°E, the counter current runs along the southern flank. McCartney (1976) supposes that a large scale cyclonic circulation exists over the Indian-Antarctic Ridge between 100°E and 140°E. Smith and Fandry's (1978) model reveals that the position of the west wind maximum mainly determines the strength of the meridional density gradients at the northern flank. The SF and the associated current core are strongest when the west wind maximum is situated slightly north of the crest. Seasonal meridional variations of the west wind maximum are reflected in the zonal currents. The vertical velocity shear attains its maximum at the SF in the model if the ridge is elevated. Computations by Spillane (1978) reveal that the counter current at the southern flank of the Indian-Antarctic Ridge requires a southward component of the generally eastward zonal flow.

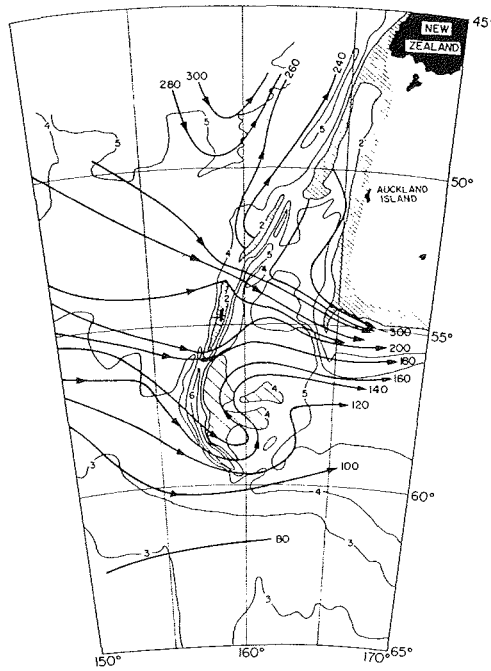

Figure 31: Depth of the salinity maximum layer southwest of New Zealand (scale factor 10 m) (Gordon, 1972).

The Tasman Plateau and the Macquarie Ridge deflect the ACC to the south by about 1000 km. One branch of the ACC flows around the southern tip of the Macquarie Ridge, other branches cross the ridge through gaps at 53.5°S and 56°S (Fig. 31). The geopotential anomaly of the sea surface relative to 40 MPa is a linear function of the depth of the salinity maximum in this region. Thus, the isobaths of the salinity maximum coincide with stream lines of the geostrophic flow. East of the northern gap anti-cyclonic eddies form with periods of about 1 month (Colton and Chase, 1983). Due to the meandering of the most southerly branch, a warm water tongue is situated over the southern Macquarie Ridge. A model by Boyer and Guala (1972) generates a large southward velocity at the western flank in this region. Probably meso-scale eddies also develop at the southern tip.

The branches of the ACC which cross the Macquarie Ridge converge at the southern slope of the Campbell Plateau and form a strong current core with relative geostrophic velocities of up to 45 cms^{-1} (Fig. 32). At the base of the slope 100 m above the

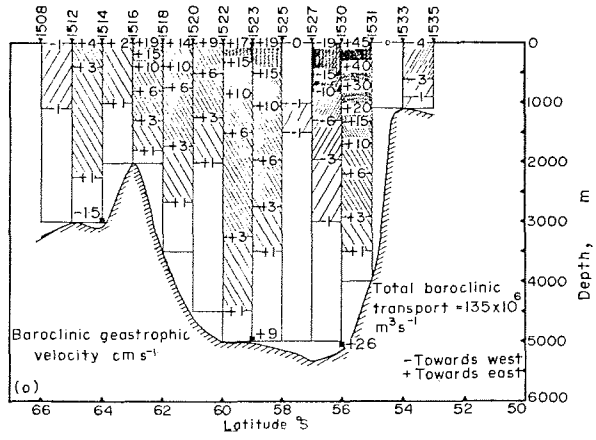

Figure 32: Geostrophic velocities relative to the deepest common level of a station pair along 170°E. The squares refer to the locations of current meters (Gordon, 1975).

bottom, a mean zonal velocity of 26 cms^{-1} was recorded, indicating a surface velocity of 70 cms^{-1}. The counter current at 56°-57°S suggests a cyclonic circulation south of the Campbell Plateau. Other current cores of the ACC are situated at 59°S and at the northern flank of the South Pacific Ridge near 62°-63°S.

2.4.2.1.4 Pacific sector

In the zone from 155°W to 125°W, the isolines in Fig. 28 indicate an intensification of the ACC which crosses the East Pacific Ridge at 145°W and 125°W. Bottom topography causes barotropic standing Rossby waves in the ACC east of the ridge in the central Southeast Pacific Basin, with wave lengths of about 1000 km (Gordon and Bye, 1972). In this region the flow field is divergent, whereas it converges above the eastern Southeast Pacific Basin due to the influence of the Antarctic Peninsula and South America. At the west coast of South America, the northernmost part of the ACC is deflected northwards and finally feeds into the Humboldt Current.

2.4.2.1.5 Drake Passage (DP)

The Drake Passage (DP) connects the Pacific and the Atlantic Oceans and forms simultaneously a broad western entrance into the Scotia Sea. Two submarine ridges extend from South America (westerly) and Antarctica (easterly) in a southeast-northwest direction into the middle of the Drake Passage. Their depths increase from <2000 m at the northern and southern boundaries to >4000 m in the central DP. They direct the northern and central ACC at 2700 m depth to the north and the southern part to the east (Bryden and Pillsbury, 1977).

Hydrographic sections from South America to the South Shetlands suggest that the ACC is composed of four distinct water masses, which are separated by three fronts reaching down to the ocean bottom (Fig. 33).

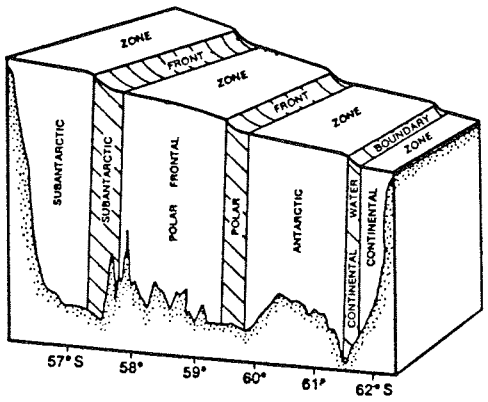

Figure 33: Schematic representation of the four water mass zones separated by three fronts across Drake Passage from Cape Horn to Livingston Island (Nowlin and Clifford, 1982).

According to Whitworth (1980), the four water mass zones are:

- the Subantarctic Zone (SAZ)
- the Polar Frontal Zone (PFZ)
- the Antarctic Zone (AAZ) and
- the Continental Zone (CZ)

The three fronts known as Subantarctic Front (SF), Polar Front (PF) and Continental Water Boundary (CWB) (Sievers and Emery, 1978) are referred to as current cores, which may be permanent in the DP, with a maximum geostrophic velocity relativ to 25 MPa of 25-30 cms^{-1} (Nowlin et al., 1977) The speed reduces in the water mass zones to less than 5 cms^{-1}. The fronts vary geographically in time by nearly two hundred kilometers. They meander with phase velocities of 10-15 cms^{-1} and create eddies with diameters of 60-80 km which migrate to the north (Sciremammano et al., 1980).

Measurements at depths 2500 m indicate that the currents vary with periods of about two weeks and with spatial scales of less than 80 km. The mean flow velocity ranges from 7.6 cms^{-1}(eastwards) to 2.9 cms^{-1}(westwards), with vector average of 1.56 cms^{-1} to the east (Bryden and Pillsbury, 1977). These fluctuations may result from alterations of the atmospheric surface winds which have periods between 2 and 14 days (Baker et al., 1977).

Most of the ACC baroclinic transport (75 %) is primarily associated with the SF and PF and to a lesser extend with the CWB. This fact is noteworthy since the fronts cover only 19 % of the Drake Passage (Nowlin and Clifford, 1982).

Current meters deployed for one year during DRAKE 79 (Dynamic Response and Kinematics Experiment) reveal an eastward net transport in the upper 2500 m of 121 x 10^6 m^3s^{-1}. Hence the total transport through the entire cross-sectional area of DP probably has a range of 118 to 146 x 10^6 m^3s^{-1} (Whitworth, 1983).

Using the FDRAKE 75 data Bryden and Pillsbury (1977) have calculated a total transport of 139x$10^6$$m^3s^{-1}$, whilst Fandry and Pillsbury (1979) arrive at a value of 127x$10^6$$m^3s^{-1}$. Both calculations include a baroclinic transport of 100x$10^6$$m^3s^{-1}$ found by Nowlin et al. (1977). The total transport varies from 28 to 290 x $10^6$$m^3s^{-1}$ within the 35 weeks estimate. These temporal changes may not fully cover the total transport since the mooring

separation of about 80 km is rather large (Sciremammano et al., 1980). Gordon (1983) states that the net transport through the DP may in fact be quite steady. Whitworth (1980) compares the baroclinic transport relative to 25 MPa of summer and winter data and finds an insignificant difference of only 10 %.

Gill and Bryan (1971) show with the aid of a baroclinic model, that the ACC transport through DP is increased by submarine ridges. They also demonstrate that the displacement of the current to the north in the southwest Atlantic is mainly caused by continental boundaries. At the southern continental rise, a westward flow develops so that two different cells are separated at latitude 60°S.

A quasi-geostrophic wind-forced two-layer model of McWilliams et al. (1978) generates baroclinic mesoscale eddies with diameters of up to 200 kilometers as well as meanders with wave lengths from 400 to 800 kilometers. The bottom topography prescribed in this model produces a stationary cyclonic gyre south of the main flow axis. Considerable amounts of momentum are transferred from the mean zonal flow to smaller scales of motion by friction forces in both of the boundary layers.

2.4.2.2 East Wind Drift (EWD)

The westward flow along the Antarctic continental slope is called the EWD. It is basically driven by easterly winds which prevail south of 65°S (Gordon, 1974). Observations of Tchernia and Jeannin (1980) support the assumption that the EWD is composed of the southern part of 3 to 4 individual gyres enclosing the Antarctic continent rather than a continuous flow.

With the aid of satellite tracked icebergs one may conclude that the EWD has a mean velocity of 5-10 cms^{-1}. Maximum values of 25-50cms^{-1} have been measured off the coast of Wilkes Land (Gordon, 1974). Time variability of the flow is difficult to record because the movements of icebergs can be disturbed by the presence of sea ice, ice shelves, local winds, and bottom topography on the track line.

2.4.2.3 Antarctic Divergence (AAD)

The position of the AAD corresponds with the location of the atmospheric low pressure belt at 65°S which separates the southerly east winds from the northerly west winds. The Ekman transports driven by these wind systems cause and maintain the AAD. It forms nearly a complete circle which is broken only in the western Weddell Sea caused by the Antarctic Peninsula (Fig.34).

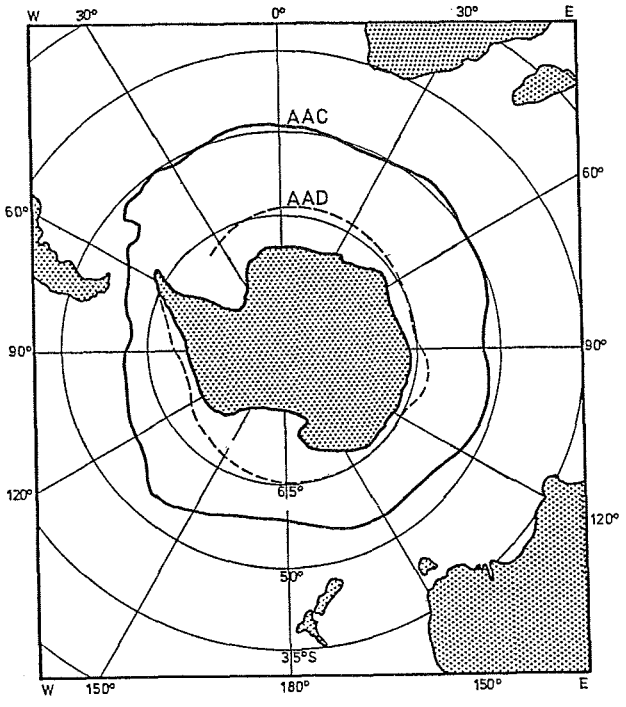

Figure 34: Position of the Antarctic Divergence (dashed line) and the Antarctic Convergence (solid line) around Antarctica (after Deacon, 1982).

Gordon and Taylor (1975b) calculate, from annual wind data, mean vertical water velocities at the bottom of the Ekman layer of $10 \times 10^{-5} cms^{-1}$ for the area between 20°W-155°E and 58°-63°S and $17 \times 10^{-5} cms^{-1}$ for the area between 160°E-25°W and 63°-68°S.

During summer, two divergences exist in the Atlantic-Indian sector; the AAD at about 65°S and the Bouvet Divergence (BD) at about 55°S (Koopmann, 1953). The BD extends from 20°W to 30°E. It forms a transition zone of Weddell Sea Deep Water and Southeast Pacific Deep Water (Gordon, 1967). However, the forcing mechanism of this divergence is not clearly specified.

3. The Weddell Sea

3.1 Bottom topography

The Weddell Sea covers the southerly part of the Southern Ocean in the Atlantic sector. It is bounded to the south by the Antarctic continent, to the west by the Antarctic Peninsula (ca. 60°W) and to the north by the South Scotia Ridge (60°S). No significant natural boundary exists on the eastern side (see Fig. 1). Carmack and Foster (1977) have artifically chosen a straight line from the South Sandwich Islands (26°W) to Cape Norvegia (12°W) as the eastern boundary. Since the Weddell Gyre extends much further to the east, the above defined area may be considered as the minimal extension of the Weddell Sea. Using these limits, it covers about $2.3 \times 10^6 km^2$, which is approximately equal to the Mediterranean Sea. With a mean depth of about 4400 m the volume of the Weddell Sea amounting to 7.6×10^6 km^3 represents about 0.5 % of the water volume of the World Ocean.

The South Scotia Ridge has sill depths of 3000 m and therefore the exchange of water masses between the Weddell and Scotia Seas is possible.

The continental shelf region occupies one-quarter of the area but forms only 4 % of the volume of the Weddell Sea. The 600 m-isobath is generally defined as the shelf edge. This rule is broken only on the eastern side off Dronning Maud Land where the 400 m isobath is chosen instead (Johnson et al., 1981). The width of the shelf increases from about 90 kilometers in the east to about 500 kilometers off the Filchner-Ronne Ice Shelf. The gently sloping shelf area is cut by a trough, called Filchner Depression, which extends from 82°S, 73°W about 600 km northeastwards (Behrendt, 1962). It has a sill depth of about 700 m at the shelf break and deepens to 1200 m at the edge of the Filchner Ice Shelf. It is speculated that the trough was formed by a grounded glacier at the end of the Pleistocene. Information about the western shelf along the Antarctic Peninsula is meagre since heavy sea ice prevents shipborne measurements in this region throughout the year.

The continental slope east of 25°W is relatively steep (approx. 9°) whereas the broad shelf further to the west has a slope of less than 3°.

3.2 Marine atmosphere

3.2.1 Surface heat budget in the pack ice zone

The air-sea heat exchange in the Weddell Sea depends strongly on the coverage and the thickness of sea ice. Due to the high albedo of ice and snow surfaces, solar heating of the ocean is small in pack ice regions. But the sea ice also reduces heat losses of the water column by long wave radiation and interaction with the atmosphere. On the average, the albedo of the inner pack ice zone (ice concentration > 85 %) amounts to 75 %, and of the outer pack ice zone (ice concentration between 15 % and 85 %) to 54 % (Weller, 1981). In particular it is a function of ice concentration, ice composition and snow cover.

The albedo may vary from 20 % for pancake ice to 95 % for the ice shelves (Babarykin et al., 1964). The maximum radiative heat loss of the ocean during the winter season occurs in the open water adjacent to the ice edge which migrates in autumn from the Antarctic coast northwards to a latitude at about 55°S (Schwerdtfeger, 1970). The energy of the solar radiation during the summer period is mainly used to melt the sea ice. Only a small portion is accumulated in the water column directly.

The sensible heat flux from the ocean to the atmosphere is generally strong in leads and polynyas where it attains maximum values of more than 700 Wm^{-2} in winter (Gube-Lenhardt and Hoeber, 1985). Here the latent heat flux can also be considerably high. This happens frequently at the east coast of the Weddell Sea when cold and dry continental air flows across coastal polynyas. The latent heat fluxes there may exceed 100 Wm^{-2}. This heat loss compensates for the summer radiative heating so that the sea surface temperature in polynyas stays near freezing point (-1.92°C to -2.10°C) (Ledenev, 1964). A thin ice cover already reduces the sensible and latent heat fluxes drastically. Maykut (1978) points out that an ice cover of 5 cm thickness reduces the sensible heat flux by 40 % and the latent heat flux by 70 %.

Measurements of Weller (1968, 1981) and Allison et al. (1982) near Mawson (67°34'S 62°53'E) support the following scheme:

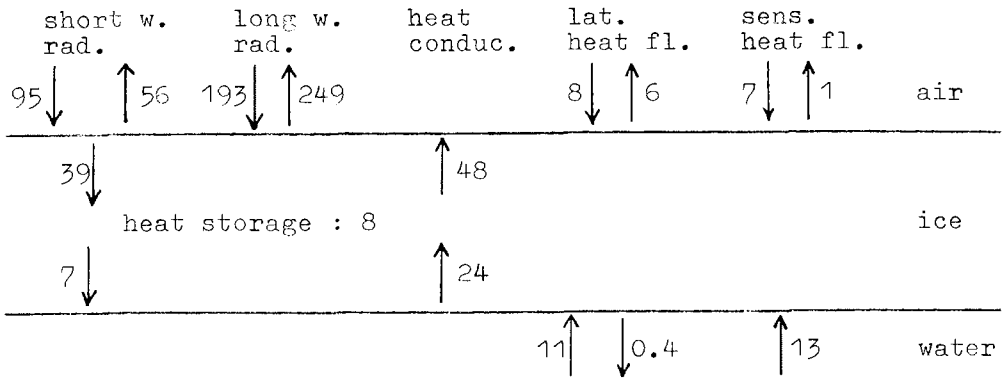

Figure 35: The heat balance at the upper and lower sea ice boundaries averaged from 1 July to 15 November near Mawson. Units in Wm^{-2} (after Weller, 1968).

From mid summer to March the ocean gains heat by net radiation (maximum values ≥ 200 Wm^{-2}) and sensible heat fluxes. During March the direction of the net radiative and heat fluxes reverses and in April the oceanic heat loss may reach as high as 200 Wm^{-2}. This value drops remarkably when ice formation starts. As soon as the ice cover is about 20 cm thick, the oceanic heat loss drops below 75 Wm^{-2}. From May to July the heat transfer across the ocean surface remains nearly constant at 50 Wm^{-2}, while the ice thickness increases to 1.8 m. In mid-winter the coastal pack ice zone still loses energy of 56 Wm^{-2}, which is twice as much as inland on the Antarctic continent. With increasing solar radiation, melting of ice starts in October again.

Month	Q_S	Q_B	H	LE	Q_{WA}	Q_{IA}	R	P	Q_o
Jan.	162	35	7	39	81	29	0,36	0,3	65
Feb.	109	36	15	47	11	3	0,28	0,1	10
March	56	36	15	44	- 39	- 8	0,20	0,2	-32
Apr.	21	36	50	72	-138	-32	0,23	0,4	-95
May	12	36	60	63	-148	-25	0,17	0,5	-87
June	4	36	80	66	-178	-21	0,12	0,6	-84
July	2	36	100	72	-206	-25	0,12	0,7	-79
Aug.	38	36	100	72	-171	-16	0,09	0,7	-62
Sept.	76	36	90	68	-118	- 8	0,07	0,8	-30
Oct.	106	36	50	69	- 49	- 7	0,15	0,7	-20
Nov.	128	35	20	60	13	2	0,14	0,6	6
Dec.	142	36	8	52	47	13	0,27	0,4	33
Averages	71	36	49	61	- 75	- 8	0,18	0,5	-31

Table 5: Seasonal variations of surface heat budget components zonally averaged between 60°S and 70°S in Wm^{-2}.

Qs: global radiation absorbed by the ocean
Q_B: net long wave radiation
H: sensible heat flux
LE: latent heat flux
Q_{WA}= Q_S-Q_B-LE-H: net heat flux between an ice-free ocean and the atmosphere
Q_{IA}: net heat flux between an ice-covered ocean and the atmosphere
R= Q_{IA}/Q_{WA}
P: ratio of the ice-covered area to the total area (from NAVY-NOAA ice charts)
Q_O: net heat flux for a realistic sea ice extent

(Gordon, 1981).

Since neither the atmospheric flow, nor the ice coverage of the pack ice zone are known well enough, heat budget estimates for the entire pack ice region are quite uncertain. Nevertheless, the results of Gordon (1981) and Sasamori et al. (1972), presented in Table 5, and the values obtained at Mawson Station in Figure 35 provide some informations. According to the tabulated values, the long wave emission exceeds the short wave absorption from April to July. Sensible and latent heat fluxes are generally directed from the ocean to the atmosphere, increasing from summer to winter time. A net warming of the ocean occurs from November to February. The annual oscillation of the air-sea heat exchange is damped by the sea ice. Because of the glaciological annual cycle, the mean heat loss in winter (June to September) amounts to 64 Wm^{-2} and the mean heat gain in summer (December to March) to 19 Wm^{-2}. Leads and polynyas in the pack ice zone which form about 30 % of the total area, are of particular importance for the oceanic heat loss in winter. They contribute about 44 % to the mean annual heat loss of the ocean to the atmosphere (Ackley, 1981 a).

3.2.2. Air temperature at the lower boundary of the atmosphere

The air temperature of the Weddell Sea region is controlled by the northward transport of sea ice and cold water along the Antarctic Peninsula. This cooling effect results in a negative surface layer temperature anomaly extending from the Antarctic Peninsula to the South Indian Ocean (Fig. 36, Table 6). The annually averaged surface air temperature in the Weddell Sea

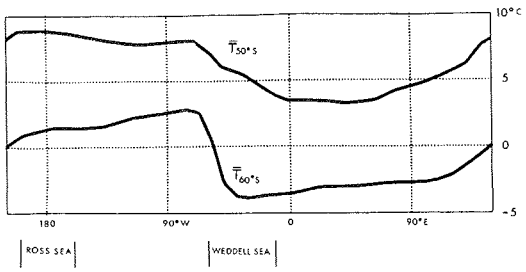

Figure 36: Zonal distributions of the annual averaged air temperature at the sea surface along 50°S and 60°S (Schwerdtfeger, 1979).

decreases southwards from -4.3°C (Orcadas) to -22.2°C (Belgrano) (Schwerdtfeger, 1975). The monthly mean temperatures amount to -10°C and +1°C at the South Orkney Islands and to -30°C and -8°C at the Filchner Ice Shelf for July and January, respectively (Schwerdtfeger, 1970).

	110°W	90°W	70°W	50°W	30°W	10°W	10°E	30°E	
60°S	+2.2	+2.2	+2.6	-2.4	-3.9	-3.6	-3.3	-3.0	°C
65°S	-2.8	-2.7	-3.2	-8.6	-8.3	-7.5	-6.8	-6.4	°C

Table 6: Zonal distributions of the annual averaged air temperature at the sea surface along 60°S and 65°S (Schwerdtfeger, 1975).

Drifters on the pack ice of the western Weddell Sea have indicated temperature fluctuations with a characteristic period of 2 weeks which are obviously caused by large scale atmospheric disturbances. Compared to other regions of the Antarctic pack ice zone, the Weddell Sea exhibits the largest interannual sea ice and surface air temperature variations (Streten and Pike, 1980). These features may have certain impacts on the year to year changes of large scale global circulation.

3.2.3 Antarctic pressure trough

The axis of the Antarctic pressure trough over the Weddell Sea has its most southerly position on the western side. A stationary low pressure centre exists at 62°S 20°E and sometimes a secondary low lies at 66°S 20°W (Schwerdtfeger, 1970)

In summer and autumn, cyclones occur over the Weddell Sea with an average period of 20 days (Ackley, 1981 b). The majority of the cyclones created in the west wind zone are deflected northwards by the Antarctic Peninsula so that they circumnavigate the Weddell Sea (Taljaard, 1972).

3.2.4 West and east wind zones

The zonal distribution of the meridional pressure gradient at the sea surface between 40°S and 60°S (Fig. 9) exhibits a local minimum at the Antarctic Peninsula. Eastwards up to 10°W the strength of the west wind increases on a seasonal average by 10-30 % (Streten, 1980).

West winds are dominant north of about 65°S. Between 65°S and 70°S, both west and east winds are observed, while south of about 70°S, east winds prevail (Schwerdtfeger, 1975). Table 7 portrays the monthly averaged zonal geostrophic wind over the Weddell Sea.

		60°S	65°S	70°S	75°S
January	20°W	3.6	-0.1	-3.2	-4.8
	30°W	3.0	-0.1	-2.5	-4.1
	40°W	2.3	0.0	-1.6	-2.9
	50°W	2.2	-0.1	-1.3	-1.9
April	20°W	6.6	0.1	-4.9	-5.5
	30°W	6.7	1.6	-3.2	-5.1
	40°W	6.1	2.7	-1.5	-4.3
	50°W	5.6	3.1	-0.5	-3.3
July	20°W	6.4	1.7	-3.2	-5.4
	30°W	5.5	2.7	-1.2	-4.5
	40°W	4.4	2.8	0.1	-3.3
	50°W	3.5	2.2	0.4	-2.2
October	20°W	9.3	5.8	-0.7	-5.3
	30°W	9.2	6.9	0.7	-5.2
	40°W	8.8	6.9	1.5	-4.4
	50°W	8.4	6.0	1.4	-3.5

Table 7: Monthly averaged zonal geostrophic wind field above the Weddell Sea in ms^{-1}, positive for west winds (Jenne et al., 1971).

The mountain barrier of the Antarctic Peninsula causes a south wind which transports cold continental air of -20° to -30°C along the Antarctic Peninsula into the west wind zone (Schwerdtfeger, 1975). Its strength depends on the zonal temperature gradient, which in this part of Antarctica amounts to 2-4°C per 100 km (Ackley, 1981 b).

The annual mean wind speed ranges up to about 14 ms^{-1} (Schwerdtfeger 1979). Drifter measurements on the western Weddell Sea pack ice display temperature fluctuations of 10-15°C with periods of 2-3 days caused by outbreaks of cold continental air from the south (Ackley, 1981 b). From February to May, when the barrier winds are strongest, the sea ice frequently piles up to form large ridges in the northwestern Weddell Sea (Schwerdtfeger, 1979).

The east wind zone over the southern Weddell Sea is influenced by katabatic winds reaching some 10 km off the coast. They are strong enough to create and maintain coastal polynyas, even in winter. The low air temperature, which sometimes reaches -40°C, simultaneously favours sea ice production (Ledenev,1964; Weller, 1981). The newly-formed ice is advected off the coast by these surface winds.

3.2.5 Precipitation

Precipitation decreases from about 400 mma^{-1} at the South Orkney Islands to less than 200 mma^{-1} at the Antarctic coast (Streten, 1977). Newton (1972) estimates a 270 mma^{-1} difference between precipitation and evaporation for the zonal belt between 60°S and 70°S. If the melting of icebergs is included, the fresh water gain of this region amounts to about 400 mma^{-1} (Gordon, 1981). Piola and Georgi (1981) determined the fresh water source of the Scotia Sea near the PF at 276 ± 190 mm per 6 months, which is in rough agreement with the above value.

3.3 Glaciological aspects

3.3.1 Sea ice

Large parts of the Weddell Sea are permanently covered with sea ice.The latter reaches its maximum extent of $4.36 \cdot 10^6 km^2$ in August, and the minimum coverage of $1.14 \cdot 10^6 km^2$ is observed in February (Ropelewski, 1983). Compared to other Antarctic regions the Weddell Sea shows the largest annual sea ice variation as demonstrated on Fig.37. The large amplitude of this signal is mainly attributed to dynamic, rather than to thermodynamic effects (Hibler and Ackley, 1983).

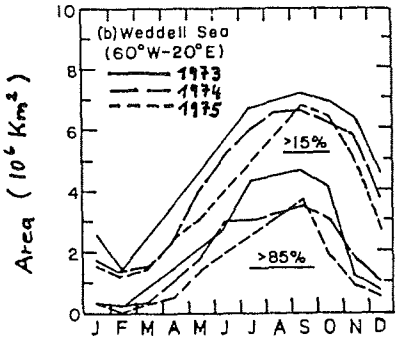

Figure 37: Annual variations of the sea ice extent between 60°W and 20°E for areas with different ice concentrations (Ackley, 1981 a).

In the Weddell Sea the pack ice edge occupies its northernmost position at the South Sandwich Islands (56°S 26°W) in September (Fig. 38). The sea ice retreat begins in late September and is accellerated in November. During spring and summer the ice-free

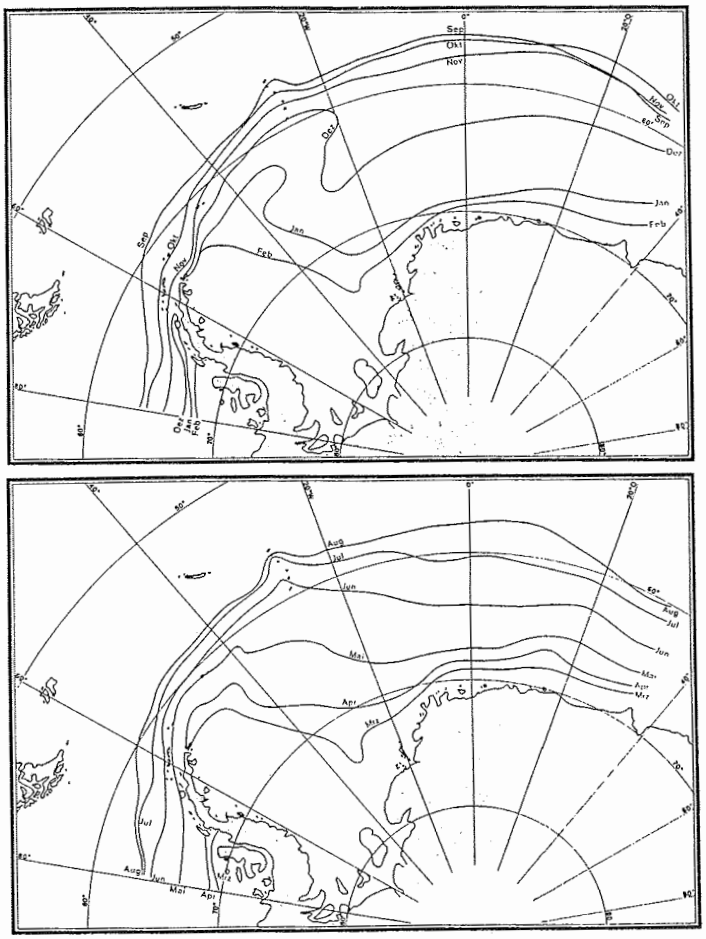

Figure 38: Monthly averaged positions of the pack ice edge between 1973 and 1979 (Deut. Hydrogr. Inst., 1981).

region expands along the coast of Coats Land and sometimes even to the Filchner-Ronne Ice Shelf. A tongue of relative high ice concentration from the tip of the Antarctic Peninsula to about 20°W is preserved by an eastward transport of the pack ice in

the northern part of the Weddell Gyre. Due to the barrier effect of the Antarctic Peninsula to the oceanic circulation and the northward flow of continental air, an area of about 8 x $10^5 km^2$ in the western Weddell Sea is covered by sea ice throughout the year. Occasionally the whole area west of 25°W stays covered with ice. During cold air outflow conditions sea ice can also be formed in summer at the Filchner Ice Shelf edge (Foster, 1972b).

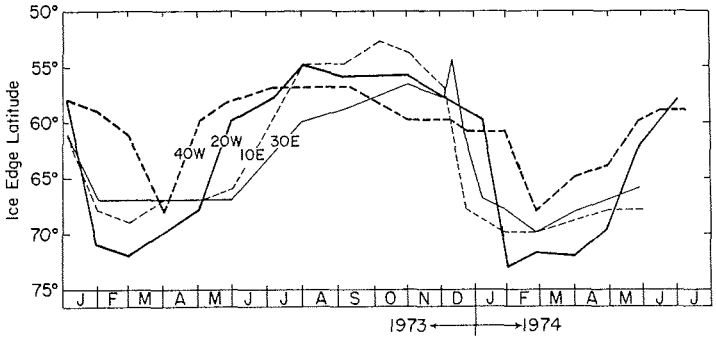

Figure 39: Annual variations of the pack ice edge along 40°W, 20°W, 10°E and 30°E from satellite data, Jan. 1973 to July 1974 (Ackley, 1979).

The eastward advection of sea ice by the Weddell Gyre causes a considerable phase shift of the annual meridional migration of the pack ice between the western and eastern Weddell Sea (Fig. 39). At about 30°W the maximum sea ice extent is reached in July/August, at 10°E it appears in September/October, and at 30°E the ice edge occupies its northernmost position in December.

The strong kinematic forcing is an important contribution to annual and interannual fluctuations of the sea ice extent in the Weddell Sea region predominantly between 20°W and 40°W (Streten and Pike, 1980).

According to ship and iceberg drift observations, sea ice motion along the Antarctic Peninsula amounts to about 4.5 cms^{-1} on an annual average, with a maximum of about 8 cms^{-1} during the winter months (Brennecke, 1921). Thus, the migration of sea ice from the southwestern shelf to the tip of the Antarctic Peninsula lasts more than one year. Satellite-tracked buoys dropped at 70°-75°S/50°-60 °W reveal northeastward velocities from 2 to 12 cms^{-1} during summer and autumn. The larger values have been observed in autumn, when strong southerly winds prevail along the Antarctic Peninsula. Westward migrating cyclones frequently cause short-time convergences and divergences in the pack ice field of the western Weddell Sea.

The thickness of sea ice increases from 1 m for first-year to 3 m for multi-year ice. Consequently, 1 to 1.5 m ice thickness dominates in the eastern Weddell Sea, whilst it measures more than 3 m at the tip of the Antarctic Peninsula. These mean values are locally exceeded by pressure ridges which may amount to 10 m. The compact sea ice cover along the Antarctic Peninsula prevents the surface water from solar heating in summer. Summer melting of the underwater part of the ice floes is therefore small and no remarkable fresh water production occurs (Ackley 1979). During the "Deutschland" drift, an ice growth of 1 to 1.5 m was observed along the trajectory (Foster, 1972 b).

About 50 - 70 % of the sea ice in the Weddell Sea is frazil ice, which seems to be formed at high growth rates (>1cmh^{-1}) in polynyas and leads (Ackley et al., 1980; Gow et al., 1982; Clarke and Ackley, 1984). Bauer and Martin (1983) indicate that ice accumulation can lead to ice layers of more than 50 cm thickness within a few hours. Obviously this process inhibits the brine drainage so that the salinity of sea ice is still 4 to $10x10^{-3}$ in early spring (at 59°-62°S 0°-5°E). Congelation at the bottom of ice sheets through heat loss at the top depends on the actual ice thickness, but it is generally much slower than by accumulation of frazil ice (Clarke and Ackley, 1984).

Comparatively large growth rates are observed during the formation of grease ice. The latter forms in leads and polynyas with high sea-air heat fluxes. However, in this case, salt is strongly precipitated (Bauer and Martin, 1983).

3.2.2 Weddell Polynya

From 1973 to 1977 a large polynya with an area of about $2.5 \cdot 10^5 km^2$ appeared in the pack ice of the eastern Weddell Sea (63°-71°S 30°W-15°E) (Martinson et al., 1981). Satellite images show spatial as well as temporal variations of this phenomenon

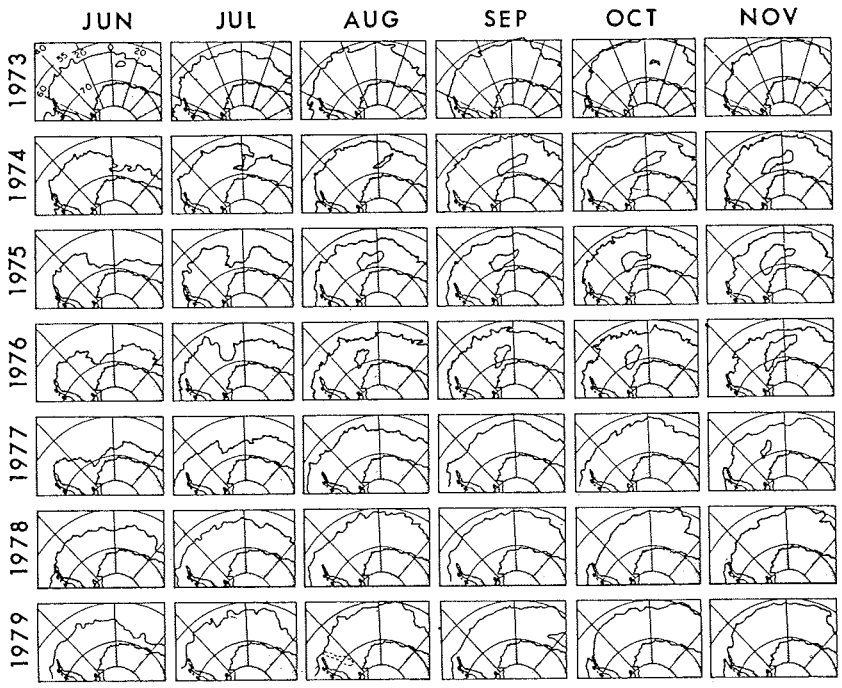

Figure 40: Locations of the pack ice edge over the Weddell Basin during June to November 1973 - 1979 from satellite images (Martinson et al., 1981).

(Fig. 40). On the average, the Weddell Polynya migrated with a velocity of 1 cms^{-1} westwards from 1973 to 1977 (Carsey, 1980). Figure 41 shows the development of the polynya in winter 1974. During sea ice growth a large bight from 64° to 69°S and from 0° to 10°E stays ice-free and the open water area is fully surrounded by pack ice in July. The polynya enlarges its area from July to December.

The mechanisms of creation and maintenance of this open water area in the pack ice belt are not yet clearly identified. Speculations that perturbations originating from the Maud Rise (65°S 0°) and deep convection may be predominantly involved in the above processes seem to have some likelihood.

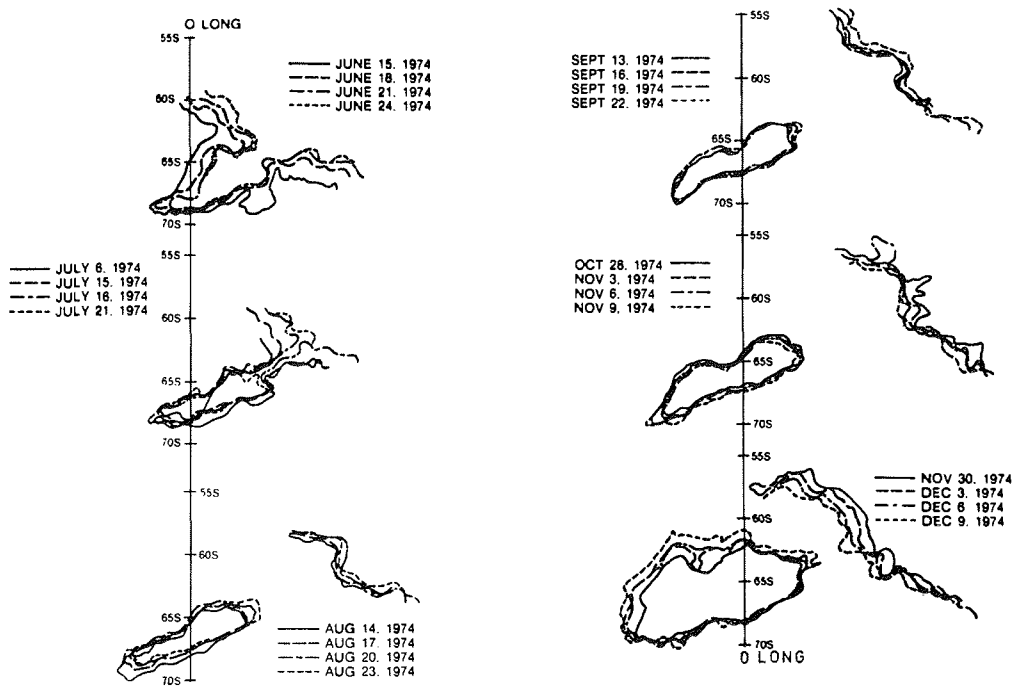

Figure 41: Locations of the pack ice edge and the Weddell Polynya during June to December 1974 (Carsey, 1980).

3.3.3 Ice Shelves

Two large ice shelves flow into the Weddell Sea: the Filchner-Ronne Ice Shelf in the south and the Larsen Ice Shelf at the east coast of the Antarctic Peninsula. Radio-echo soundings indicate that the thickness of the Filchner-Ronne Ice Shelf increases from 200 - 300 m at the floating ice front to 1400 -1500 m farther south where it rests on the ground (Robin et al., 1983). In the north, the shelf ice is divided into two parts by Berkner Island. Between Berkner Island and Coats Land the ice stream convergences. At the front the ice attains velocities of up to 1500 ma^{-1}. West of Berkner Island, the flow speed reduces to about 1050 ma^{-1} (Kohnen, 1982). The major ice discharge occurs at the eastern and western sides of the shelf. On the average the annual calving amounts to about 400 km^3a^{-1} (Zotikov et al., 1974).

Bottom melting of the ice shelves plays some role where surface water is forced downward on its way under the ice. Rough estimates indicate that, west of Berkner Island the melting rate is as large as 3.2 ma^{-1} (Robin et al., 1983) and at the eastern slope of the Filchner Depression it increases to even 10 ma^{-1} (Behrendt, 1968; Carmack and Foster, 1975 a).

3.4 Hydrography

The ice conditions hamper systematic hydrographic observations in the Weddell Sea throughout the year. Therefore, information about seasonal phenomena is rare. Winter data are available only from the drifting ships "Deutschland" (1911-1912) and "Endurance" (1915-1916) and the 1981 expedition with the RV Somov. Basic studies of the hydrography of the Southern Ocean featuring the Weddell Sea as the main source of Antarctic Bottom Water have been conducted by Brennecke (1921), Wüst (1933), Mosby (1934) Deacon (1933, 1937) and Mackintosh (1946) using measurements of several sea trials. The Weddell Sea investigations have been supplemented by ELTANIN data from 1963-64 and by the observations during the International Weddell Sea Oceanographic Expeditions (IWSOE) 1968 and 1973 to 1976 (Fig. 42).

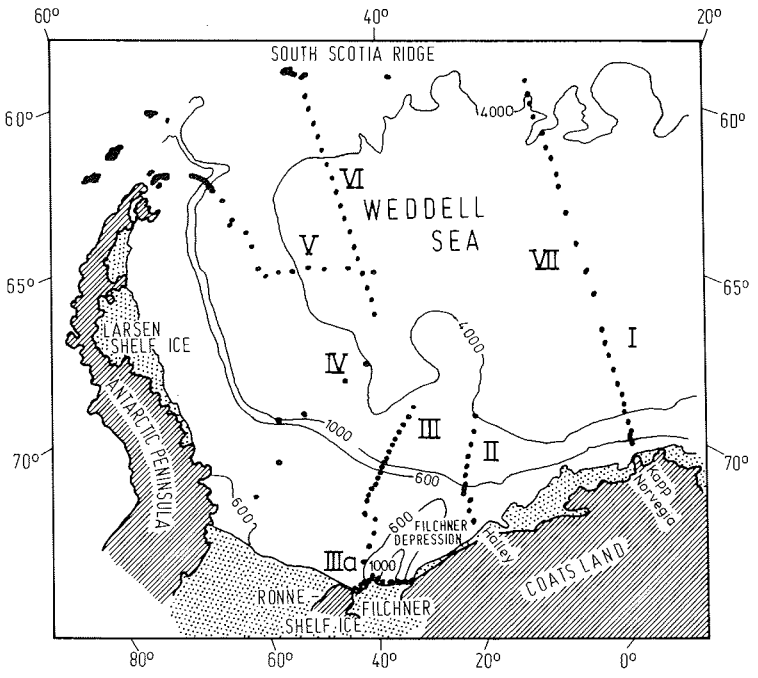

Figure 42: Locations of hydrographic sections carried out during the International Weddell Sea Oceanographic Expedition (IWSOE) 1973: I, II, III, IIIa and VII, IWSOE 1975: VI and IWSOE 1976: V
Section IV originates from GLACIER cruise 1968
Dots mark hydrographic stations.

3.4.1 Water masses

Characteristics and spatial distribution of the Weddell Sea water masses will be described with the aid of potential temperature θ, salinity S and oxygen O_2.

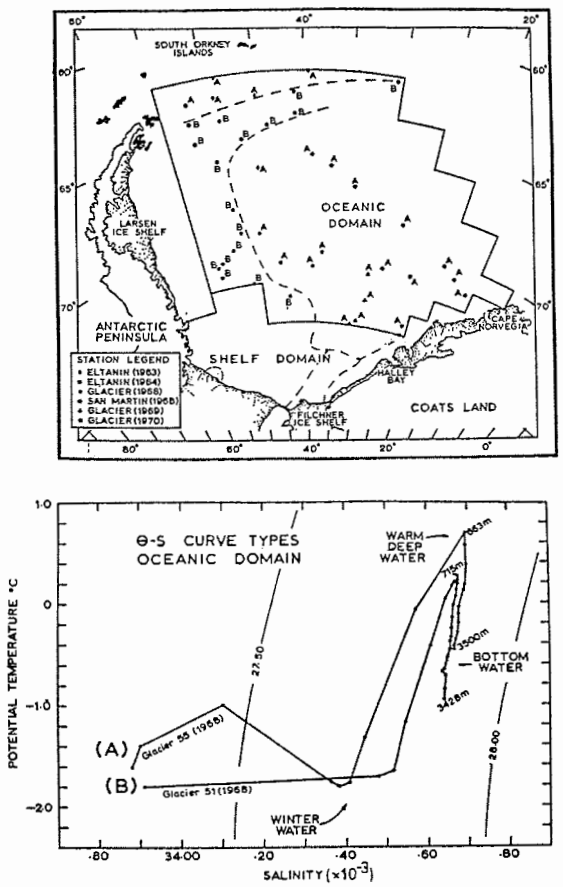

Figure 43: Two characteristic θ/S correlation curves representing stations in the oceanic domain
A: central Weddell Sea
B: continental slope and rise of the western and northern Weddell Sea.
Curve A shows the beginning of surface cooling, whilst the influence of summer heating is still present below. According to permanent ice cover, curve B shows no summer heating (Carmack, 1974).

The θ/S-diagrams on Figures 43 and 50 show distinct differences between the water masses of the oceanic and of the shelf domain as well as between Weddell Sea Bottom Water and Antarctic Bottom Water. Characteristic properties of the individual water masses are displayed in Table 8 and their volumes are indicated in Table 9.

Water mass	potential temperature interval θ (°C)	salinity interval S ($x10^{-3}$)	oxygen interval O_2 ($x10^{-3}$)
Winter Water (WW)	$-2 \leqslant \theta \leqslant -1.6$ (I)	$34.4 \leqslant S \leqslant 34.52$ (I)	$6.6 \leqslant O_2 \leqslant 6.9$ (I)
Warm Deep Water (WDW)	$0 < \theta \leqslant 0.8$ (II)	$34.6 \leqslant S \leqslant 34.76$ (II)	$4.3 \leqslant O_2 \leqslant 4.9$ (I)
Antarctic Bottom Water (AABW)	$-0.8 \leqslant \theta \leqslant 0$ (I)	$34.64 \leqslant S \leqslant 34.68$ (I)	$5.1 \leqslant O_2 \leqslant 5.7$ (I)
Weddell Sea Bottom Water (WSBW)	$-1.4 \leqslant \theta < -0.8$ (I)	$34.64 \leqslant S \leqslant 34.68$ (I)	$5.9 \leqslant O_2 \leqslant 6.5$ (I)
Weddell Sea Deep Water (WSDW)	$-0.4 \leqslant \theta \leqslant -0.1$ (III)	$34.66 \leqslant S \leqslant 34.67$ (III)	$5.4 \leqslant O_2 \leqslant 5.6$ (III)
Modified Warm Deep Water (MWDW)	$-1.6 < \theta \leqslant 0$ (II)	$34.4 \leqslant S \leqslant 34.64$ (II)	
Eastern Shelf Water (ESW)	$-2 < \theta \leqslant -1.6$ (I)	$34.28 \leqslant S \leqslant 34.44$ (I)	$7.2 \leqslant O_2 \leqslant 7.4$ (I)
Western Shelf Water (WSW)	$-2 < \theta \leqslant -1.6$ (I)	$34.56 \leqslant S \leqslant 34.84$ (I)	$6.9 \leqslant O_2 \leqslant 7.3$ (I)
Ice Shelf Water (ISW)	$-2.4 \leqslant \theta \leqslant 2$ (II)	$34.56 \leqslant S \leqslant 34.68$ (II)	

Table 8: Potential temperature θ (°C), salinity S ($x10^{-3}$) and oxygen O_2 ($x10^{-3}$) intervals for the water masses of the Weddell Sea given by:

I: Carmack (1974); II: Carmack and Foster (1977); III: Gordon (1978).

Oceanic domain

water mass	volume (km^3)	percent of TV
AASW	592×10^3	7.8
WW	125×10^3	1.6
WDW	2260×10^3	29.7
AABW	4350×10^3	57.2
WSBW	223×10^3	3.0

Shelf domain

MWDW	14×10^3	0.2
ESW	61×10^3	0.8
WSW	84×10^3	1.1
ISW	16×10^3	0.2
total volume (TV)	7600×10^3	100

Table 9: Volume and percent of the total volume of the Weddell Sea water masses listed in Table 8. The volume for AASW comprises both domains; MWDW can be observed only on the shelf (Carmack and Foster, 1977).

3.4.1.1 Winter Water (WW)

The Winter Water is a remnant of thermohaline convection during sea ice growth. It forms an isothermal layer with the temperature minimum below the seasonal pycnocline from 100 to 200 m depth. Compared to the Antarctic Surface Water, WW has lower temperature and higher salinity values (Weiss et al., 1979). Jacobs et al. (1979 b) suggest that a particularly thick WW layer forms in areas of high iceberg frequency. The surface layer flattens in comparison to the interior of the Weddell Sea, where the prevailing winds cause an Ekman upwelling of deep water (Foster and Carmack, 1976 b).

3.4.1.2 Warm Deep Water (WDW)

The Warm Deep Water underlies the WW and is characterized by temperature and salinity maxima. The temperature maximum ascends from 400 - 600 m depth at the shelfbreak to 200 m in the centre of the Weddell Gyre (Fig. 44). A parallel rise in the salinity maximum from 1000 to 500 m depth is also observed (Gordon and Molinelli, 1982; Table 210).

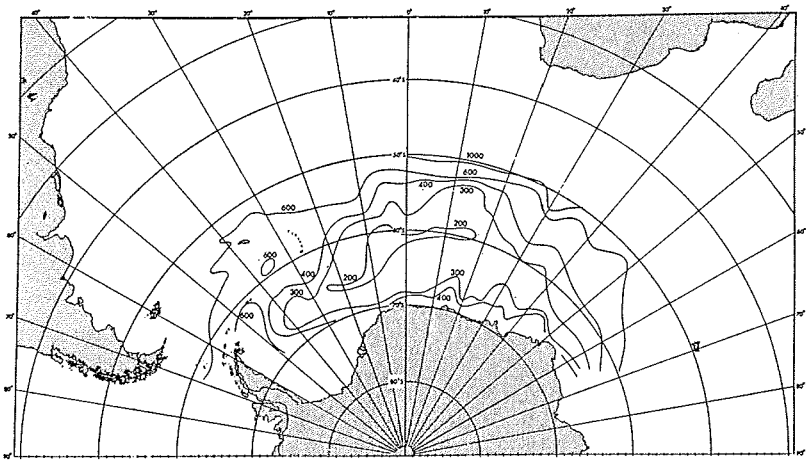

Figure 44: Depth contours of the deep temperature maximum layer over the Weddell Basin (Deacon, 1979).

As Gordon (1982) has pointed out, WDW has cooled by 0.3°C from 1973 to 1977 to the west of Maud Rise. This heat loss of the water column seems to be a consequence of the earlier mentioned polynya existing during this time period. It is worthwhile to point out that the temperature maximum in 1977 has passed the lower limit of the WDW characteristic indicated in Table 8. For more details see paragraph 3.5.2.4.

3.4.1.3 Antarctic Bottom Water (AABW)

Temperature and salinity change gradually from WDW to Antarctic Bottom Water. The latter, which is characterized by temperatures below 0°C, a salinity minimum and an oxygen maximum near the ocean bottom, represents by far the largest water mass of the Weddell Sea (Table 9). It fills the entire basin below the depth of about 2000 m, as indicated in Figures 45 to 47. According to Foster and Middleton (1979), AABW is composed of Warm Deep Water and Weddell Sea Bottom Water.

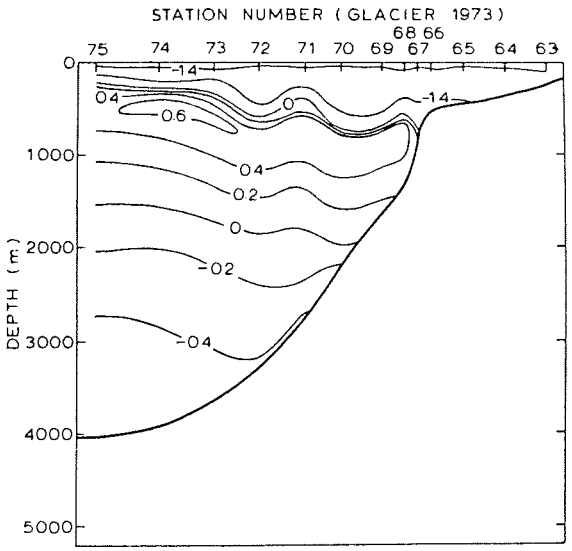

Figure 45: Vertical distribution of the potential temperature (°C) along section II (IWSOE 1973) crossing the shelf break at about 29°W (Foster and Carmack, 1977).

3.4.1.4 Weddell Sea Bottom Water (WSBW)

The newly formed bottom water in the Weddell Sea is called Weddell Sea Bottom Water. Carmack and Foster (1977) estimate a production rate of 3.5 $x10^6 m^3 s^{-1}$ for this type of water mass.

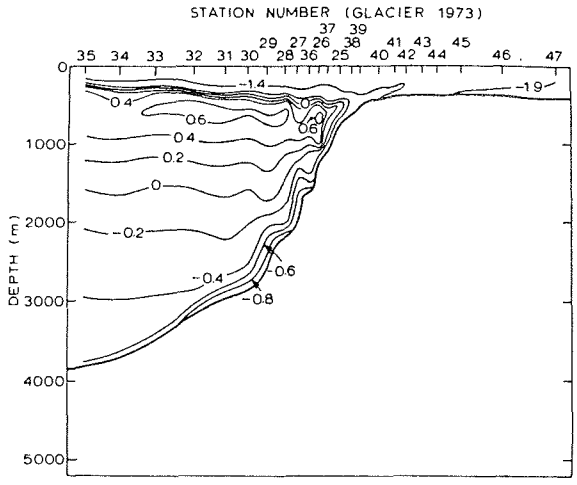

Figure 46: Vertical distribution of the potential temperature (°C) along section III (IWSOE 1973) crossing the shelf break at about 40°W (Foster and Carmack, 1977).

At 40°W (Fig. 46) the WSBW was detected at the continental slope between 2000 m and 3500 m depth with no direct inflow from the shelf. One may therefore speculate that this water mass originates from the Filchner Depression. Further to the west, subsidence of cold shelf water down into the deep basin is confirmed in Figure 47. This section crosses the shelf break at about 51°W. A thin layer with potential temperatures below -0.8°C can be traced all the way along the slope up to the shelf. At present no measurements are available to verify the production of WSBW in the western Weddell Sea although the region along the Antarctic Peninsula should be favourable for such a process (Carmack and Foster, 1977). The coldest bottom water of the Weddell Sea with a potential temperature of -1.4°C was detected just south of the tip of the Antarctic Peninsula (Foster and Middleton, 1980).

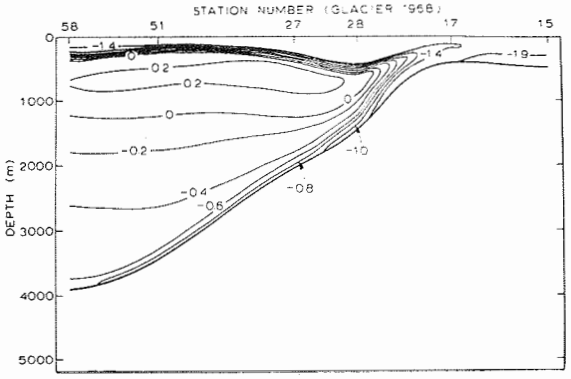

Figure 47: See Figure 45. Section IV (GLACIER cruise 1968) crosses the shelf break at about 51°W (Foster and Carmack, 1977).

Salinity measurements in the same area portrayed in Figure 48 indicate a decreasing salinity with depth in the bottom layer.

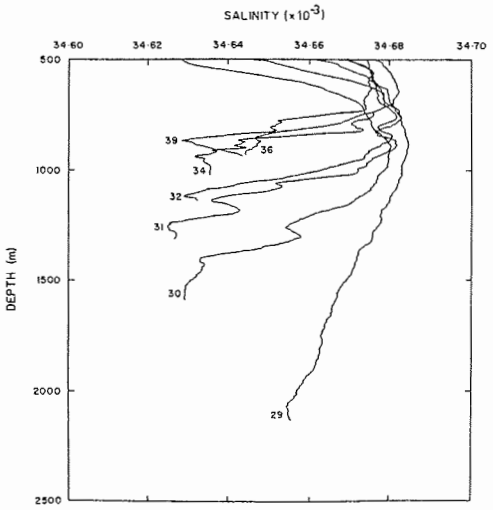

Figure 48: Salinity profiles at stations over the continental slope in section V (IWSOE 1976) (Foster and Middleton, 1980).

These profiles furthermore show some intrusions of saltier water which suggest an intermittent bottom water formation in space and time in this region (Foster and Carmack, 1976 a). Similar arguments seem to hold for the slope of the South Scotia Ridge. Foster and Carmack (1977) conclude, from the slightly higher temperature and the larger volume of bottom water, that WSBW is mixing with the overlaying WDW. A repetition of section VI in 1976 revealed that the bottom water was cooler, saltier and higher in oxygen than one year before. These findings provide evidence for considerable variations in bottom water production in the Weddell Sea.

3.4.1.5 Weddell Sea Deep Water (WSDW)

The WSDW, characterized by Reid et al. (1977), ranges near the warm saline end of AABW. According to Gordon (1978), WSDW formation takes place in the centre of the Weddell Gyre. The required vertical mixing of the cold low saline Winter Water with the warm salty Deep Water could be supported by westward moving eddies generated at Maud Rise. The perturbation extends down to 4000 m depth as documented by the isolines of potential temperature and density, in Figure 49.

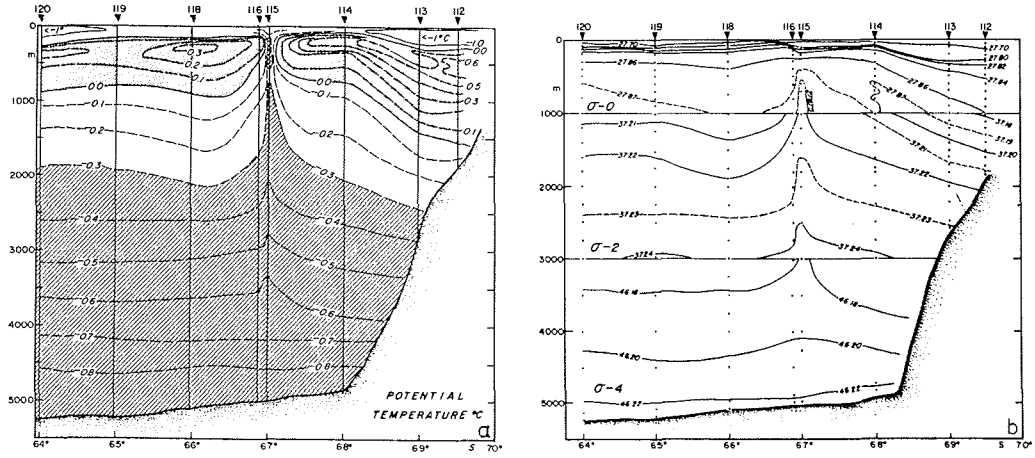

Figure 49: Vertical distribution of potential temperature (a) and sigma-p (b) west of Maud Rise (Gordon, 1978).

3.4.1.6 Shelf Water (SW)

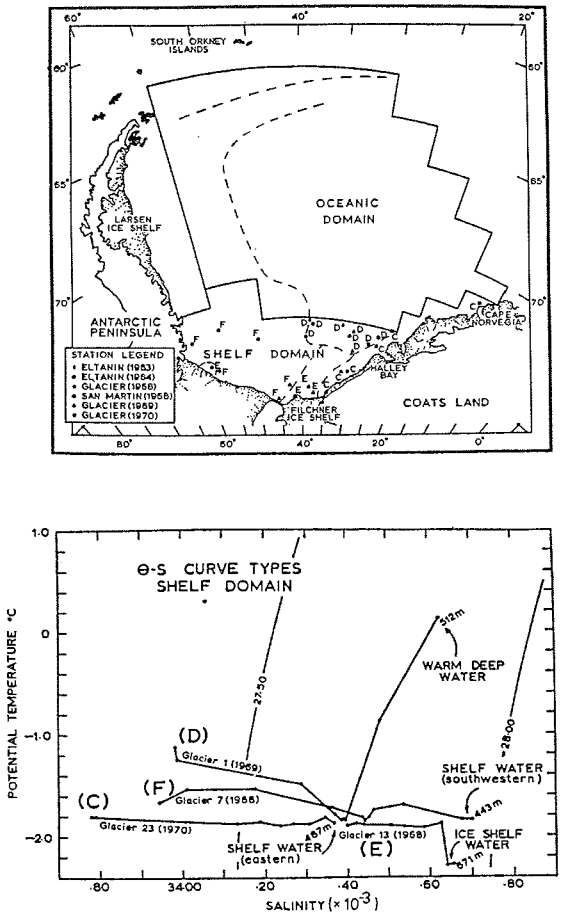

Figure 50: Characteristic θ/S correlation curves from different regions of the Weddell Sea shelf.
C: eastern shelf
D: shelf break (25°-40°W)
E: Filchner Depression
F: western shelf

(Carmack, 1977)

Eastern Shelf Water (ESW) covers the narrow shelf east of the Filchner Depression. It differs from the Western Shelf Water (WSW) by lower salinity values. The latter lies in the density interval of 27.85 to 28.08 (Carmack, 1974) and is thus the densest water mass in the Weddell Sea. WSW occupies the broad shelf region west of the Filchner Depression. The salinity increases from east to west with a maximum at the Antarctic Peninsula.

3.4.1.7 Ice Shelf Water (ISW)

Ice Shelf Water exists near the ice shelves primary in the Filchner Depression at depths around 400 m. According to Carmack and Foster (1975 a), WSW, which flows under the ice shelf lowers its temperature and salinity due to melting of shelf ice. The resulting water mass is called Ice Shelf Water (ISW).

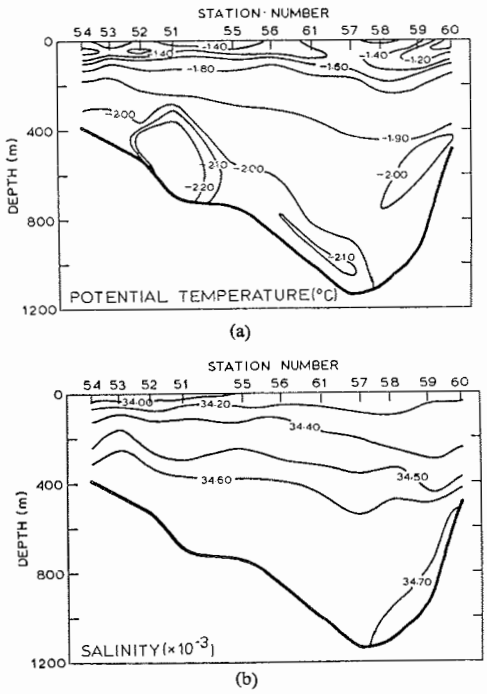

Figure 51: Potential temperature (a) and salinity (b) along section IIIa (IWSOE 1973) across the Filchner Depression at about 78°S. The western slope is represented to the left (Carmack and Foster, 1975 a).

The temperature and salinity sections along the Filchner Ice Shelf front (Figure 51) feature ISW cores with potential temperatures < -2.0°C over the western and eastern slope of the Filchner Depression in 200-600 m depth. The density distribution predicts a cyclonic flow of ISW in the depression. At about 77°S (Station 49 of Figure 52), ISW overrides the warmer high salinity WSW. Foldvik (private communication) has measured an outflow of ISW at the sill of the Filchner Depression near 74°S.

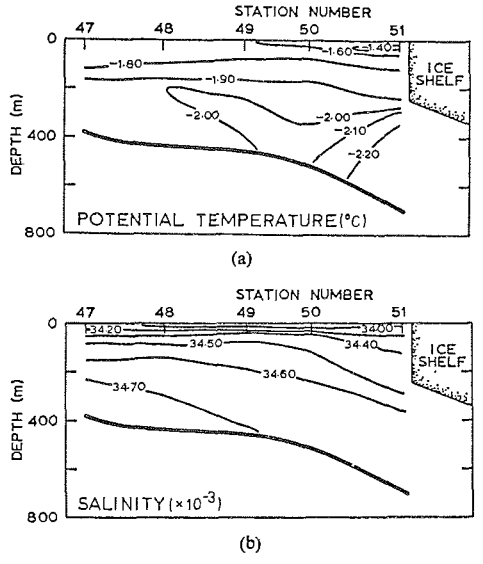

Figure 52: Potential temperature (a) and salinity (b) along section III (IWSOE 1973) (Carmack and Foster, 1975 a).

Occasionally ISW ascends at the ice shelf front with temperatures of -2.2°C, close to the freezing point at 400 m depth. The upwelling of this in situ-supercooled water could be caused by katabatic winds.

3.4.2 Circulation

3.4.2.1 Weddell Gyre

An elongated cyclonic gyre dominates the oceanic circulation of the Weddell Sea. It extends from the Antarctic Peninsula to about 20°-30°E (Deacon, 1937) or even 40°E (Gordon et al., 1981), as one can conclude from the dynamic topography relativ to 5MPa in Figure 53.

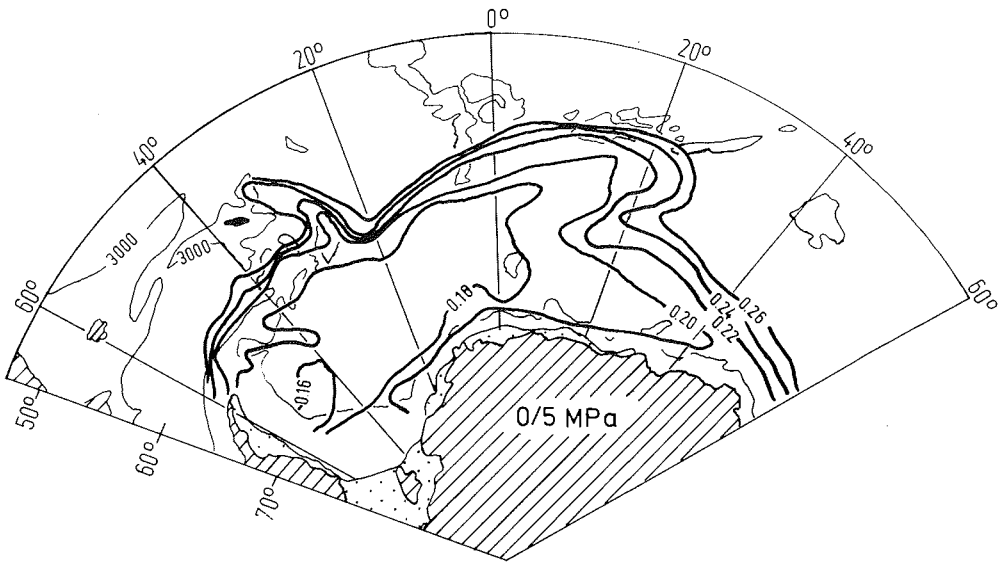

Figure 53: Dynamic topography of the sea surface relative to 5 MPa in dynm (Gordon et al., 1981).

The flow direction is to the northeast along the South Scotia Ridge (west of 25°W), the America-Antarctic Ridge (25°W-0°) and the Mid-Ocean Ridge (west of 20°E). Starting at the Greenwich meridian, the current becomes weaker and turns to the south. Recycling to the west along the Antarctic coast is extended up to 40°E. Finally, the barrier of the Antarctic Peninsula forces the flow northward again. The coastal current is strongly baroclinic east of 20°W. Along the shelf break, this current is about 100 km wide. Its speed reaches 40cms^{-1} (Carmack and Foster, 1977) so that the volume transport of mainly WDW amounts to 12.5 x 10^6m^{3}s^{-1} (Seabrooke et al., 1971). At the northeastern boundary of the Filchner Depression (75°S 29°W), a divergence in the near-surface flow generally exists (Gill, 1973). The water masses propagate predominantly along the coastline towards the Filchner Ice Shelf (Fig. 54). The remaining water continues westward along the shelf break separating shelf water from WDW below 200 m depth. This contour current was investigated at 74.4°S 40°W by Foldvik and Kvinge (1974 a) with the aid of two current meters, moored at 634 m and 640 m water depth (about 21 m above the bottom) for one year. They found a more or less westerly (280°) current with a northward deflection from the isobaths of 7°. The mean velocity in summer (February to March) was 6.1 cms^{-1}. Higher values with a maximum of 7.3 cms^{-1} appeared in the winter months June and July. The component normal to the isobaths obtained its maximum during the period of strongest sea ice growth from April to May. Since the sea surface velocities

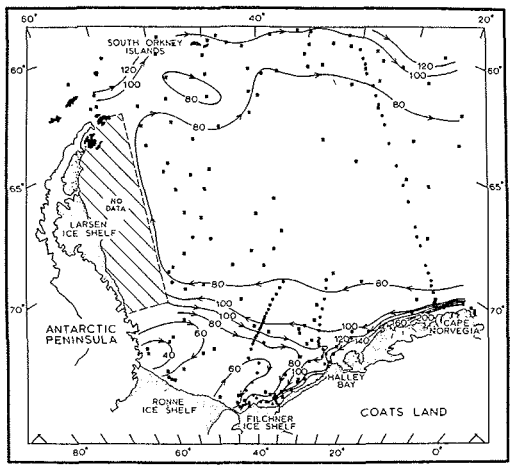

Figure 54: Dynamic topography of the 0.5 MPa-surface relative to 3 MPa. Arrows indicate relative direction of the flow (Carmack and Foster, 1977).

derived from the "Deutschland" and "Endurance" drifts ranged from 5 to 6 cms^{-1}, respectively in the same area, one may, as a first approximation, assume that this flow is primarily barotropic.

Only sparse information exists about the circulation along the Antarctic Peninsula due to the permanent ice cover. The "Deutschland" drift revealed a northward surface current with a mean velocity of 7.3 cms^{-1} (Brennecke, 1921). More recent buoy drift data covered the velolcity range from 1.7 to 8.8 cms^{-1} (Gordon et al., 1981). The total volume transport has been estimated to be 76 x $10^6 m^3 s^{-1}$ (Gordon, 1983).

The north-western branch of the Weddell Gyre is described with the aid of the hydrographic sections VI and VII in Figure 42 and a one-year current meter record at 66°S 41°W in 4504 m depth (50 m above the bottom). The annual mean of the current vector pointed to the northeast, with an easterly component of 0.14 cms^{-1} and a northerly component of 1.3 cms^{-1}. Velocity and temperature fluctuations are larger in summer than in winter. They seem to be caused by cyclonic cold-core eddies with the baroclinic Rossby Radius of Deformation of approximately 17 km (Foster and Middleton, 1979).

The hydrographic sections VII and I (Fig. 42) combined with current measurements along a profil between the South Sandwich Islands and Cape Norvegia were applied to determine the water mass outflow of the Weddell Sea. The mean velocity between 60°S and 67°S was estimated at 0.8 to 4.34 cms^{-1} with an easterly to northeasterly direction in a depth of 4100 m. Maximum speed values were found at the base of the South Scotia Ridge decreasing towards the centre of the Weddell Gyre at 67°38'S 20°26'W (Carmack and Foster, 1975 b). The velocity field of the adjusted geostrohpic flow (relative velocity profiles adjusted to direct current measurements) is displayed on Figure 55.

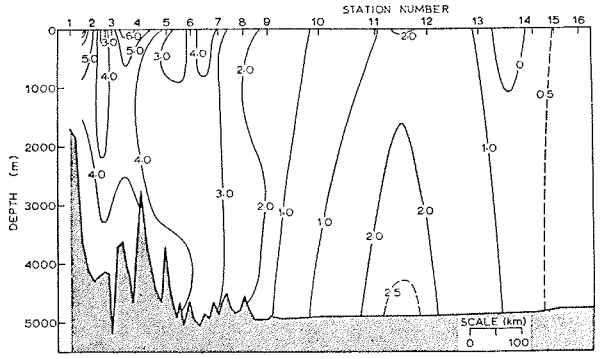

Figure 55: Adjusted velocity distribution along section VII (IWSOE 1973). Velocities are in cms^{-1} and positive values are to the east (Carmack and Foster, 1975 b).

The calculated transport of water out of the Weddell Sea in units $10^6 m^3 s^{-1}$ amounts to:

1.2 Winter Water
25.6 Warm Deep Water (including Modified Warm Deep Water)
53.1 Antarctic Bottom Water
15.6 Weddell Sea Bottom Water for $\Theta \leq -0.7°C$
1.4 Antarctic Surface Water for $S < 34.3 \times 10^{-3}$

96.9 Total transport (Carmack and Foster, 1975 b)

This total transport exceeds the maximum Sverdrup value of the western boundary current of Gordon et al. (1981) by about 20 %. The difference may be explained by the contribution of the Antarctic Circumpolar Current to the Weddell Gyre. But considerable uncertainties still exist since the record length of the current measurements of 96-345 hours does not cover the whole variability of the flow.

The major portion of AABW exported from the Weddell Sea consists of water that has entered the Weddell Sea with the southeastern branch of the gyre.

Carmack and Foster (1977), analysing the abyssal ocean with the aid of potential temperature and salinity in the bottom layer of the southwestern shelf and the western Weddell Sea Basin, found that the cold water from the wide shelf advances to the north and mixes in a frontal zone near the continental shelf break west of 40°W (Fig. 56). A tongue of WSBW with potential temperatures of $\theta < -0.85$°C spreads along the continental rise up to 63°S. There it turns to the east forced by the topography of the South Scotia Ridge, which also causes a southward deflection at about 32°W. East of 25°W the outflow of the Weddell Sea gains a northeasterly direction.

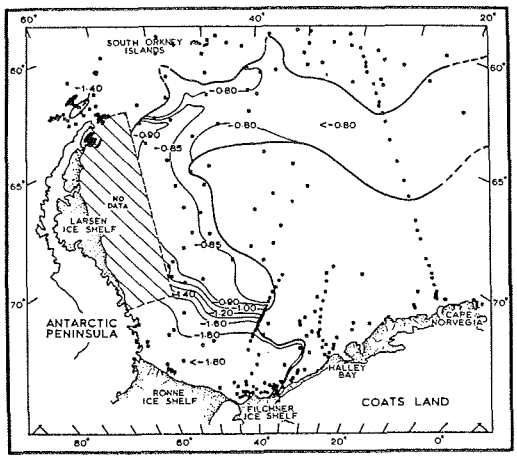

Figure 56: Potential temperature distribution (°C) in the bottom layer of the Weddell Sea shelf and western oceanic domains (Carmack and Foster, 1977).

The amplitudes of the tidal currents in the deep water of the Weddell Sea for the main harmonics are:

$K_1 = 0.46$ cms^{-1} $\quad M_2 = 0.69$ cms^{-1}
$O_1 = 0.45$ cms^{-1} $\quad S_2 = 0.58$ cms^{-1}

K_1: Luni-solar diurnal $\quad M_2$: Principal lunar semi-diurnal
O_1: Principal lunar diurnal $\quad S_2$: Principal solar semi-diurnal

(Middleton and Foster, 1977).

In each case the current vectors rotate clock-wise. 72 % and 50 % of the respective diurnal and semi-diurnal tidal motion are barotropic in agreement with the predominantly barotropic nature of the Weddell Sea circulation.

At the shelf edge (74°8'S 39°20'W) the corresponding velocities are:

K_1 = 11 cms^{-1} M_2 = 3 cms^{-1}
O_1 = 4 cms^{-1} S_2 = 3 cms^{-1}

(Foldvik and Kvinge, 1974 a).

3.4.2.2 Circulation on the shelf

According to the dynamic topography of the 0.5 to 3 MPa layer (Fig. 54) the surface circulation on the southern shelf of the Weddell Sea is characterized by a cyclone with two centres. Since the data base supporting the flow pattern of Figure 54 in the southern region is sparse, future observations may lead to some revision of details.

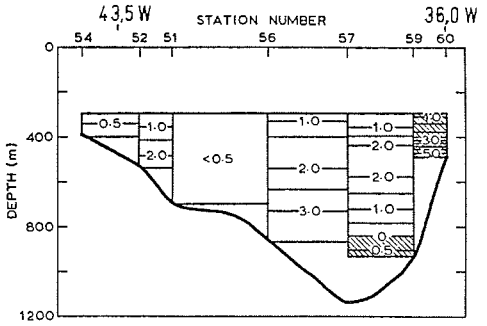

Figure 57: Geostrophic velocities (cms^{-1}) relativ to 3 MPa along section III a (IWSOE 1973). Hatched areas indicate a southward transport (Carmack and Foster, 1975 a).

The circulation within the Filchner Depression is governed by the cyclonic flow of Ice Shelf Water that advances to the north over the western slope and recirculates southwards along the eastern flank (Fig. 57). Velocities relative to 3 MPa along the depression are relatively small. They do not exceed 8 cms^{-1} so that the northward transport over the western slope amounts to 0.4 x $10^6 m^3 s^{-1}$ only (Carmack and Foster, 1975 a).

4. The Bottom water formation

4.1 Influence of the wind

The production of AABW seems to be strongly controlled by atmospheric wind forcing. Along the coast, easterly and off shore winds generate and maintain Ekman transports which result in a distinct vertical circulation. On the Weddell Sea shelf this effect is generally supported by the geostrophic flow. The surface wind stress and the horizontal mass distribution support an on-shore flow component in the upper 200 metres and an off-coastal transport in deeper layers.

Gill (1973) concludes from simple model calculations that these processes account already for 36 % of the discharge of high salinity water from the Weddell Sea shelf. The major portion of the Shelf Water produced by sea ice growth at a rate of 2.75 x $10^6 m^3\ s^{-1}$ is obviously removed by the Weddell Gyre. Assuming that the Western Shelf Water mixes with Warm Deep Water and Winter Water in a (1:1) ratio $5.5 \times 10^6 m^3 s^{-1}$ WSBW would be formed. This is the upper limit of the range given by Carmack and Foster (1975 b).

The importance of wind and buoyancy-driven motions in the production of Weddell Sea Bottom Water is studied by Killworth (1973) with the aid of a two-dimensional, numerical model. His results fall in the same range as Gill's values but the density contours in the model show no bottom water formation. The bottom water produced by buoyancy-driven motions alone is negligible. However, if, additionally, the convection is forced by a surface wind stress of $\tau^x = -0.4 Nm^{-2}$ (east winds), a remarkable agreement with observations is obtained. The transport values are the same as in the purely wind driven system ($1-1.5 \times 10^6 m^3 s^{-1}$), yet the densest water is found over the shelf. The lower half of the southern slope and the flat bottom are covered by a water mass with the characteristics of bottom water (Fig. 58). Higher values for the wind stress do not change bottom water generation but do improve the density structure of the model. In spite of some uncertainties in detail, these model experiments clearly emphazise the importance of windstress in bottom water formation.

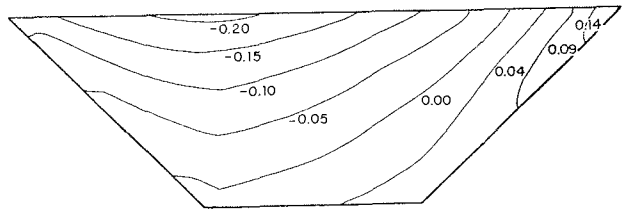

Figure 58: Modeled density structure in the Weddell Sea for $\tau^x = -0.4 Nm^{-2}$. Right corner symbolized the shelf area (Killworth, 1973).

A further wind effect in this respect is the weakening of the pycnocline in the centre of the Weddell Gyre through Ekman divergence. Gordon and Huber (1984) speculate that this fact may form a necessary condition for deep oceanic convection during sea ice growth and thus favour the initiation of polynyas.

4.2 Surface cooling and salt rejection during freezing periods

4.2.1 Sea ice growth and haline convection

Compared to the World Ocean and especially to the Arctic Ocean, the Southern Ocean is characterized by a weak pycnocline, which is a consequence of the small fresh water input and the upwelling of warm, more saline Circumpolar Deep Water at the AAD. In the Weddell Gyre the pycnocline lies in about 100 m depth in the centre and slopes down to about 200 m in the outer parts. The Brunt-Väisälä frequency, which characterizes the maximum frequency of possible internal gravity waves, ranges around 2×10^{-3} s^{-1} (Foster and Carmack, 1976 b; Middleton and Foster, 1980). Ocean-atmosphere heat exchange and sea ice formation in winter enhance mixing across the pycnocline and thus the intensity of upward heat and salt fluxes. Hence the pycnocline is weakest at the end of winter.

With decreasing solar radiation, the cooling of the surface waters generally begins in February in the southern part of the Antarctic pack ice zone. The induced thermal convection generates a mixed layer which finally accommodates the Winter Water of the last winter. The growth rate of the mixed layer critically depends on the density difference at the lower boundary. Prior to freezing, the most important contributions to surface cooling come from sensible and latent heat fluxes into the atmosphere (Danard et al., 1983).

Sea ice growth is the result of closely coupled dynamic and thermodynamic processes. Dynamic effects are related to wind and current stresses, the Coriolis force, the dynamic topography of the sea surface, ice interaction, and inertial forces. They influence the distribution and thickness of the sea ice (Hibler, 1979).

Melting and freezing during the sea ice development is thermodynamically controlled by the heat transport across the ice boundaries (Killworth, 1979) in the form:

$$\frac{dh_I}{dt} = \frac{1}{\rho_I L} (Q_{IA} - Q_{WI})$$

Q_{IA}: heat flux from the ice to the atmosphere including radiation

Q_{WI} : heat flux from the water to the ice

h_I : ice thickness

ρ_I : ice density

$L \approx 3 \times 10^5$ J/kg: latent heat of ice melting.

Q_{IA} is proportional to the vertical temperature gradient in the sea ice. For thin ice (h_I<0.8m), the subsequent linear relationship holds approximately (Parkinson and Washington, 1979):

$$Q_{IA} = \frac{k_I}{h_I} (T_F - T_{IS})$$

T_{IS}: surface temperature of the sea ice

T_F : freezing point temperature of sea water

k_I : thermal conductivity of sea ice.

When the ice gets thicker, it stores heat and the temperature profiles become nonlinear. In this situation surface heat fluxes do not immediately cause freezing or melting (Maykut, 1982). The thermal conductivity of sea ice depends on temperature and salinity. It is the first approximation given by (Untersteiner, 1961):

$$k_I = k_{I0} + \gamma S_I/T_I$$

S_I, T_I: salinity and temperature of sea ice, respectively

k_{I0} = 2.04 $J(ms°C)^{-1}$: thermal conductivity of pure ice

γ = 117.3 $J(ms)^{-1}$

The freezing rate is reduced when snow covers the sea ice. In such situations the heat flux at the surface diminishes according to (Maykut, 1982):

$$Q_{SA} = \frac{k_I k_S}{k_S h_I + k_I h_S} (T_F - T_{SS})$$

Q_{SA} : heat flux from the snow to the atmosphere

T_{SS} : surface temperature of the snow

h_S : thickness of the snow cover

k_S = 0.31 $J\ (ms°C)^{-1}$: thermal conductivity of snow.

The release of latent heat during the freezing process and the reduction of the freezing point temperature with increasing salinity due to brining diminish sea ice growth. The heat exchange between water and ice is, to a large extent, also controlled by the vertical mixing in the water column by e.g. haline convection.

A molecular layer of less than 1 cm in thickness with a relatively high salt content forms just below the sea ice (Lake and Lewis, 1970; Lewis, 1974). The vertical salinity gradient predominantly determines the vertical density distribution. When the latter becomes unstable, haline convection in the form of filaments and fingers with vertical scales of 25 - 30 cm and radii of 0.1 - 0.2 cm is initiated in the upper layer of the

water column (Foster, 1969). When the density of this layer has passed some critical value, larger convective elements can extend the mixing into greater depths as far down as 2000 m (Foster, 1972 b). Actually, neither models nor measurements are available to describe the details of these processes sufficiently.

Apart from vertical mixing horizontal advection by e.g. tidal currents may also contribute to the heat transfer between ice and the adjacent water (Csanady, 1972). Measurements near Mawson Station indicate that the sensible heat flux from water to ice drops from 20 - 40 Wm^{-2} in autumn to 10 Wm^{-2} in mid-winter. A parallel reduction in the vertical haline mixing also takes place. In September/October,a secondary maximum of 15 to 20 Wm^{-2} sensible heat flux from water to ice is observed at several Antarctic coastal stations (Mawson, Molodezhnaya, Halley, Mirny, Davis). This phenomenon is caused by a southward advection of warm saline surface water. On the average the sensible heat flux from the ocean to the sea ice amounts to 10-15 Wm^{-2} during the period of ice growth (Allison, 1981).

During periods of rapid freezing, more salt is captured in the ice than by slow ice growth, although due to gravity, the brine migrates downwards with time. Thus, a vertical salinity gradient develops in older sea ice , which is proportional to the brine release at the bottom. In spite of this retardation of salt injection, the salinity of the surface water is more or less proportional to the ice growth rate (Killworth, 1979):

$$\frac{dS}{dt} = \frac{\sigma}{h}\frac{dh}{dt}$$

h: thickness of the surface layer
σ: salinity difference between sea water and sea ice.

4.2.2 Large-scale salt and heat fluxes

Upwelling of Circumpolar Deep Water at the AAD transports heat and salt from lower layers to the sea surface. The zonally integrated upwelling amounts to about $60x10^6$ m^3s^{-1}. This volume flux is associated with an upward salt flux of $36x10^6$ kgs^{-1}. Since the freshwater input of about 500 mma^{-1} south of the PF compensates only for $11x10^6$ kgs^{-1}, deep convection must exchange $25x10^6$ kgs^{-1} between the Antarctic Surface Water and the bottom water. The latter advects the salt northwards (Gordon and Taylor, 1975 a).

Gordon (1981) relates the upward heat flux through CDW upwelling to the melting rate of the Antarctic pack ice in spring and summer. Between mid-November and mid-January the Antarctic pack ice area reduces from $17.5x10^6km^2$ to $6.5x10^6km^2$. This requires a heat flux of 64 Wm^{-2} for a mean ice thickness of 1.25 m (Heating of the surface water and iceberg melting are neglected). The ocean gains heat of 34 Wm^{-2} through sea surface heating and about 30 Wm^{-2} must be supplied by vertical transports. If an

upwelling velocity of $1x10^{-4}$ cms^{-2} (Gordon et al., 1977 a) and a temperature difference of 3°C between CDW and AASW are assumed, the heat flux amounts to 13 Wm^{-2}. Consequently 17 Wm^{-2} are still left for small scale processes such as convection and turbulent diffusion.

To compensate for the mean annual heat loss of about 30 Wm^{-2} of the Southern Ocean a poleward heat transport of about $60x10^{13}W$ across 60°S is required (Gordon, 1981; Hastenrath, 1980, 1982). This value is half as large as the atmospheric poleward heat flow across 60°S (Trenberth, 1979). Apparently the major portion of the heat is transported southwards by a small number of ocean eddies with time scales of 5 to 60 days (Sciremammano, 1980; DeSzoeke and Levine, 1981).

4.2.3 Convection on the shelf

In front of the Filchner-Ronne Ice Shelf, cold katabatic winds frequently push the sea ice off-shore and generate leads. Sea ice formation and thus also an increase of salt in the water column, is here intensified (Mather and Miller, 1967; Gill, 1973). The mean northward drift of the sea ice in the southwestern Weddell Sea lies at 2600 md^{-1}. This coastal effect leads to an increase of sea ice production in the entire shelf area from 1.6 m (Foster, 1972 b) to 2.1 m for 6 months during winter. The ice growth has its maximum of about 1 m per month in a 30 km wide zone along the ice front and decreases seawards. Since about 0.4 m of ice melts during 6 months of the summer season, an annual ice growth rate of 1.7 m must be assumed in the southern shelf area of the Weddell Sea (Gill, 1973). Ackley (1979) speculates that this rate might be even 3.7 ma^{-1} because freezing occurs also in summer and ridging effects are not included in the above estimates. Foster and Carmack (1976 a) compute a northward sea ice transport across the shelf break of $1.5x10^{4}$ m^3s^{-1}, which corresponds to an ice growth rate of 0.95 ma^{-1} (the shelf occupies an area of $5x10^{5}km^2$). This value would mean a salt release of about $4x10^{5}$ kgs^{-1}. Due to the great width of the southern Weddell Sea shelf, the salinity of the shelf water is one of the highest encountered on the Antarctic shelves.

The katabatic coastal winds cause an upwelling of Ice Shelf Water which may become supercooled on its way upwards and ice crystals may form (Dieckmann et al., in press). The latter are buoyant, ascend to the surface layer and may thus contribute to the growth of pack ice. The rejected brine mixes with the surrounding water and descends to greater depths. The intensity of these processes depends on the production rate of ISW and the wind forcing (Foldvik and Kvinge, 1974 b, 1974 c). Since icebergs act as heat sinks of the surface water and sources of supercooled water on their upwelling side, they may generate similar phenomena as the ice shelf edge but in offshore regions.

The shelf water circulation on the basis of the above-mentioned processes is simulated with the aid of a baroclinic two layer model by Killworth (1974). In his model the shelf has a flat bottom, and the Filchner Depression and the continental slope are not specified. The density is a function of salinity only. The salt input at the sea surface decreases northwards and does not vary zonally. The mean salt input corresponds to an ice growth of 2 m per 6 months with a maximum of 8 m per 6 months at the ice front of the Filchner-Ronne Ice Shelf. Wind forcing on the shelf water is neglected. The inital stratification is chosen by a density difference of 0.25 σ_T -units between the two layers, which approximates the summer conditions of the shelf water.

The salt injection at the sea surface causes a southward density gradient and thereby an eastward geostrophic current in the upper layer. The lower layer velocity compensates for the mass transport of the upper one. Downwelling at the eastern and upwelling at the western boundary result in southward geostrophic currents at both boundaries in the upper layer. This cycle of positive coupling is damped by the horizontal turbulent diffusion of salt. Convective overturning starts at the southern boundary after 2.5 months in the model. During summer the salt input at the sea surface is turned off.

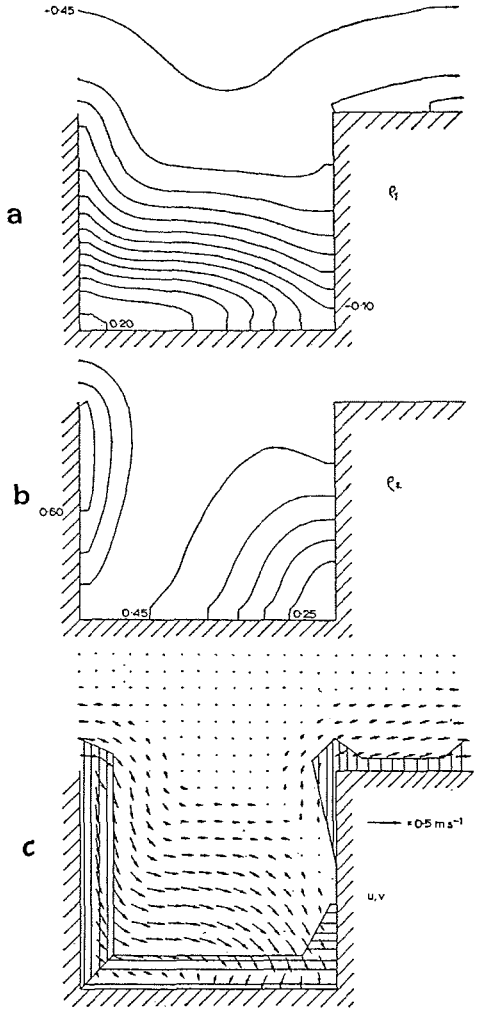

Figure 59:

Conditions at the end of the first summer.

a) Density distribution of the upper layer (difference of isopycnals: 0.05≙0.025)
b) density distribution of the lower layer
c) velocity field of the upper layer.
The horizontal hatched area indicates the downwelling region, the vertical hatched area the upwelling region (Killworth, 1974).

Figure 59 shows the results of the model at the end of the first summer. The upper layer exhibits a large meridional density gradient. The zonal density difference across the total region amounts to 0.15 σ_T-units in agreement with observations. In the lower layer both the density maximum and the upwelling centre migrate northwards along the western boundary. In this region dense shelf water leaves the shelf at a rate of 0.20 to 0.33 x 10^6 m^3s^{-1}, which is about half as much as estimated by Gill (1973). During winter, the model outflow increases slightly in agreement with the observations of Foldvik and Kvinge (1974 a). At the end of the second summer, a secondary density maximum appears in the southwestern corner of the shelf and the meridional density gradient increases in contrast with their observations. Obviously long term integration requires a closer adaptation of the model to the actual situation.

4.2.4 Convection in the open ocean

Deep convection in the central Weddell Sea is favoured by a relatively weak pycnocline. This could be achieved by the cyclonic circulation of the Weddell Gyre and some freshwater input into the Antarctic Surface Water. Observations of Gordon (1978, 1982) suggest further more that conditions for deep convection may also exist in mesoscale cyclonic eddies and in polynyas.

In eddies a rapid cooling of a relatively shallow mixed layer can initiate overturning which finally extends down to nearly 2000 m depth, as observed by Gordon (1978). In the centre of convection elements vertical velocities of 10 cms^{-1} are possible (Gascard, 1973). Volume and characteristics of the deep water formed by such processes depend on duration and intensity of the surface cooling (Lacombe, 1974).

Chimney convection has been studied by Killworth (1979) with the aid of a one-dimensional model. The initial state of the water column is given by the temperature and salinity distribution observed by Gordon (1978). The sea surface is assumed to be ice-free at the beginning. Figure 60 shows the results of the quasi-static model for Station 115 of Gordon (1981). The continuous line refers to case A: heat transfer between the mixed layer and the ice cover assumes its maximum. The dotted line refers to case B: no heat flux from the mixed layer to the sea ice. The entire heat loss of the water column is compensated by sea ice formation. The real behaviour lies between these extremes.

The ocean heat loss Qo can be related to the time axis: Qo=O, equals early autumn; Qo=2.7×10^4 characterizes the beginning of winter; Qo = 7.8×10^4 marks the beginning of spring. In case A, the mixed layer reaches the freezing point during the first winter month. Due to the continuous growth of the mixed layer by convection, its heat content increases and the ice cover melts

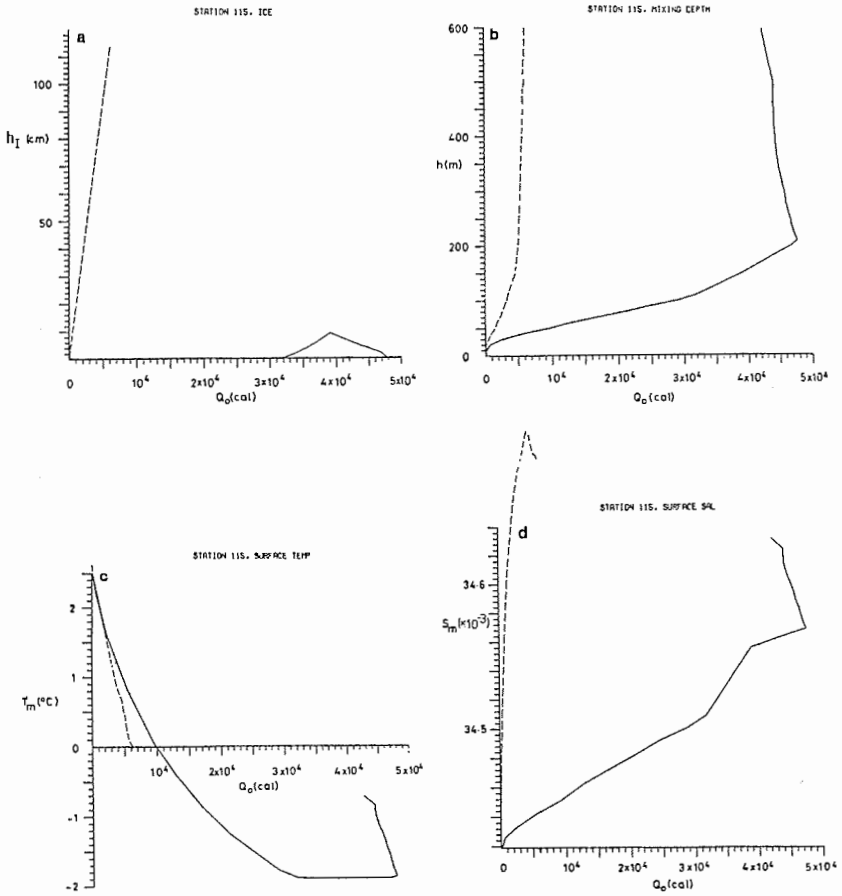

Figure 60: Results of the quasi-static model for CTD 115. a) Ice thickness (h_I), b) depth of the mixed layer (h), c) temperature of the mixed layer (T_m), d) salinity of the mixed layer (S_m) as a function of the heat loss at the sea and ice surfaces (Q_o) (Killworth, 1979).

away after 24 days. From then on a strong surface cooling causes an intensive vertical mixing down to more than 3000 m depth. Stations outside the eddy experience enhanced mixing 3 to 4 months later as in case A with a mixed layer growth to depths of 180 to 290 m. The overturning starts where the influence of Warm Deep Water is strongest.

Deep convection develops only within eddies when cyclonic circulation diminishes the static stability of the upper 300 m in the eddy centre by a positive density anomaly of 0.1 σ_T-units. This preconditioning seems to be necessary to enable surface cooling and salt rejection in winter to generate the observed chimney effect.

Maintenance of the Weddell Polynya has been examined with the aid of a one-dimensional convection model by Martinson et al. (1981). The authors also give a rough estimate of the production of Weddell Sea Deep Water in the open water area. According to temperature profiles obtained during winter in the Weddell Sea

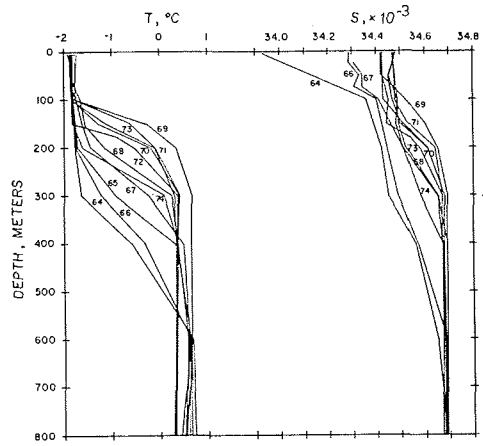

Figure 61: Potential temperature and salinity profiles based on data obtained during the DEUTSCHLAND-drift from March to December 1912 by Brennecke (1921). Numbers indicate the profiles (Foster, 1972 b).

(Fig. 61) the model consists of two ideally mixed layers. The two-layer approximation assumes one of four possible states, sketched in Figure 62. States 2 and 4 show the stratified situation with $\rho_1 < \rho_2$, while states 1 and 3 indicate a fully mixed water column.

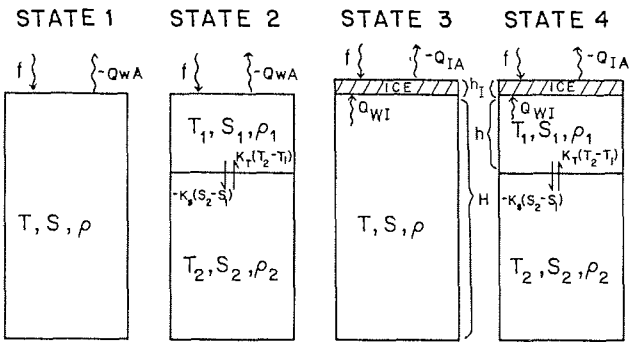

Figure 62: Schematic representation of the four states used to describe the situation within the Weddell Polynya.
f: freshwater input
K_T, K_S: exchange coefficients for heat and salt parameterizing upwelling, turbulent exchange and double diffusion
$K_T(T_2-T_1)$: heat exchange between the two levels
$K_S(S_2-S_1)$: salt exchange between the two levels
T_1, S_1: temperature and salinity of the upper level (WW)
T_2, S_2: temperature and salinity of the lower level (WDW); $T_2 > T_1$
h: depth of the upper level = 200 m
H: total depth = 4000 m

(after Martinson et al., 1981)

A realistic diagram of sequences of states is displayed on Figure 63. The polynya starts at point P, i.e. the ice is melted

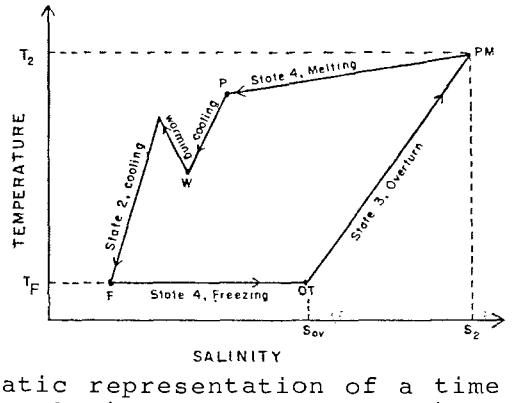

Figure 63: Schematic representation of a time dependent T/S-diagram showing a one-year cycle in the upper level of the polynya water column. Indices are explained in the text (Martinson et al., 1981).

and the water column assumes state 2. Surface cooling and the continuous fresh-water input of $0.78 my^{-1}$ ($0.21\ cmd^{-1}$) cause a strong temperature drop and a slight salinity decrease to point W when summer radiative warming starts until in autumn cooling leads again to a density increase of the upper layer. Finally, the freezing point of seawater is reached (point F). During the ice growing phase the salinity of the upper level increases to:

$$S_{ov} = S_2 + \alpha\beta^{-1} (T_F - T_2) = 34.526 \times 10^{-3}$$

α: thermal expansion coefficient, const. = $5.82 \times 10^{-5}\ ^{o}C^{-1}$
β: haline expansion coefficient, const. = 0.8

Beyond this value overturning occurs if, at the beginning of sea ice growth (point F), S_1 is not less than a certain critical value S_{crit}, as shown in Figure 64. This quantity decreases with increasing duration of ice production time.

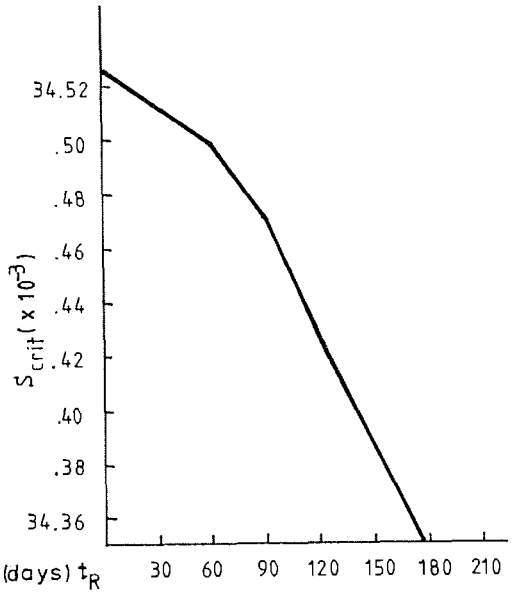

Figure 64: S_{crit} as a function of time remaining in the cooling season after ice onset (t_R) in days (after Martinson et al., 1981).

Assuming $S_1 > S_{crit}$, the system overturns at point OT and reaches state 3. The heat input to the upper layer by upward mixing of warmer and more saline water causes ice melting and thus a new formation of the stratification assigned to state 4. Melting continues until the starting point P is reached again. The proposed cycle of states is only possible under certain assumptions of fresh water supply, a sufficient freezing period and special vertical temperature and salinity distributions.

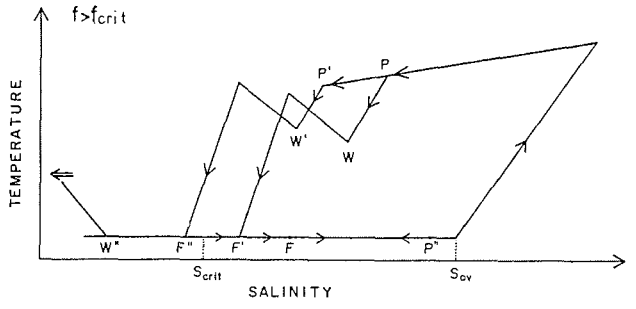

Figure 65: As Figure 63 for $f > f_{crit}$ over several years up to stable cycling (Martinson et al., 1981).

For the freshwater input there exists a critical value $f_{crit} = 0.77 my^{-1}$. In case $f > f_{crit}$, the cycle represented in Figure 63 modifies to the one reproduced in Figure 65. Here a polynya opens up during two seasons only since the ice growing period is also growing because of the decreasing salinity of the upper level in time.

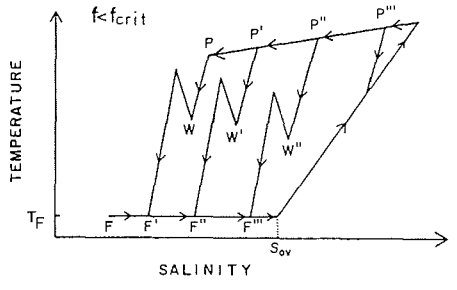

Figure 66: As Figure 63 for $f < f_{crit}$ over several years up to stable cycling (Martinson et al., 1981).

For $f < f_{crit}$ the cycle of Figure 66 is likely. The permanent increase of S_1 reduces the required period of winter cooling. Eventually overturning results just from cooling without an additional salt input through ice growth. Then the mixing state 1 is valid and the polynya exists permanently.

The lower limit of Weddell Sea Deep Water production in the Weddell Polynya is estimated by Martinson et al. (1981) to be $1 \times 10^6 m^3 s^{-1}$. This water mass has a density of σ_2 =37.22-37.23 and is 0.1°C cooler and 0.01×10^{-3} less salty than the surrounding deep water.

Gordon (1982), assuming that the entire Warm Deep Water ($1.5 \times 10^{15} m^3$) with temperatures $\Theta < 0$°C observed in the polynya area 1977 was formed by surface cooling during three polynya years, derives a maximum production of $31.7 \times 10^6 m^3 s^{-1}$ during a 6 month winter season. Since Winter Water contributes 10 - 20 % to WDW the minimum WSDW production amounts to 3.2 to 6.4 x $10^6 m^3 s^{-1}$ for the same time interval.

4.3 Mixing processes

4.3.1 Mixing on the continental slope

Bottom water production on the continental slope in the southwestern Weddell Sea proceeds in three steps which are schematically portrayed in Figure 67.

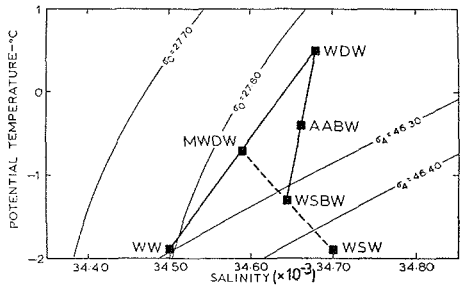

Figure 67: Mixing scheme for the bottom water production in the southwestern Weddell Sea (Foster and Carmack, 1976 a).

At first Winter Water ($T \approx -1.9$°C and $S = 34.50 \times 10^{-3}$) and Warm Deep Water (0.5°C, 34.68×10^{-3}) combine to form Modified Warm Deep Water (-0.7°C, 34.59×10^{-3}). Then MWDW mixes with Western Shelf Water (1.9°C, 34.70x10-3) to form Weddell Sea Bottom Water (-1.3°C, 34.645×10^{-3}). Finally, WSBW descending down the continental slope and following the isobaths of the western and northern Weddell Sea mixes with WDW to become Antarctic Bottom Water (-0.4°C, 34.663×10^{-3}). Details of the mixing processes are still uncertain and will not be discussed here.

On the average AABW is composed of 1/8 WW, 2/8 WSW and 5/8 WDW, as can be concluded from oxygen distribution (Foster and Carmack, 1976 a). Production and characteristics of the AABW depend on the production of WSW and its mixing with WDW.

The descent of dense shelf water and the mixing with surrounding waters are studied with the aid of entraining plume models by Killworth (1977). The plume is driven by the density difference between the plume and its environment. Laboratory experiments reveal a proportionality between the plume velocity and the entrainment (Turner, 1973). The models yield realistic results only if the dependence of the thermal expansion coefficient on pressure is taken into account. No such details are important for the haline expansion coefficient.

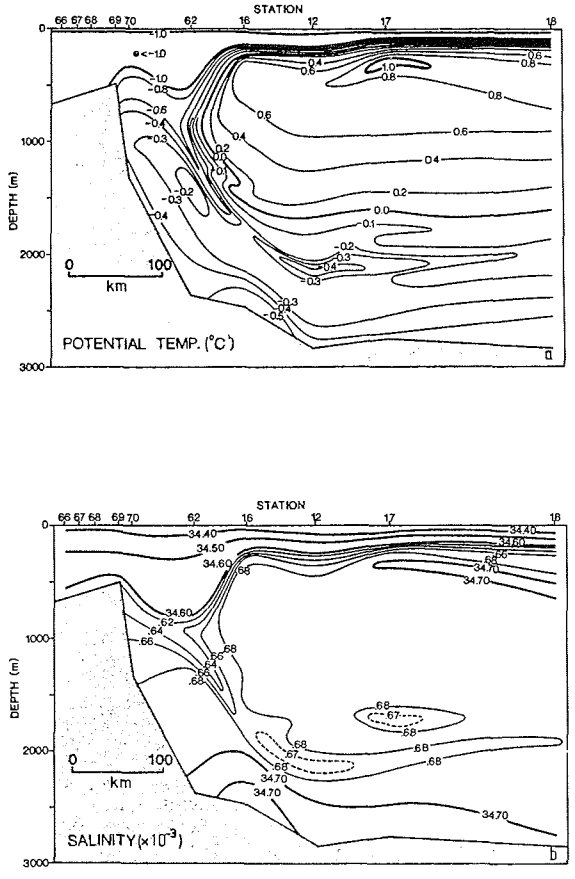

Figure 68: Vertical sections of potential temperature (a) and salinity (b) off Wilkes Land. Between stations 66 and 70 the sections run at a right angle against the shelf break, between stations 70 and 18 nearly parallel (Carmack and Killworth, 1978).

The plume model and observational data agree sufficiently with each other off Wilkes Land (150°-160°W) (Carmack and Killworth 1978). Temperature and salinity sections exhibit a relatively cold, less saline water lens at 2150 m depth with a mean width of 100 km and a mean height of 200 m, extending 800 km along the continental slope parallel to the shelf break (Figure 68). Its high oxygen and low nitrate contents suggest a formation region near the sea surface. The sinking of dense shelf water down the continental slope is also indicated by the V-shaped frontal zone, which extends from the shelf break to 1800 m depth. The sinking occured along σ_0=27.86 down to 1000 m depth and followed σ_2=37.20-37.24 farther downwards. The Coriolis force has deflected the sinking plume westwards. At the equilibrium position at about 2000 m depth, the plume water spreads out laterally. The temperature and salinity values of the lens result from the mixing of shelf water (θ=-1.9°C, S=34.64x10^{-3}) and Circumpolar Deep Water (θ=0.8°C, S=34.69x10^{-3}) at ratio of 1:1.4.

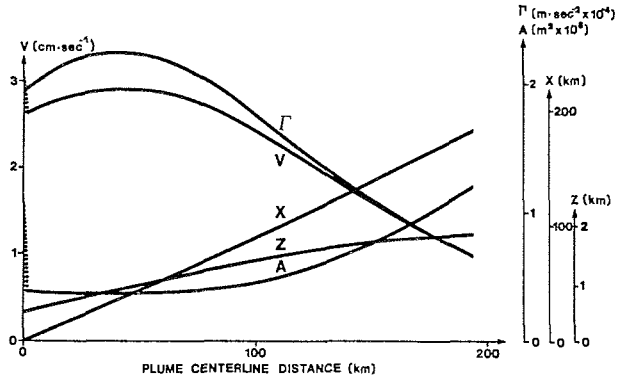

Figure 69: Results of the plume model for sinking of dense shelf water down the continental slope off Wilkes Land. The X-axis is directed westwards parallel to the shelf break, the Z-axis vertically downwards. A: cross-section area of the plume, V: plume-velocity, Γ: buoyancy force (Carmack and Killworth, 1978).

The main quantities of the plume model are displayed in Figure 69. Variations of the initial values of A and V hardly influence the results. More effective are the mean vertical ambient temperature and salinity gradients, the density and temperature differences between shelf water and CDW, and the inclination of the continental slope (Table 10). Relative cold and dense plume water, a weak stratification of the CDW and a steep continental slope favour vertical mixing. Seasonal density changes of the shelf water and temperature variations of the CDW can cause fluctuations of the plume descending depth with the result that lenses of plume water spread laterally along various density surfaces.

Parameter	Max. depth of plume
$\Gamma_o = 3.9 \times 10^{-4}\ ms^{-2}$	2458 m
$\Gamma_o = 1 \times 10^{-4}\ ms^{-2}$	1318 m
$\Delta T_o = -4\ ^oC$	3607 m
$\Delta T_o = -1\ ^oC$	1000 m
$\Phi = 3 \times 10^{-2}$	2168 m
$\Phi = 1 \times 10^{-2}$	805 m
$\delta\theta_e/\delta z = 4.7 \times 10^{-5}\ ^oCm^{-1}$; $\delta S_e/\delta z = -1 \times 10^{-8}\ m^{-1}$	2382 m
$\delta\theta_e/\delta z = 4 \times 10^{-5}\ ^oCm^{-1}$; $\delta S_e/\delta z = -1 \times 10^{-8}\ m^{-1}$	4000 m
$\delta S_e/\delta z = 0$	2220 m
$\delta\theta_e/\delta z = 6.7 \times 10^{-5}\ ^oCm^{-1}$	1676 m

Table 10: Influence of several parameters on the sinking depth of the plume.
$\Gamma_o = g/\rho_R \cdot \Delta\rho_o$: initial buoyancy force
($\Delta\rho_o$: density difference between shelf water and CDW, g: gravitational acceleration, ρ_R : reference density)
ΔT_o : temperature difference between shelf water and CDW
ϕ: inclination of the continental slope
dT_e/dz and dS_e/dz : mean vertical environmental temperature and salinity gradients (Carmack and Killworth, 1978).

The observations of Foster and Middleton (1979, 1980) suggest that such a mechanism governs the spreading of WSBW along the continental slope of the southwestern Weddell Sea. If the mean vertical ambient temperature gradient is sufficiently weak ($\leq (3\text{-}4)\times10^{-5}\,°Cm^{-1}$), the plume can sink down to the deep sea bottom. In contrast, stratification caused by the CDW does not allow plume water to sink down to the deep sea bottom (Carmack and Killworth, 1978).

4.3.2 Mixing in the open ocean

Deep water formation in the central and eastern Weddell Sea requires that cold, low saline WW mixes with warmer, more saline WDW. Surface cooling, salt rejection and the stability of the undisturbed water column determine the intensity of the mixing process. From temperature and salinity variations of the WDW Gordon (1982) estimates the mixing ratio of WW and WDW to be 1:4 to 1:9. Generally, the volume of surface water, which is included in the deep water production of the eastern Weddell Sea, is larger than its contribution to bottom water production at the continental slope. Enhanced deep water formation during the appearance of the Weddell Polynya has possibly reduced the contribution of WW to the bottom water production.

4.3.3 Double diffusive convection

The decrease of stability and salinity near the bottom towards the shelf break suggest that double diffusion controls mixing between Western Shelf Water and Modified Warm Deep Water predominantly at the shelf break in the southwestern Weddell Sea (Foster and Carmack, 1976 a).

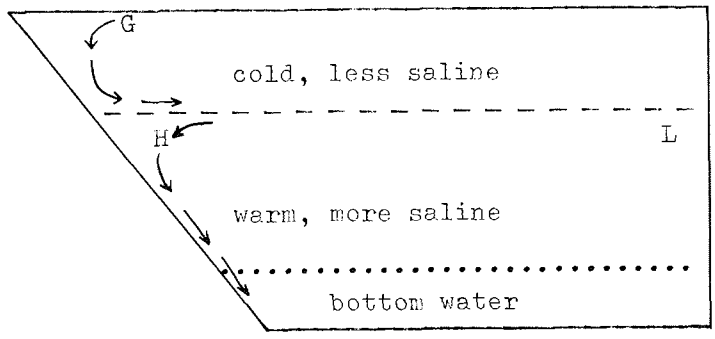

Figure 70: Sketch of the laboratory experiment by Gill and Turner (1969).

According to laboratory studies of Gill and Turner (1969), double diffusive convection, caused when cold, less saline WW lies above warmer, more saline WDW, may intensify the bottom water production at the continental slope (Figure 70). Under such conditions, convection develops in both layers. Due to the sloping depth, the density increases quicker at point H than at L. The dense water formed at H sinks down the slope and accumulates on the bottom. Salt rejection at point G forces downward motions in the upper layer, which join the low level circulation at H. At the boundary between the slope current and the surrounding waters, salt fingers may form.

Generally, the double diffusion process across the interface of WW and WDW causes step-like vertical temperature and salinity profiles. These jumps intensify towards the centre of the Weddell Gyre, where the WDW ascends closer to the sea surface (Figure 71). Obviously, the thickness of homogeneous layers depends on the strength of the mean vertical temperature and salinity gradients. Between 100 m and 530 m depth, the static stability of the water column is rather weak (the Brunt-Väisälä frequency amounts to $5.6 \times 10^{-4} s^{-1}$).

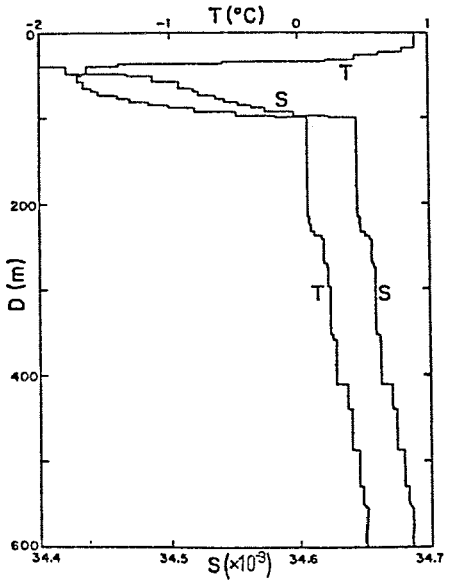

Figure 71: Smoothed vertical profiles of temperature and salinity at 68°50'S 18°20'W (Foster and Carmack, 1976 b).

The step structure of the vertical temperature and salinity profiles is maintained by the upward heat flux between WDW and WW. Tank experiments by Turner (1968) confirm the development of step structures under similar conditions. Formulae of the heat and salt flux between the small-scale layers are given by Huppert (1971) and Huppert and Turner (1972). It is not actually clear, to which extent double diffusion contributes to the deep and bottom water formation in the Weddell Sea.

4.3.4 Cabbeling-instability

Cabbeling-instability was first described by Witte (1902). Two neighbouring water masses of similar density, but with different temperatures and salinities may mix at their interface and form a water mass which is more dense than each of the original ones. The higher density is a consequence of volume contraction due to the non-linearity of the equation of state. From T/S-diagrams, the conclusion can be drawn that cabbeling-instability occurs when the mixing line between two water masses forms a tangent of an isopycnal.

From a comparison of the vertical density distribution around Antarctica, Gordon (1971 b) shows that cabbeling-instability between WW and WDW is most probable in the central Weddell Sea and in the northwestern Ross Sea. Fofonoff (1956) already pointed out that cabbeling-instability may be involved in the formation of AABW. Gill (1973) indicates that mixing of WW (θ=-1.9°C, $S > 34.465 \times 10^{-3}$) and WDW ($\theta$=0.4°C, $S=34.68 \times 10^{-3}$) enables the mixture to sink below the WDW. Foster and Carmack (1976 b) and Middleton and Foster (1980) conclude from observations that the cabbeling-instability is possibly active in summer in the central Weddell Sea between 100 m and 530 m depth. This mechanism may also become active in winter when the salinity of the WW exceeds 34.495×10^{-3} at 100 m or 34.478×10^{-3} at 300 m depth (Foster and Carmack, 1976 b).

In a two-dimensional two layer model with upper layer quantities

$T = -1.9°C, \quad S = 34.568 \times 10^{-3}$ and lower layer values
$T = 0.6°C, \quad S = 34.700 \times 10^{-3}$

Foster (1972a) deduced, for a mixing ratio of 1:1, a maximum vertical velocity of 1.6 cms^{-1} and a density increase in the lower layer. For an upper layer salinity of 34.520×10^{-3} the maximum vertical velocity reduces to 0.5 cms^{-1} and for salinities $< 34.51 \times 10^{-3}$, no cabbeling-instability exists. The formation of a 85 cm thick ice layer would cause the Weddell Sea surface water to exceed the latter value.

It has, however, not been proven that cabbeling-instability between WW and WDW or shelf water and WDW does, in fact, contribute to the deep water and bottom water formations in the Weddell Sea.

4.6 Spreading of Antarctic Bottom Water from the Weddell Sea

In the southern hemisphere, the distribution of Antarctic Bottom Water produced in the Weddell Sea can be traced by the 0°C-isotherm as well as by the 34.68×10^{-3}-isohaline. Schlemmer (1978) subdivides the AABW into three layers with potential densities relative to 40 MPa of σ_4=46.08; 46.15 and 46.21. He determines the spreading of AABW from the horizontal distribution of these isopycnals. According to the UNESCO-Equation of State for Sea Water (1980), a potential density of σ_4=46.11 (relativ to 40 MPa) results in a potential temperature of 0°C and a salinity of 34.68×10^{-3}. AABW, produced in the Weddell Sea, is evident in the Θ/S-diagrams of the Atlantic Ocean to about 40°N (Tchernia, 1980) and of the Indian Ocean to about 20°N (Kolla et al., 1976).

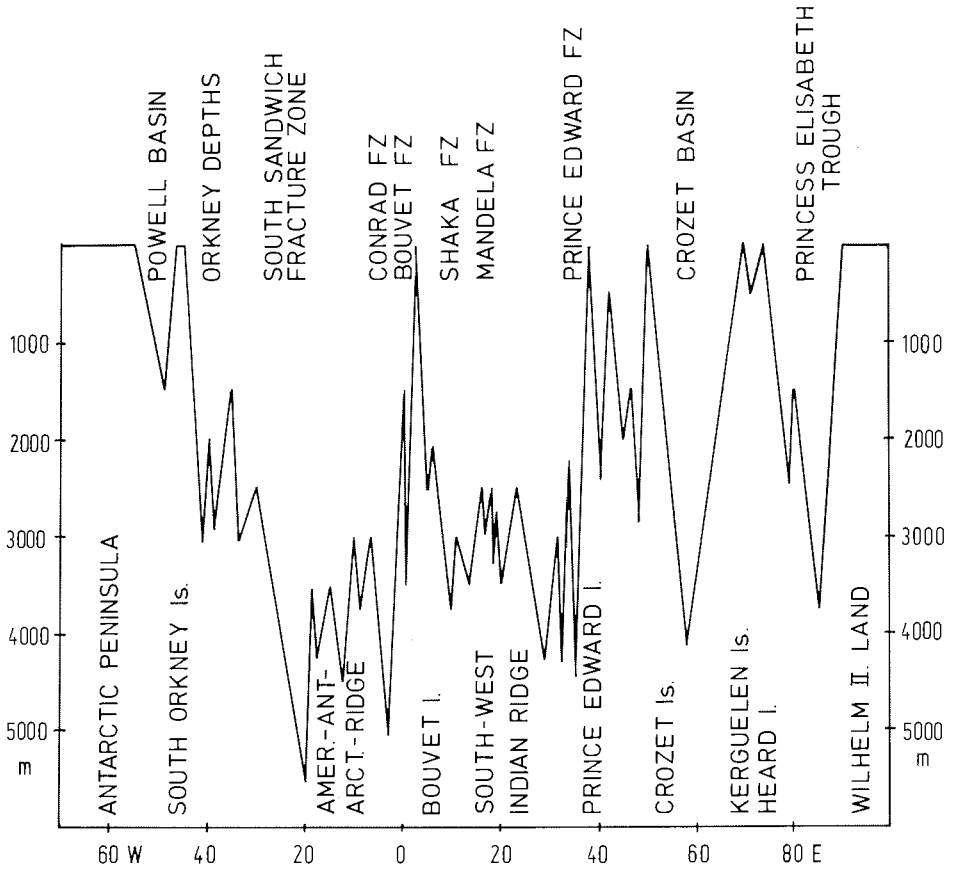

Figure 72: Distribution of sill depths along the ridges bounded the Weddell Basin (doted line in Figure 75). According to General Bathymetric Chart of the Oceans (GEBCO), 1981. Series established by H.S.H. Prince Albert I of Monaco in 1903.

The Weddell Basin is bounded by ridges which have, at some locations, sill depths greater than 3000 metres (Figure 72) enabling the migration of AABW to the north. One pathway to the Scotia Sea exists at about 40°W (IV in Figure 74), where the South Scotia Ridge has passages with sill depths of 3000 to 3200 metres. According to the isotherms in the bottom layer (Figure 73), an outflow into the Pacific Ocean seems to be unlikely. Hitherto no bottom water with $\Theta \leq 0°C$ and $S < 34.68 \times 10^{-3}$ could be observed in the northern part of the Scotia Sea, possibly due to vigorous mixing with the water masses of the ACC.

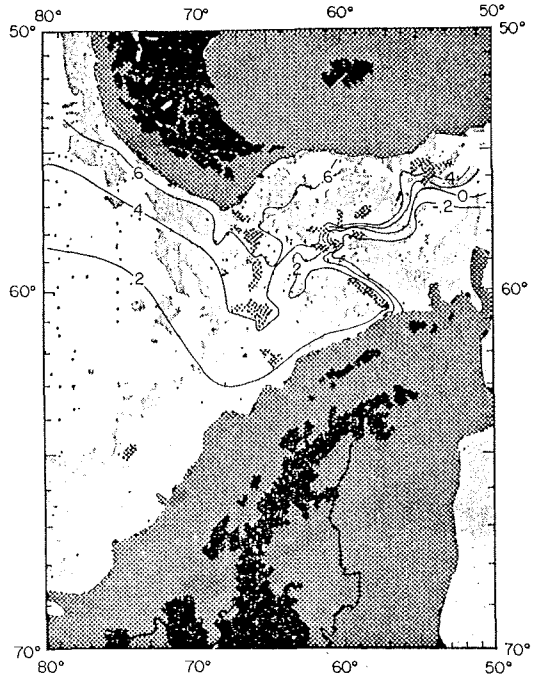

Figure 73: Potential temperature (°C) at depths greater than 3000 m in Drake Passage. Dark shading indicates depth 0-3000 m; light shading 3000-4000 m; white areas > 4000 m (Reid and Nowlin, 1971).

The measurements east of South Georgia (II in Figure 74) are insufficient to deduce an easterly flow of the AABW out of the Scotia Sea (Gordon, 1966). Georgi (1981) argues that bottom water from the South Sandwich Trench may advance westward into the Scotia Sea. Although the South Scotia Ridge has a sill depth greater than 3000 m at about 33°W (III, Figure 74), it has not yet been established that AABW enters the Scotia Sea through this passage (Patterson and Sievers, 1980).

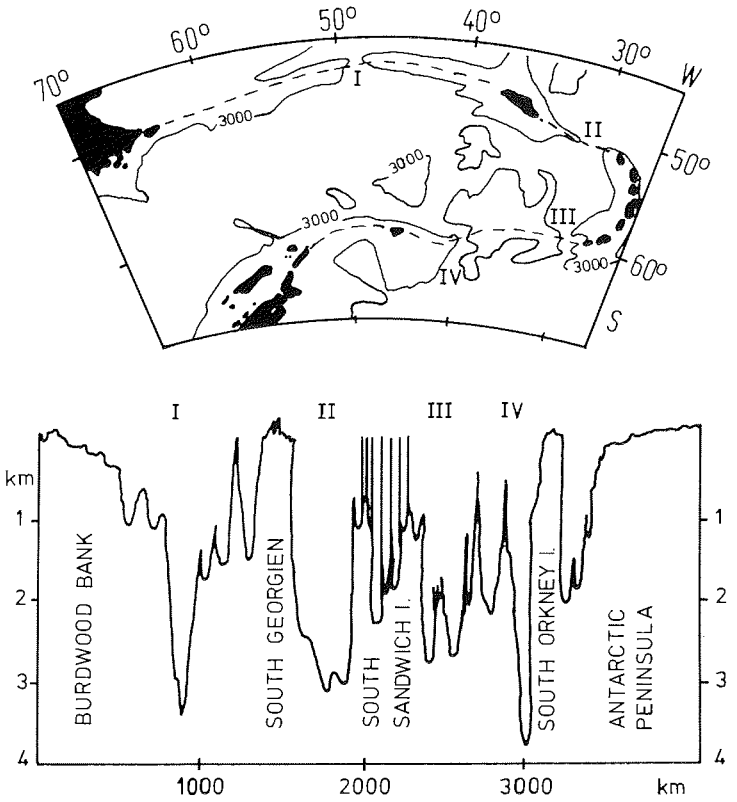

Figure 74: Schematic representation of the ridge system (broken line) bounding the Scotia Sea, and the distribution of sill depths along these line (Gordon, 1979).

South of the South Sandwich Trench, the flow of the bottom water diverges. The main portion moves to the east while the rest reaches the trench in a weak northward flow (Gordon, 1966). Below 5000 m the whole trench area is occupied by water with potential temperatures $\theta \leq -0.75$°C and salinities $S < 34.65 \times 10^{-3}$, which classify Weddell Sea Bottom Water (Carmack, 1977; Foster and Middleton, 1979).

WSBW can neither leave the trench nor advance further north. On the basis of a potential temperature section across the South Sandwich Trench Georgi (1981) assumes that a cyclonic deep circulation exists. AABW, limited by the 0°C-isotherm, flows in the upper layer to the east over the eastern flank of the trench. At the northern end it enters the Georgia Basin and possibly the Scotia Sea.

The Falkland Fracture Zone, which forms the northern boundary of the Georgia Basin, has a sill depth of less than 5000 m so that only AABW with $\theta > -0.5$°C can reach the Argentine Basin.

The cyclonic deep circulation of the Argentine Basin transports the 1000 m thick bottom layer with the Falkland (Malvinas) Current along the Falkland Plateau westwards. The motion turns then northwards forced by the Argentine continental slope (Georgi, 1981). At about 40°S the current detaches from the slope due to the influence of the southward flowing Brazil Current, and migrates northward to the Rio Grande Rise. Further extension to the north is blocked, as can be concluded from the distribution of the 0°C-isotherm (Figure 75). However Hogg et al. (1982) have demonstrated that a small portion of AABW enters the Brazil Basin through the Vema Channel. Gordon (1978) assumes that this bottom water is formed by deep convection in the oceanic domain of the Weddell Basin.

No evidence has been provided that AABW spreads northward through the more than 4000 m deep Hunter Channel (28°W 35°S). The Mid-Ocean Ridge forces the flow to turn cyclonically back toward the ACC. Consequently AABW with potential temperatures 0°C remains in the Argentine Basin in depths of more than 4000 m.

WSBW which flows to the east south of the South Sandwich Trench is observed only in the central and western part of the Weddell Basin (Schlemmer, 1978). The remaining bottom water of the Weddell Sea may flow into the eastern basins of the South Atlantic and the southwestern basins of the Indian Ocean through several passages in the Mid-Ocean Ridge (see Fig. 75). The bottom water of the Agulhas Basin with potential temperatures < -0.1°C originates from a transport of AABW through the Conrad, Bouvet, Shaka or Mandela Fracture Zone west of 20°E. AABW moves also into the Crozet Basin, mainly through the western part of the Crozet-Kerguelen Passage at about 50°S (Jacobs and Georgi, 1977).

Within the cyclonic deep circulation of the Weddell Basin, AABW flows first southward along the Kerguelen Plateau and then turns westward toward the Weddell Sea. At about 60°E it overrides the bottom water which has newly formed at the Enderby Land-/Prydz Bay Coast (Jacobs and Georgi, 1977). It has not been determined whether or not the eastward spreading of AABW is blocked by the Kerguelen Plateau. Gordon (1974) assumes that bottom water of the South Indian Basin consists of a mixture of bottom water originating from the Ross Sea and from the Adélie Coast. Kolla et al. (1979) demonstrate with the aid of 8-day current measurements, that a weak eastward flow exists between the southern tip of the plateau and Antarctica.

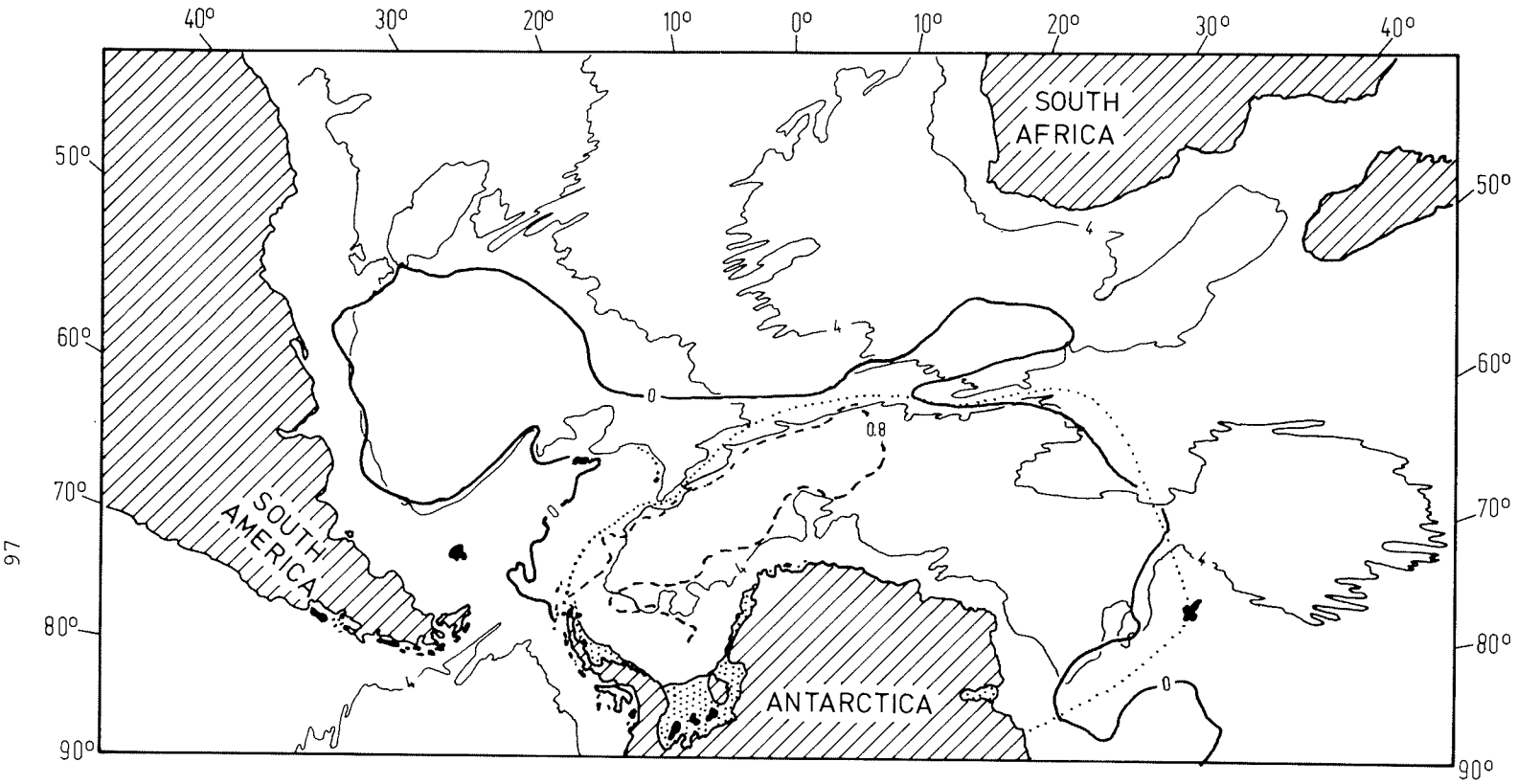

Figure 75: Distribution of the 0°C- and -0.8°-isotherms in the bottom layer south of 25°S between 90°W and 90°E (after Gordon and Molinelli, 1982).

ACKNOWLEDGEMENTS

The authors thank Dr. F. Westall for the critically reading of this paper and C. Schwake for typing the manuscript.

SUBJECT INDEX

	page
Adélie Coast Bottom Water	24,96
Agulhas Current	29,38,39
albedo	46
Antarctic Bottom Water (AABW)	
- formation	74ff.
- general	21,24,33
- Ross Sea	24
- Scotia Sea	95
- Weddell Sea	24,58,59,62,74,86ff.
- -transport	71
- -spreading	93ff.
Antarctic Circumpolar Current (ACC)	
- general	26,29,36ff.,71,94
- Atlantic sector	38ff.
- Drake Passage	42ff.
- Indian sector	39ff.
- Pacific sector	42
Antarctic continent	4,15
Antarctic Convergence	4,7,8,26
Antarctic Discordance	39
Antarctic Divergence (AAD)	17,22,23,36,44ff.,75,77
Antarctic Intermediate Water (AAIW)	22,25,37
Antarctic Peninsula	4,8,18,42,44,49,55
Antarctic pressure trough	10,11,50
Antarctic Surface Water (AASW)	
- general	21,22,26,80
- Weddell Sea	61
- -transport	71
Antarctic Zone (AAZ)	43
Atlantic-Indian Ridge	39
Argentine Basin	39,96
bottom water formation	74ff.
Bouvet Divergence (BD)	45
Brazil Current	38,96
cabbeling instability	92
circulation	
- atmospheric	5
- oceanic	36ff.
- Filchner Depression	73
- Weddell Basin	68ff.
- Weddell Sea shelf	73,79
Circumpolar Deep Water (CDW)	21,23,24,33,75,89
- upwelling of CDW	77
Continental Water Boundary (CBW)	36,43
Continental Zone (CZ)	43

	page
convection	
- haline	76ff.
- in the open ocean	80ff.
- -deep convection	18,75,80,82,96
- -chimney convection	80,82
- on the shelf	78ff.
- overturning	79,84ff.
- thermal	75
deep water formation	90,92
divergence	
- Antarctic Divergence (AAD)	17,22,23,36,44ff.,75,77
- Bouvet Divergence (BD)	45
double diffusive convection	90ff.
downwelling	79
Drake Passage	28,42ff.
East Wind Drift (EWD)	44
east wind zone	14,50ff.
Eastern Shelf Water (ESW)	67
Falkland (Malvinas) Current	25,38,39,96
Filchner Depression	46,58,63,67,73
fresh water input	14,84ff.
frazil ice	55
heat flux	47ff.,75,77,80,92
Humboldt Current	42
iceberg	21,44,78
Ice Shelf Water (ISW)	
- general	24,26
- Weddell Sea	67ff.
- upwelling	78
ice shelves	
- general	21,46
- Ross Sea	4,21
- Weddell Sea	57ff.
- -Filchner-Ronne	21,46,54,57,69,78,79
- -Larsen	57
Indian-Antarctic Ridge	39,40
Kerguelen Plateau	4,39,96
lead	47,49,55,78
Macquarie Ridge	39,41
Modified Circumpolar Deep Water (MCDW)	24ff.
Modified Warm Deep Water (MWDW)	25,86ff.,90ff.
North Atlantic Deep Water (NADW)	23
plume model	87ff.
Polar Front (PF)	22,26ff.,36,43
Polar Front Zone (PFZ)	26ff.,43

	page
polynya	19,47,49,52,55,75,80
- Weddell Polynya	56,75,82ff.,90
precipitation	14,52
pycnocline	
- Southern Ocean	75
- Weddell Sea	80
Ross Sea	4,18,26
Ross Sea Bottom Water (RSBW)	24
salt finger	76,91
Scotia Sea	33ff.,39,42,94ff.
sea ice	
- freezing	76ff.,84ff.
- melting	18,76ff.,84ff.
- Southern Ocean	
- -concentration	19ff.
- -extension	5ff.
- -seasonal variation	15ff.
- -thickness	21
- Weddell Sea	52ff.
- -thickness	55
- growth	75,77,84
shelf water	
- general	24,25
- High Salinity Shelf Water (HSSW)	24,26
- Low Salinity Shelf Water (LSSW)	26
South Indian Basin	4,96
South Sandwich Trench	95
Southeast Pacific Deep Water (SPDW)	23,45
Subantarctic Front (SF)	26,29,30,33,36,40,43
Subantarctic Surface Water (SASW)	26,30
Subantarctic Zone (SAZ)	43
supercooled water	67,77,78
surface cooling	75,82,85
Warm Deep Water (WDW)	23,61ff.,65,71,74,82,86ff.,90ff.
water masses	21ff.,59ff.
Weddell Gyre	10,46,54,61,65,68ff.,74,75,80,91
Weddell-Scotia Confluence (WSC)	34ff.
Weddell Sea	4,46ff.,94,96
- circulation	68ff.
- hydrography	58ff.
- topography	26,46
- water masses	59ff.
- -mixing on the cont. slope	86ff.
- -mixing in the open ocean	90
Weddell Sea Bottom Water (WSBW)	63ff.,71,72,74,86ff.,90ff.,96
Weddell Sea Deep Water (WSDW)	45,65,82,86
West Australian Current	39
Western Shelf Water (WSW)	67,74,86ff.,90ff.
west wind zone	11,50ff.
Winter Water (WW)	22,24,61,65,71,74,75,86ff.,90ff.
wind	
- east wind zone	14,50ff.
- katabatic	14,19,52,68
- west wind zone	11ff.,50ff.

REFERENCES

ACKLEY, S.F. 1979. Mass balance aspects of Weddell pack ice. J. Glaciol., 24, 391-406.

ACKLEY, S.F. 1981a. A review of sea-ice weather relationships in the Southern Hemisphere. In: Sea Level, Ice, and Climate Change, Proceedings of the Canberra Symposium, Dec. 1979, IAHS Publ. No. 131, 127-159.

ACKLEY, S.F. 1981b. Sea-ice atmosphere interactions in the Weddell Sea using drifting buoys. In: Sea Level, Ice, and Climatic Change, Proceedings of the Canberra Symposium, Dec. 1979, IAHS Publ. No. 131, 177-191.

ACKLEY, S.F. and T.E. KELIHER 1976, Antarctic sea ice dynamics and its possible climatic effects. AIDJEX Bull., 33, 53-76.

ACKLEY, S.F., A.J. GOW, K.R. BUCK and K.M. GOLDEN 1980. Sea ice studies in the Weddell Sea aboard USCGC Polar Sea. Antarct. J. of the U. S., 15, 84-86.

ALLISON, I. 1981. Antarctic sea ice growth and oceanic heat flux. In: Sea Level, Ice, and Climatic Change, Proceedings of the Canberra Symposium, Dec. 1979, IAHS Publ. No. 131, 161-170.

ALLISON, I., C.M TIVENDALE, G.J. AKERMAN, J.M. TANN and R.F.WILLS 1982. Seasonal variations in the surface energy exchanges over Antarctic sea ice and coastal waters. Ann. Glaciol., 3, 12-16.

BABARYKIN, V.K., G.I. BARANOV, G.I. BARDIN and G.G. SAKUNOV 1964 Albedo of the surface of Antarctic ice. Sov. Ant. Exp. Inf. Bull., 5, 203-204.

BAKER, D.J. 1979. Ocean-atmosphere interaction in high southern latitudes. Dyn. Atmos. Oceans, 3, 213-229.

BAKER, D.J., W.D. NOWLIN, jr., R.D. PILLSBURY and H.L. BRYDEN 1977. Antarctic Circumpolar Current: space and time fluctuations in the Drake Passage. Nature, 268, 696-699.

BAUER, J. and S.L. MARTIN 1983. A model of grease ice growth in leads. J. Geophys. Res., 88, 2917-2925.

BEHRENDT, J.C. 1962. Geophysical and glaciological studies in the Filchner Ice Shelf area of Antarctica. J. Geophys. Res., 67, 221-234.

BEHRENDT, J.C. 1968. The structure of the Filchner Ice Shelf and its relation to bottom melting. ISAGE Symposium Hanover, USA, Sept. 1968, 488-496.

BOTNIKOV, V.N. 1963. Geographical position of the Antarctic Convergence Zone in the Antarctic Ocean. Soviet Ant. Exped. Inf. Bull., 4, 324-327.

BOTNIKOV, V.N. 1964. Seasonal and long-term fluctuations of the Antarctic Convergence Zone. Soviet Ant. Exped. Inf. Bul., 5, 92-95.

BOYER, D.L. and J.R. GUALA 1972. Model of the Antarctic Circumpolar Current in the vicinity of the Macquarie Ridge. In: Antarctic Oceanology II: The Australian - New Zealand sector, D. Hayes, ed., Ant. Res. Ser., 19, 79-93.

BRENNECKE, W. 1921. Die ozeanographischen Arbeiten der deutschen antarktischen Expedition 1911-1912. Arch. Deutsche Seewarte, 39(1), 1-216.

BRYDEN, H.L. 1979. Poleward heat flux and conversion of available potential energy in Drake Passage. J. Mar. Res., 37, 1-22.

BRYDEN, H.L. and R.D. PILLSBURY 1977. Variability of deep flow in the Drake Passage from year-long current measurements. J. Phys. Oceanogr., 7, 803-810.

CALLAHAN, J.E. 1971. Velocity structure and flux of the Antarctic Circumpolar Current south of Australia. J. Geophys. Res., 76, 5859-5864.

CALLAHAN; J.E. 1972. The structure and circulation of Deep Water in the Antarctic. Deep-Sea Res., 19, 563-575.

CARMACK, E.C. 1974. A quantitative characterization of water masses in the Weddell Sea during summer. Deep-Sea Res., 21, 431-443.

CARMACK, E.C. 1977. Water characteristics of the Southern Ocean south of the Polar Front. In: A Voyage of Discovery, M.V. Angel, ed., Deep-Sea Res., Suppl. to Vol. 24, 15-41.

CARMACK, E.C. and T.D. FOSTER 1975a. Circulation and distribution of oceanographic properties near the Filchner Ice Shelf. Deep-Sea Res., 22, 77-90.

CARMACK, E.C. and T.D. FOSTER 1975b. On the flow of water out of the Weddell Sea. Deep-Sea Res., 22, 711-724.

CARMACK, E.C. and T.D. FOSTER 1977. Water masses and circulation in the Weddell Sea. Proceedings of the Polar Oceans Conference, Montreal, May 1974. In: Polar Oceans, M.J. Dunbar, ed., Arctic Inst. of North America, 151-165.

CARMACK, E.C. and P.D. KILLWORTH 1978. Formation and interleaving of abyssal water masses off Wilkes Land, Antarctica. Deep-Sea Res., 25, 357-369.

CARSEY, F.D. 1980. Microwave observations of the Weddell Polynya. Mon. Wea. Rev., 108, 2032-2044.

CAVALIERI, D.J. and C.L. PARKINSON 1981. Large scale variations in observed antarctic sea ice extent, and associated atmospheric circulation. Mon. Wea. Rev., 109, 2323-2336.

CLARKE, A.J. 1982. The dynamics of large-scale, wind-driven variations in the Antarctic Circumpolar Current. J. Phys. Oceanogr., 12, 1092-1105.

CLARKE, D.B. and S.F. Ackley 1984. Sea ice structure and biological activity in the Antarctic marginal ice zone. J. Geophys. Res., 89, 2087-2095.

COLTON, M.T. and R.R. CHASE 1983. Interaction of the ACC with bottom topography: An investigation using satellite altimetry. J. Geophys. Res., 88, 1825-1843.

CSANADY, G.T. 1972. Geostrophic drag, heat and mass transfer coefficients for the diabatic Ekman layer. J. Atmos. Sc., 29, 488-496.

DANARD, M., M. GRAY and G. LYV 1983. A model for the prediction of initial sea ice formation. Month. Wea. Rev., 111, 1634-1645.

DEACON, G.E.R. 1933. A general account of the hydrology of the South Atlantic Ocean. Discovery Reports, 7, 171-238.

DEACON, G.E.R. 1937. The hydrology of the Southern Ocean. Discovery Reports, 15, 1-124.

DEACON, G.E.R. 1979. The Weddell Gyre. Deep-Sea Res., 26A, 981-995.

DEACON, G.E.R. 1982. Physical and biological zonation in the southern Ocean. Deep-Sea Res., 29, 1-15.

DEACON, G.E.R. 1983. Kerguelen, Antarctic and Subantarctic. Deep-Sea Res. 30, 77-81.

DE SZOEKE, R.A. and M.D. LEVINE 1981. The advective flux of heat by mean geostrophic motions in the Southern Ocean. Deep-Sea Res., 28A, 1057-1085.

DEUTSCHES HYDROGRPAHISCHES INSTITUT 1981. Handbuch des Atlantischen Ozeans.

DIECKMANN, G., G. ROHARDT, H.H. HELLMER and J. KIPFSTUHL 1986. The occurence of ice platelets at 250 meters depth near the Filchner Ice Shelf and its significance for sea ice biology. Deep-Sea Res., in press.

EMERY, W.J. 1977. Antarctic Polar Frontal Zone from Australia to the Drake Passage. J. Phys. Oceanogr., 7, 811-822.

EYRE, W.S. 1972. The spherical harmonic analysis of global wind stress field and atmospheric angular momentum. Flinders Inst. f. Atmosph. and Marine Sciences Res., Rep.6.

FANDRY, Ch. and R.D. Pillsbury 1979. On the estimation of absolute geostrophic volumne transport applied to the Antarctic Circumpolar Current. J. Phys. Oceanogr., 9(3), 449-455.

FLETCHER, J.O., U. RADOK and R. SLUTZ 1982. Climatic signals to the Antarctic Ocean. J. Geophys. Res., 87, 4269-4276.

FOFONOFF, N.P. 1956. Some properties of sea water influencing the formation of Antarctic Bottom Water. Deep-Sea Res., 4, 32-35.

FOLDVIK, A. and T. KVINGE 1974a. Bottom currents in the Weddell Sea. Rep. Geophys. Inst., Univ. Bergen, No. 37.

FOLDVIK, A. and T. KVINGE 1974b. Conditional instability of sea water at the freezing point. Deep-Sea Res., 21, 169-174.

FOLDVIK, A. and T. KVINGE 1974c. Thermohaline convection in the vicinity of an ice shelf. Rep. Geophys. Inst., Univ. Bergen, No. 36.

FOSTER, T.D. 1969. Experiments on haline convection induced by the freezing of sea water. J. Geophys. Res., 74, 6967-6974.

FOSTER, T.D. 1972a. An analysis of the cabbeling instability in sea water. J. Phys. Oceanogr., 2, 294-301.

FOSTER, T.D. 1972b. Haline convection in polynyas and leads. J. Phys. Oceanogr., 2, 462-469.

FOSTER, T.D. and E.C. CARMACK 1976a. Frontal zone mixing and Antarctic Bottom Water formation in the southern Weddell Sea. Deep-Sea Res., 23, 301-317.

FOSTER, T.D. and E.C. CARMACK 1976b. Temperature and salinity structure in the Weddell Sea. J. Phys. Oceanogr., 6, 36-44.

FOSTER, T.D. and E.C. CARMACK 1977. Antarctic Bottom Water formation in the Weddell Sea. Proceedings of the Polar Oceans Conference, Montreal, May 1974. In: Polar Oceans, M.J. Dunbar, ed., Arctic Inst. of North America, 167-177.

FOSTER, T.D. and J.H. MIDDLETON 1979. Variability in the bottom water of the Weddell Sea. Deep-Sea Res., 26A, 743-762.

FOSTER, T.D. and J.H. MIDDLETON 1980. Bottom water formation in the western Weddell Sea. Deep-Sea Res., 27A, 367-381.

GASCARD, J.C. 1973. Vertical motion in a region of deep water formation. Deep-Sea Res., 20, 1011-1028.

GEORGI, D.T. 1981. Circulation of bottom waters in the southwestern South Atlantic. Deep-Sea Res., 28A, 959-979.

GILL, A.E. 1973. Circulation and bottom water production in the Weddell Sea. Deep-Sea Res., 20, 111-140.

GILL, A.E. and K. BRYAN 1971. Effects of geometry on the circulation of a three-dimensional southern-hemisphere ocean model. Deep-Sea Res., 18, 685-721.

GILL, A.E. and J.S. TURNER 1969. Some new ideas about the formation of Antarctic Bottom Water. Nature, 224, 1287-1288.

GORDON, A.L. 1966. Potential temperature, oxygen and circulation of bottom water in the Southern Ocean. Deep-Sea Res., 13, 1125-1138.

GORDON, A.L. 1967. Structure of Antarctic Waters between 20°W and 170°W. Antarctic Map Folio Series - Folio 6, V.C. Bushnell, ed., Amer. Geogr. Soc., 10 pp.

GORDON, A.L. 1971a. Antarctic Polar Front Zone. In: Antarctic Oceanology I, J. Reid, ed., Ant. Res. Ser., 15, 205-221.

GORDON, A.L. 1971b. Oceanography of Antarctic waters. In: Antarctic Oceanology I, J. Reid, ed., Ant. Res. Ser., 15, 169-203.

GORDON, A.L. 1972. On the interaction of the Antarctic Circumpolar Current and the Macquarie Ridge. In: Antarctic Oceanology II: The Australian - New Zealand sector, D. Hayes, ed., Ant. Res. Ser., 19, 71-78.

GORDON, A.L. 1974. Varities and variability of Antarctic Bottom Water. Colloques Internationaux du C.N.R.S., No. 215 - Processus de formation des eaux océaniques profondes, 33-47.

GORDON, A.L. 1975. An Antarctic oceanographic section along 170°E. Deep-Sea Res., 22, 357-377.

GORDON, A.L. 1978. Deep Antarctic convection west of Maud Rise. J. Phys. Oceanogr., 8, 600-612.

GORDON, A.L. 1979. Circulation of Weddell Gyre and Antarctic Circumpolar Current in South Atlantic. Antarctic J. of the U.S., 14 (5), 112-113.

GORDON, A.L. 1980. Comments on Southern Ocean near-surface circulation and its variability. Ann. Glaciol., 1, 57-60.

GORDON, A.L. 1981. Seasonality of Southern Ocean sea ice. J. Geophys. Res., 86 (C5), 4193-4197.

GORDON, A.L. 1982. Weddell Deep Water variability. J.Mar. Res., Suppl. to Vol. 40, 199-217.

GORDON, A.L. 1983. Polar Oceanography. Rev. Geophys. and Space Phys., 21 (5), 1124-1131.

GORDON, A.L. and J.A. BYE 1972. Surface dynamic topography of Antarctic waters. J. Geophys. Res., 77, 5993-5999.

GORDON, A.L. and R.D. GOLDBERG 1970. Circumpolar characteristics of Antarctic waters. Antarctic Map Folio Series, 18, V. Bushnell, ed., Amer. Geogr. Soc., New York.

GORDON, A.L. and B.A. HUBER 1984. Thermohaline stratification below the Southern Ocean sea ice. J. Geophys. Res., 89 (C 1) 641-648.

GORDON, A.L. and E. MOLINELLI 1982. Southern Ocean Atlas: Thermohaline and Chemical Distributions. Columbia University Press, New York.

GORDON, A.L. and W.D. NOWLIN, jr. 1978. The basin waters of the Bransfield Strait. J. Phys. Oceanogr., 8, 258-264.

GORDON, A.L. and H.W. TAYLOR 1975a. Heat and salt balance within the cold waters of the world ocean. In: Numerical Models of Ocean Circulation, National Academy of Sciences, Washington, 54-56.

GORDON, A.L. and H.W. TAYLOR 1975b. Seasonal change of Antarctic sea ice cover. Science, 187, 346-347.

GORDON, A.L. and P. TCHERNIA 1972. Waters of the continental margin off Adélie coast, Antarctica. In: Antarctic Oceanology II: The Australian - New Zealand sector, D.E. Hayes, ed., Ant. Res. Ser., 19, 59-69.

GORDON, A.L., D.T. GEORGI and H.W. TAYLOR 1977b. Antarctic Polar Front Zone in the western Scotia Sea-summer 1975. J. Phys. Oceanogr., 7, 309-328.

GORDON, A.L., D.G. MARTINSON and H.W. TAYLOR 1981. The wind-driven circulation in the Weddell-Enderby Basin. Deep-Sea Res., 28A, 151-163.

GORDON, A.L., E. MOLINELLI and T. BAKER 1978. Large-scale relative dynamic topography of the Southern Ocean. J. Geophys. Res., 83, 3023-3032.

GORDON, A.L., H.W. TAYLOR and D.T. GEORGI 1977a. Antarctic oceanographic zonation. In: Polar Oceans, M.J. Dunbar, ed., Arctic Inst. of North America, 45-76.

GOW, A.J., S.F. ACKLEY, W.F. WEEKS and J.W. GOVONI 1982. Physical and structural characteristics of Antarctic sea ice. Annals of Glaciology, 3, 113-117.

GUBE-LENHARDT, M. and H. HOEBER 1985. The development of the atmospheric boundary layer over the coastal region of the Weddell-Sea during offshore winds. To be published in: J.de Recherches Atmosphériques.

HASTENRATH, S. 1980. Heat budget of tropical ocean and atmosphere. J. Phys. Oceanogr., 10, 159-170.

HASTENRATH, S. 1982. On meridional heat transports in the World Ocean. J. Phys. Oceanogr., 12, 922-927.

HELLERMAN, S. 1967. An updated estimate of the wind stress on the world ocean. Mon. Wea. Rev., 95, 607-626.

HIBLER, W.D. 1979. A dynamic thermodynamic sea ice model. J. Phys. Oceanogr., 9, 815-846.

HIBLER, W.D. and S.F. ACKLEY 1983. Numerical simulation of the Weddell Sea pack ice. J. Geophys. Res., 88, 2873-2887.

HOGG, N., P. BISCAYE, W. GARDNER and W.J. SCHMITZ jr. 1982. On the transport and modification of Antarctic Bottom Water in the Vema Channel. J. Mar. Res., Suppl. to Vol. 40, 231-263.

HUPPERT, H.E. 1971. On the stability of a series of double diffusive layers. Deep-Sea Res., 18, 1005-1021.

HUPPERT, H.E. and J.S. TURNER 1972. Double -diffusive convection and its implications for the temperature and salinity structure of the ocean and Lake Vanda. J. Phys. Oceanogr., 2, 456-461.

JACOBS, S.S. and D.T. GEORGI 1977. Observations in the southwest Indian/Antarctic Ocean. In: A Voyage of Discovery. M.V. Angel, ed., Deep-Sea Res., Suppl. to Vol. 24, 43-89.

JACOBS, S.S., A.F. AMOS and P.M. BRUCHHAUSEN 1970. Ross Sea oceanography and Antarctic Bottom Water formation. Deep-Sea Res., 17, 935-962.

JACOBS, S.S., A.L. GORDON and J.L. ARDAI 1979a. Circulation and melting beneath the Ross Ice Shelf. Science, 203, 439-443.

JACOBS, S.S., A.L. GORDON and A.F. AMOS 1979b. Effect of glacial ice melting on the Antarctic surface water. Nature, 277, 469-471.

JENNE, R.L., H.L. CRUTCHER, H. VAN LOON and J.J. TALJAARD 1971. Climate of the Upper Air: Southern Hemisphere. Vol.III: Vector Mean Geostrohpic Winds, Isogon and Isotach Analyses. National Center for Atmospheric Research, Boulder, Colorado.

JOHNSON; G.L., J.R. VANNEY, A. ELVERHØI and J.L. LA BRECQUE 1981. Morphology of the Weddell Sea and southwest Indian Ocean. Deutsche Hydrogr. Z., 34, H. 6, 263-272.

JOYCE, T.M., S.L. PATTERSON and R.C. MILLARD 1981. Anatomy of a cyclonic ring in the Drake Passage. Deep-Sea Res., 28 A, 1265-1287.

JOYCE, T.M., W. ZENK and J.M. TOOLE 1978. The anatomy of the Antarctic Polar Front in the Drake Passage. J.Geophys. Res., 83, 6093-6113.

KILLWORTH, P.D. 1973. A two-dimensional model for the formation of Antarctic Bottom Water. Deep-Sea Res., 20, 941-971.

KILLWORTH, P.D. 1974. A baroclinic model of motions on Antarctic continental shelves. Deep-Sea Res., 21, 815-837.

KILLWORTH, P.D. 1977. Mixing on the Weddell Sea continental slope. Deep-Sea Res., 24, 427-448.

KILLWORTH, P.D. 1979. On "chimney" formations in the ocean. J. Phys. Oceanogr., 9, 531-554.

KOHNEN, H. 1982. Glaciological investigations in the frontal zone of the Filchner and Ronne Ice Shelves, Ann. Glaciol., 3, 160-165.

KOLLA, V., L. SULLIVAN, S.S. STREETER and M.G. LANGSETH 1976. Spreading of Antarctic Bottom Water and its effects on the floor of the Indian Ocean inferred from bottom-water potential temperature, turbidity, and sea-floor photography. Mar. Geol., 21, 171-189.

KOOPMANN, G. 1953. Entstehung und Verbreitung von Divergenzen in der oberflächennahen Wasserbewegung der antarktischen Gewässer. Deutsche Hydrogr. Z., Ergänzungsheft Reihe A, 2, 38 pp.

KORT, V.G. 1962. The Antarctic Ocean. Scientific American, 207, 113-121.

KORT, V.G. 1981. Mesoscale variability of currents and temperature in the Southern Ocean from drifting buoy data. Oceanology, 21, 291-298.

KUKSA, V.J. and S.G. POYARKOV 1977. Large-scale characteristics of the distribution of Antarctic Intermediate Water in the world ocean. Oceanology, 17 (2), 121-126.

LACOMBE, H. 1974. Deep effects of energy transfers across the sea surface: the formation of deep waters. The western Mediterranean, as an example. Procès-Verbaux, 13, IAPSO First Special Assembly at Melbourne, Jan. 1974.

LAKE, R.A. and E.L. LEWIS 1970. Salt rejection by sea ice during growth. J. Geophys. Res., 75 (3), 583-597.

LEDENEV, V.G. 1964. Influence of evaporation on the formation of cold Antarctic water. Sov. Ant. Exp. Inf. Bull., 5, 50-52.

LEGECKIS, R. 1977. Oceanic polar front in the Drake Passage-satellite observations during 1976. Deep-Sea Res., 24, 701-704.

LEWIS, E.L. 1974. Convection beneath sea ice. Colloque Internationaux du C.N.R.S. No. 215 - Processus de formation des eaux océaniques profondes, 49-55.

LUTJEHARMS, J.R. and D.J., BAKER 1980. A statistical analysis of the meso-scale dynamics of the Southern Ocean. Deep-Sea Res., 27 A, 145-159.

MAC AYEAL, D.R. 1984. Thermohaline circulation below the Ross Ice Shelf: a consequence of tidally induced vertical mixing and basal melting. J. Geophys. Res., 89 (C 1), 597-606.

MACKINTOSH, N.A. 1946. The Antarctic Convergence and the distribution of surface temperatures in Antarctic Waters. Discovery Reports, 23, 177-212.

MARTINSON, D.G., P.D. KILLWORTH and A.L. GORDON 1981. A convective model for the Weddell Polynya. J. Phys. Oceanogr., 11, 466-488.

MATHER, K.B. and G.S. MILLER 1967. Note on topographic factors affecting the surface wind in Antarctica, with special reference to katabatic winds. Geophys. Inst. Un. Alaska Tech. Rep. UAG R-189 Antarctic (unpublished manuscript).

MAYKUT, G.A. 1978. Energy exchange over young sea ice in the central Arctic. J. Geophys. Res., 83, 3646-3658.

MAYKUT, G.A. 1982. Large-scale heat exchange and ice production in the central Arctic. J. Geophys. Res., 87, 7971-7984.

MC CARTNEY, M.S. 1976. The interaction of zonal currents with topography with applications to the Southern Ocean. Deep-Sea Res., 23, 413-427.

MC WILLIAMS, J.C., W.R. HOLLAND and J.H. CHOW 1978. A description of numerical Antarctic circumpolar currents. Dyn. Atmos. Oceans, 2, 213-291.

MIDDLETON, J.H. and T.D. FOSTER 1977. Tidal currents in the central Weddell Sea. Deep-Sea Res., 24, 1195-1202.

MIDDLETON, J.H. and T.D. FOSTER 1980. Fine structure measurements in a temperature-compensated halocline. J. Geophys. Res., 85, 1107-1122.

MOROZ, I.F. 1979. Thermohaline structure of waters of the Pacific Ocean sector of the Antarctic. Oceanology, 19 (3), 253-256.

MOSBY, H. 1934. The waters of the Atlantic Antarctic Ocean. Scientific Results of the Norwegian Antarctic Exped. 1927 - 1928, 1 (11), 1-131.

NEAL, V.T. and W.D. NOWLIN 1979. International Southern Ocean studies of circumpolar dynamics. Polar Record, 19, 461-470.

NEWTON, C.W. 1972. Southern hemisphere general circulation in relation to global energy and momentum balance requirements. In: Meteorology of the Southern Hemisphere, Meteor. Monogr., 13, 215-246.

NOWLIN, W.D. and M. CLIFFORD 1982. The kinematic and thermohaline zonation of the Antarctic Circumpolar Current at Drake Passage. J. Mar. Res., 40, Suppl., 481-507.

NOWLIN, W.D., T. WHITWORTH and R.D. PILLSBURY 1977. Structure and transport of the Antarctic Circumpolar Current at Drake Passage from short-term measurements. J. Phys. Oceanogr., 7, 788-802.

OSTAPOFF, F. 1962. The salinity distribution at 200 meters and the Antarctic frontal zones. Deutsche Hydrogr. Z., 15, 133-142.

PARKINSON, C.L. and D.J. CAVALIERI 1982. Interannual sea-ice variations and sea-ice/atmosphere interactions in the Southern Ocean, 1973-1975. Ann. Glaciol., 3, 249-254.

PARKINSON, C.L. and W.M. Washington 1979. A large-scale numerical model of sea ice. J. Geophys. Res., 84, 311-337.

PATTERSON, S.L. and H.A. SIEVERS 1980. The Weddell-Scotia Confluence. J. Phys. Oceanogr., 10, 1584-1610.

PETERSON, R.G., W.D. NOWLIN and T. WHITWORTH 1982. Generation and evolution of a cyclonic ring at Drake Passage in early 1979. J. Phys. Oceanogr., 12, 712-719.

PILLSBURY, R.D., T. WHITWORTH, W.D. NOWLIN and F. SCIREMAMMANO 1979. Currents and temperatures as observed in Drake Passage during 1975. J. Phys. Oceanogr., 9, 469-482.

PIOLA, A.R. and D.T. GEORGI 1981. Sea-air heat and freshwater fluxes in the Drake Passage and western Scotia Sea. J. Phys. Oceanogr., 11, 121-126.

PIOLA, A.R. and D.T. GEORGI 1982. Circumpolar properties of Antarctic Intermediate Water and Subantarctic Mode Water. Deep-Sea Res., 29, 687-711.

RADOK, U., N. STRETEN and G. WELLER 1975. Atmosphere and ice. Oceanus, 18, 17-27.

RAYNER, J.N. and D.A. HOWARTH 1979. Antarctic sea ice: 1972-75. Geogr. Rev., 69, 202-223.

REID, J.L. and W.D. NOWLIN 1971. Transport of water through the Drake Passage. Deep-Sea Res., 18, 51-64.

REID, J.L., W.D. NOWLIN and W.C. PATZERT 1977. On the characteristics and circulation of the southwestern Atlantic Ocean. J. Phys. Oceanogr., 7, 62-91.

ROBIN, G. de, C.S. DOAKE, H. KOHNEN, R.D. CRABTREE, S.R. JORDAN and D. MÖLLER 1983. Regime of the Filchner-Ronne Ice Shelves, Antarctica. Nature, 302, 582-586.

RODMAN, M.R. and A.L. GORDON 1982. Southern Ocean bottom water of the Australian - New Zealand sector. J. Geophys. Res., 87, 5771-5778.

ROHARDT, G. and E. AUGSTEIN 1985. Hydrographie vor dem Filchner-Schelfeis. In: Filchner Ronne Ice Shelf Programme, H. Kohnen, ed., No. 2, 50-57.

ROPELEWSKI, C.F. 1983. Spatial and temporal variations in Antarctic sea-ice (1973-82). J. Clim. Appl. Met., 22, 470-473.

SASAMORI, T., J. LONDON and D.V. HOYT 1972. Radiation budget of the southern hemisphere. In: Meteorology of the Southern Hemisphere, Meteor. Monogr., 13, 9-23.

SAVCHENKO, V.G., W.J. EMERY and O.A. VLADIMIROV 1978. A cyclonic eddy in the Antarctic Circumpolar Current south of Australia: results of Soviet-American Observations aboard the R/V Professor Zubov. J. Phys. Oceanogr., 8, 825-837.

SCAR 1983. Second Post-FIBEX Hydrographic Data Interpretation Workshop. 16-20 May 1983, Hamburg, F.R.G., BIOMASS Report Series, 31, 26 pp.

SCHLEMMER, F.C. 1978. Structure and spreading of Antarctic Bottom Waters in oceanic basins adjacent to Antarctica. Ph. D., Texas A & M University, 138 pp.

SCHWERDTFEGER, W. 1970. The climate of the Antarctic. In: Climates of the Polar Regions, World Survey of Climatology, H. Landsberg, ed., 14, 253-355.

SCHWERDTFEGER, W. 1975. The effect of the Antarctic Peninsula on the temperature regime of the Weddell Sea. Mon. Wea. Rev., 103, 45-51.

SCHWERDTFEGER, W. 1979. Meteorological aspects of the drift of ice from the Weddell Sea toward the mid-latitude westlies. J. Geophys. Res., 84, 6321-6328.

SCIREMAMMANO, F. 1980. The nature of the poleward heat flux due to low-frequency current fluctuations in the Drake Passage. J. Phys. Oceanogr., 10, 843-852.

SCIREMAMMANO, F., R.D. PILLSBURY, W.D. NOWLIN and T. WHITWORTH 1980. Spatial scales of temperature and flow in Drake Passage. J. Geophys. Res., 85 (C 7), 4015-4028.

SEABROOKE, J.M., G.L. HUFFORD and R.B. ELDER 1971. Formation of Antarctic Bottom Water in the Weddell Sea. J. Geophys. Res., 76 (9), 2164-2178.

SIEVERS, H.A. and W.J. EMERY 1978. Variability of the Antarctic Polar Frontal Zone in the Drake Passage - summer 1976-1977. J. Geophys. Res., 83, 3010-3022.

SMITH, N.R. and C.B. FANDRY 1978. Combined effects of wind stress and topography in a two-layer model of the Southern Ocean. Deep-Sea Res., 25, 371-390.

SPILLANE, M. 1978. Topographic generation of intermediate-scale motions by wind-driven currents - a model for the circulation in the vicinity of the Indian-Antarctic Ridge. Dyn. Atmos. Oceans, 2, 427-453.

STEIN, M. 1981. Thermal structure of the Weddell-Scotia Confluence during February 1981. Meeresforschung, 29, 47-52.

STRETEN, N.A. 1973. Satellite observations of the summer decay of the Antarctic sea-ice. Arch. Meteor. Geophys. Bioklim., A 22, 119-134.

STRETEN, N.A. 1977. Seasonal climatic variability over the Southern Oceans. Arch. Meteor. Geophys. Bioklim., B25, 1-19.

STRETEN, N.A. 1980. Some synoptic indices of the southern hemisphere mean sea level circulation 1972-77. Mon.Wea.Rev., 108, 18-36.

STRETEN, N.A. and D. PIKE 1980. Characteristics of the broad-scale Antarctic sea ice extent and the associated atmospheric circulation 1972-1977. Arch. Meteor. Geophys. Bioklim., A29, 279-299.

TALJAARD, J.J. 1972. Synoptic meteorology of the southern hemisphere. In: Meteorology of the Southern Hemisphere, Meteor. Monogr., 13, 139-213.

TAYLOR, H.W., A.L. GORDON and E. MOLINELLI 1978. Climatic characteristics of the Antarctic Polar Front Zone. J. Geophys. Res., 83, 4572-4578.

TCHERNIA, P. 1980. Descriptive Regional Oceanography. Pergamon Press, London.

TCHERNIA, P. and P.F. JEANNIN 1980. Observations on the Antarctic East Wind Drift using tabular icebergs tracked by satellite Nimbus F (1975-1977). Deep-Sea Res., 27A, 467-474.

THOMPSON, R.O. 1971. Why there is an intense eastward current in the North Atlantic but not in the South Atlantic. J. Phys. Oceanogr., 1, 235-237.

TRENBERTH, K.E. 1979. Mean annual poleward energy transport by the oceans in the southern hemisphere. Dyn. Atmos. Oceans, 4, 57-64.

TRESHNIKOV, A.F., G.V. ALEKSEYEV, E.J. SARUKHANYAN and N.P. SMIRNOV 1980. Water circulation in the Southern Ocean. Polar Geogr. and Geology, 4, 21-35.

TURNER, J.S. 1968. The behavior of a stable salinity gradient heated from below. J. Fluid Mech., 33, 183-200.

TURNER, J.S. 1973. Buoyancy effects in fluids. Cambridge University Press, 367 pp.

UNTERSTEINER, N. 1961. On the mass and heat budget of Arctic sea ice. Arch. Meteor. Geophys. Bioklim., A 12, 151-182.

UNTERSTEINER, N. 1966. Sea ice. In: Encyclopedia of Oceanography, R.W. Fairbridge, ed., Reinhold, New York, 1021 pp.

VAN LOON, H. 1972b. Pressure in the southern hemisphere. In: Meteorology of the Southern Hemisphere, Meteor. Monogr., 13, 59-86.

VAN LOON, H. 1972d. Wind in the southern hemisphere. In: Meteorology of the Southern Hemisphere, Meteor. Monogr., 13, 87-121.

WEISS, R.F., H.G. ÖSTLUND and H. CRAIG 1979. Geochemical studies of the Weddell Sea. Deep-Sea Res., 26 A, 1093-1120.

WELLER, G. 1968. Heat energy transfer through a four-layer system: air - snow - sea ice - water. J. Geophys. Res., 73, 1209-1220.

WELLER, G. 1981. Spatial and temporal variations in the south polar surface energy balance. Mon. Wea. Rev., 108, 2006-2014.

WHITWORTH, T. 1980. Zonation and geostrophic flow of the Antarctic Circumpolar Current at Drake Passage. Deep-Sea Res., 27A, 497-507.

WHITWORTH, T. 1983. Monitoring the transport of the Antarctic Circumpolar Current at Drake Passage. J. Phys. Oceanogr., 13, 2045-2057.

WITTE, E. 1902. Zur Theorie der Stromkabbelungen. GAEA, Köln, 484-487.

WRIGHT, D.G. 1981. Baroclinic instability in Drake Passage. J. Phys. Oceanogr., 11, 231-246.

WÜST, G. 1933. Das Bodenwasser und die Gliederung der Atlantischen Tiefsee. Wiss. Ergebn. dtsch. atlant. Exped. METEOR 1925-1927, 6 (1), 1-106.

WÜST, G. 1935. Schichtung und Zirkulation des Atlantischen Ozeans. Das Bodenwasser und die Stratosphäre. Wiss. Ergebn. dtsch. atlant. Exped. METEOR 1925-1927, 6, 1-288.

WYRTKI, K. 1971. Oceanographic atlas of the International Indian Ocean Expedition. NSF, U.S. Government Printing Office, Washington, D.C., 1-531.

ZENK, W. 1981. Detection of overflow events in the Shag Rock Passage, Scotia Ridge. Science, 213, 1113-1114.

ZILLMAN, J.W. 1972. Solar radiation and air-sea interaction south of Australia. In: Antarctic Oceanology II: The Australian - New Zealand Sector, D. Hayes, ed., Ant. Res. Ser., 19, 11-40.

ZOTIKOV, I.A., YU.A. IVANOV and V.R. BARBASH 1974. Antarctic continental ice discharge, and the formation of Antarctic Bottom Waters.Oceanology, 14 (4), 485-490.

ZWALLY, H.J., C. PARKINSON, F. CARSEY, P. GLOERSEN, W.J. Campbell and R.O. RAMSEIER 1979. Antarctic sea ice variations 1973-75. Antarctic J. of the U.S., 14 (5), 102-103.

ZYRYANOV, V.N. and D.N. SEVEROV 1979. Water circulation in the Falkland Patagonia region and its seasonal variation. Oceanology, 19, 518-522.

ZYRYANOV, V.N., V.V. MASLENNIKOV and G.P. GORDIYENKO 1976. Gradient currents in the Scotia Sea. Oceanology, 16, 440-444.